STRESS RESPONSES OF CORALS AND THEIR SYMBIOTIC PARTNERS

by

Contessa Anastasia Ricci

DISSERTATION

Submitted in partial fulfillment of the requirements
for the degree of Doctor of Philosophy at The
University of Texas at Arlington
August, 2019

Arlington, Texas

Supervising Committee:

Laura Mydlarz, Supervising Professor
Saiful Chowdhury
Clay Clark
Shawn Christensen
Matthew Walsh

Acknowledgements

First, I would like to thank my advisor, Dr. Laura Mydlarz, for taking a chance on me and giving me support and guidance through to the end. Thank you also to my committee members who, without you, this would not be possible. I have learned so much from each of you and am grateful for the knowledge you have imparted along my academic journey. I would also like to thank the NSF LSAMP bridge-to-doctorate program for funding me during my PhD, my LSAMP BD cohort for giving me comradery and friendship, and the LSAMP BD directors, Dr. Minerva Cordero and Dr. Kayunta Johnson-Winters, for your boundless support and encouragement – especially when the going got tough, you pushed me to keep on going and I am grateful for it. To my current and former lab mates, Dr. Lauren Fuess, Dr. Whitney Tholen, Bradford Dimos, and Nicholas MacKnight, thank you for being a sounding board when I needed it. And to my UTA friends and colleagues, especially Rachel Wostl, Richard Adams, Kathleen Currie, Danielle Rivera, Kaitlyn Howell, and Michelle Packer – thank you for your friendship and support throughout the years. I feel so lucky to have known such talented, intelligent, and driven people.

To my close friends in Texas, Nicole Hales, Lea Jinks, Savannah Izumi, Delania Klinger, and Bren Ledbetter - I am so thankful for you. You have provided a home away from home, love, and a safe space and I am eternally grateful to you. Through the struggles, successes, ups and downs, you have been there the whole time reminding me to believe in myself and I am in constant awe of that fact. Without you, I know I could not have made it this far. Thank you.

Dedication

I dedicate this thesis to my family. To my mother, Cynthia Hennessey, step father, Peter Hennessey, and my sister, Angelina Ricci – your unconditional love has kept me going throughout these years. I couldn't have asked for a better support system. You were always there when I needed you and you listened to my struggles with compassion and empathy. I have missed you all every day and I can't believe how lucky I am to have a family like you. To my late father, George Anthony Ricci (January 15, 1951 – September 25, 2016) – thank you for our crazy, hair-brained conversations and encouraging me to think outside the box. You always believed in me and I know you would be proud of how far I've come. I miss you. Until we meet again.

Abstract

STRESS RESPONSES OF CORALS AND THEIR SYMBIOTIC PARTNER

Contessa A. Ricci, PhD

The University of Texas at Arlington, 2019

Supervising Professor: Laura D. Mydlarz

Disease and temperature are primary threats to coral persistence, and these stresses can work synergistically to accelerate coral declines. In the face of climate change, understanding the effects of these stresses is key to understanding ecosystem services of future reefs. Corals are an amalgam of the coral animal, an intracellular dinoflagellate symbiont (family Symbiodiniaceae), and a consortium of other symbiotic microbes that exist in the coral surface mucus layer. As such, it is important to consider the role of each component. It is also important to view any coral study through the lens of immunity, as the existence of these symbionts ultimately occurs through the allowance of the coral host immune system. These works examine stress responses through this lens at three levels: 1) the intracellular symbiont; 2) the coral animal; and 3) the coral reef population. I use proteogenomic and biochemical techniques to assess the molecular processes at play during temperature and disease stresses. I show that responses to temperature overlap with, but are not the same as, disease responses, providing support for the specificity that can be achieved by the innate invertebrate immune system. These works provide the first cell-surface proteome for a Symbiodiniaceae species and the first analysis of a coral immune response to consecutive bleaching seasons. Finally, they further the use of proteomics in the coral field, as the use of these techniques are still in its infancy. As such, they provide a framework for proteomic analysis within a non-model system

Table of Contents

Chapter 1

Introduction

Coral reefs are suffering global declines due to elevated sea surface temperatures and disease outbreaks. For example, the Great Barrier Reef lost 30% of coral cover during the record breaking 2016 heatwave (Hughes et al. 2018), while >90% elkhorn (*Acropora palmata*) and staghorn (*A. cervicornis*) coral (Miller, Bourque & Bohnsack 2002) have been lost in Florida due to white pox (Patterson et al. 2002) and (in part) white band (Gignoux-Wolfsohn, Marks and Vollmer 2012) diseases, respectively. In particular, the global decline of coral reefs due to elevated sea surface temperatures will likely be accelerated as bleaching events are predicted to become annual phenomena (van Hooidonk, Maynard & Plains 2013).

Both disease and temperature can work synergistically to increase pathogenicity of a disease, or to facilitate infection by opportunistic pathogens. This was demonstrated by the acceleration of black band disease transmission in staghorn coral during summer months (Boyett et al. 2007), in addition to a 60% coral cover loss in the US Virgin Islands after a disease outbreak that followed a bleaching event (Miller et al. 2009). Understanding their impacts and capacity to shape future reefs is of vital, and understanding the underlying mechanisms driving these declines is important for accurate predictions of coral persistence.

Corals are an amalgam of the coral animal, an intracellular dinoflagellate symbiont (family Symbiodiniaceae), and a consortium of other symbiotic microbes that exist in the coral surface mucus layer. These are collectively referred to as the coral holobiont. As such, any coral study should be viewed through the lens of immunity, as the existence of these symbionts ultimately occurs through the allowance of the coral host immune system. Further, the coral immune system is responsive to different stressors like disease and temperature, and has even

been implicated as a general homeostasis mechanism (Palmer 2018). Indeed, soft coral immunocytes are equally responsive to both heat and disease (Mydlarz et al. 2008). Immunity is thus the common denominator between both stresses.

During stress events the coral animal must regulate its own responses while also contending with those from their microbial symbionts. Such responses have the potential to activate the host immune systems against the symbionts. This is especially true during coral bleaching, where reactive oxygen species putatively derived from dinoflagellate photosystem breakdown are believed to elicit an immune response that results in dinoflagellate loss (Nielsen, Petrou & Gates 2018). Therefore, the simultaneous regulation of immune responses once the immune system is activated is necessary to prevent the removal of the dinoflagellate and other symbionts. On a broad scale, misregulation of immune responses may subsequently be contributing to global coral declines.

It is important to address the different components of the holobiont to understand more fully the mechanisms at play during stress events. Therefore, the overarching questions addressed by my thesis explores stress responses in the context of immunity at three levels: at the dinoflagellate symbiont level, at the individual coral level, and at the population level. Here, I explore the cell surface response of the dinoflagellate symbiont to experimentally elevated temperature (chapter 2), the coral immune response to a natural disease (chapter 3), and the immune response of two coral populations to repeated bleaching stress (chapter 4). I use proteomic and biochemical techniques to address these questions, shedding light on the consequences of stress at the cellular level and the implications they may have for future reefs.

REFERENCES

Boyett HV, Bourne DG, Willis BL (2007) Elevated temperature and light enhance progression and spread of black band disease on staghorn corals of the Great Barrier Reef. Mar Biol 151: 1711. https://doi.org/10.1007/s00227-006-0603-y

Gignoux-Wolfsohn SA, Marks CJ, Vollmer SV (2012) White Band Disease transmission in the threatened coral, *Acropora cervicornis.* Sci Rep 2:804

Miller M, Bourque A, Bohnsack J (2002) An analysis of the loss of acroporid corals at Looe Key, Florida, USA: 1983–2000. Coral Reefs 21: 179-182

Miller J, Muller E, Rogers C, Waara R, Atkinson A, Whelan KRT, Patterson M, Witcher B (2009) Coral disease following massive bleaching in 2005 causes 60% decline in coral cover on reefs in the US Virgin Islands. Coral Reefs 28: 925-937

Mydlarz LD, Holthouse SF, Peters EC, Harvell CD (2008) Cellular Responses in Sea Fan Corals: Granular Amoebocytes React to Pathogen and Climate Stressors. PLoS One 3: e1811

Nielsen DA, Petrou K, Gates RD (2018) Coral bleaching from a single cell perspective. ISME J 12:1558 - 1567

Palmer CV (2018) Immunity and the coral crisis. Commun Biol 1:91 doi: 10.1038/s42003-018-0097-4

Patterson KL, Porter JW, Ritchie KB, Polson SW, Mueller E, Peters EC, Santavy DL, Smith GW (2002) The etiology of white pox, a lethal disease of the Caribbean elkhorn coral, *Acropora palmate.* PNAS 99: 8725-8730

van Hooidonk R, Maynard JA, Planes S (2013) Temporary refugia for coral reefs in a warming world. Nat Clim Chang 3:508–511

Chapter 2

The cell-surface protein composition of a coral symbiont, *Breviolum psygmophilum*, reveals a mechanism for host-specificity and displays dynamic regulation during temperature stress

Contessa A. Ricci, Abu Hena Mostafa Kamal, Jayanta Kishor Chakrabarty, Bren E. Ledbetter, Saiful M. Chowdhury, Laura D. Mydlarz

Submitted to: Marine Biology, 2019

ABSTRACT

The symbiosis between corals and dinoflagellates in the family Symbiodiniaceae is threatened by warming trends that induce coral bleaching, or symbiosis breakdown. Current models of symbiosis breakdown evoke an immune response to symbiont-derived reactive oxygen species that ultimately results in the loss of the symbiont. However, the nature of the symbiosis implies an important role for the symbiont surface due to constant contact between the coral cell and the intracellular symbiont. The response of symbiont cell surface proteins to experimental temperature stress was therefore investigated using a cell surface biotin probe. Cell-surface protein composition was found to be dynamically regulated in response to heat stress, particularly after 24 hours of exposure to heat treatment. This pattern was primarily driven by an increased abundance in heat shock proteins, demonstrating that stress experienced by the symbiont can manifest at the cell surface. Elements known to activate host immunity were also increased in response to temperature stress, further demonstrating an avenue by which the symbiont can elicit a host immune response independent of reactive oxygen species. This work documents the first cell surface protein composition of a Symbiodiniaceae species and highlights host-symbiont interaction mechanisms that may be important during symbiosis breakdown.

INTRODUCTION

Coral reefs are important tropical ecosystems that are both economically (Spalding et al. 2017) and culturally (Cvitanovic et al. 2013) valuable. Their persistence in nutrient-poor tropical waters (Hoegh-Guldberg 1999) is made possible by an intracellular symbiosis formed between the coral animal and dinoflagellates in the family Symbiodiniaceae (formerly genus *Symbiodinium*) (LaJeunesse et al. 2018). These symbionts transfer metabolites (Sogin et al., 2017) and photosynthetic products (Hoegh-Guldberg et al. 2007) that supplement a coral's energy requirements for vital life processes such as growth (Little, van Oppen & Willis 2004), calcification (Colombo-Pallotta, Rodriguez-Roman & Iglesias-Prieto 2010), and reproduction (Edmunds & Spencer Davies, 1986). Warming trends over the past several decades have threatened this symbiosis in many ways. The most well-known threat is coral bleaching, which results from the loss of the symbiont itself (Weis 2008) or from bleaching of the symbiont's photopigments (Hoegh-Guldberg 1999). It is understood as a breakdown in symbiosis (Baker 2003), particularly when bleaching results from the loss of the symbiont cell.

Bleaching can occur through several processes such as: exocytosis of the symbiont cell, apoptosis or necrosis of the host cell containing the symbiont, pinching off the portion of the host cell occupied by symbiont, or detachment of the entire host cell (Gates, Baghdasarian & Muscatine 1992). The prevailing model in the coral field concerning the mechanism of active symbiont removal is as follows: the symbiont's photomachinery is damaged via temperature, which in turn causes the symbiont cell to release harmful reactive oxygen species that elicit a host immune response and ultimately leads to symbiont loss (Nielsen, Petrou & Gates 2018). However, the role of symbiont cell surface proteins and how they change in response to stimuli is worth consideration, as cell-cell contact persists throughout the symbiosis.

Cell surface studies are gaining in importance and it is becoming clear that the extracellular surface of all organisms is actively maintained. In plants, for example, the cell wall is constantly remodeled to accommodate osmotic pressure (Deniaud-Bouët et al. 2017). Additionally, new and emerging roles for processes like extracellular redox in maintaining the intracellular redox state (Jones et al. 2015) are coming to light. In the coral-Symbiodiniaceae symbiosis, cell surface elements such as lectins and glycans are crucial for successful symbiont infection of host tissues (Logan et al. 2010; Davy, Allemand & Weis 2012; Jimbo et al. 2010; Koike et al. 2004). Despite this, the symbiont cell-surface protein composition remains unknown. Further, it is also unknown if this composition is dynamic in nature, and if so, what role that may play during thermally-induced symbiosis breakdown.

To investigate this, the present study sought to determine the effect of elevated temperature on protein composition at the symbiont cell surface *in vitro*. Proteins were isolated from the symbiont cell surface using a membrane-impermeable biotin probe (Li et al. 2013; Pelz et al. 2018) on intact symbiont cells with three hypotheses in mind: 1) that the cell-surface protein abundance will change under elevated temperature; 2) that the symbiont cell surface will exhibit stress-mitigating mechanisms under elevated temperature; and 3) that changes occurring at the symbiont cell surface have the potential to elicit immune responses from a host. We found evidence to support all three of these hypotheses and document the first cell surface protein composition of a Symbiodiniaceae species. This work highlights host-symbiont interaction mechanisms that may be important during symbiosis breakdown.

METHODS

Study design:

Breviolum psygmophilum (formerly *Symbiodnium psygmophilum*, clade B (LaJeunesse et al. 2018); isolated from *Oculina diffusa,* Western Atlantic, Bermuda) was obtained from T. Lajeunesse (Pennsylvania State University) and grown in the Mydlarz lab. Three replicate cultures for the control treatment and three replicate cultures for the heat treatment were grown up to a target density of 500,000 cells/ml. Cultures were grown at 26 °C under a 12-hour light/dark cycle in ASP-8A media (Chang, Prezelin, & Trench 1983; McGinty, Pieczonka, & Mydlarz 2012). Once cultures reached target density, each replicate culture was separated into three 5 ml subsample volumes (referred to as replicate subsamples henceforth) that were collected and processed at 0-hour, 12-hour, and 24-hour time points after exposure to treatment. 0-hour subsamples were collected and processed immediately and were not exposed to either treatment condition.

Replicate subsamples were placed in individual water baths (e.g., 12-hour and 24-hour replicate subsamples for replicate 1 were in an individual water bath while 12-hour and 24-hour replicate subsamples for replicate 2 were placed in a separate water bath)(supplementary figure S1). Water baths were fitted with heaters set to target temperatures (26 °C ± 1 °C for control treatment and 32 °C ± 1 °C for heat treatment to simulate bleaching-inducing conditions). Air pumps were used to circulate water for an even temperature distribution. All water baths were initially set to control treatment temperatures. Once cultures were placed in their respective water baths, heat treatment water baths were subjected to a two-hour temperature ramp. Control treatment water baths remained at a constant temperature during this time. Time of exposure began once temperature ramp was completed.

2.2 Experimental sample processing

At time of collection, replicate subsamples were removed from treatment and pelleted at 3500 rpm in a benchtop centrifuge (959 X g) for 10 minutes. At this speed, it was microscopically confirmed that Symbiodiniaceae cells do not lyse. Intact cells were washed thoroughly using sterile PBS at room temperature.

Replicate subsamples were then incubated for 30 minutes at room temperature with a membrane-impermeable, cleavable biotin probe (Sulfo-NHS-SS-Biotin, G-Biosciences)(supplementary figure S2). This probe is used commonly in cell-surface studies (e.g., Elschenbroich et al. 2010; Li et al. 2013; Pelz et al 2018) due to its hydrophobic nature. In this system, the biotin probe is conjugated to a sulfonated NHS ester by a cleavable disulfide linker (Elschenbroich et al. 2010). The sulfo-group transfers hydrophobicity to the probe, and the cleavable property negates the need to chemically unbind the biotin motif from avidin when rescuing isolated proteins (Elschenbroich et al. 2010). This was ideal for a cell-surface study in Symbiodiniaceae because cell walls are negatively charged (Shomer et al. 2003) and, as such, the negatively charged biotin probe used would not be able to cross it. The probe will therefore primarily detect proteins on the external face of the symbiont cell wall.

To quench the biotinylation reaction after incubation with the biotin probe, 25mM tris buffer (Trizol, Sigma-Aldrich) was added. After five minutes at room temperature, time point subsamples were spun down at 13,000 rpm in a benchtop centrifuge (15,330 X g) for five minutes, washed thoroughly with sterile PBS, and resuspended in sterile PBS after the final wash (Howes et al. 2010; Jo et al. 2010; Suzuki et al., 2010). *B. psygmophilum* cells were then lysed via bead beating with glass beads for one minute.

Isolation of biotin-labeled cell surface proteins was conducted by avidin affinity purification using spin columns and monomeric avidin (G-Biosciences). Following established

protocols (Lee et al. 2009; Shimus, Levy & Herman 1985), replicate subsamples were incubated in spin columns with avidin for 30 minutes at room temperature. Avidin-bound proteins were freed using 50 mM DTT to cleave the probe's disulfide bond via reduction. Freed proteins were rescued via spinning out into a collection tube. The resulting protein isolates were considered cell-surface protein enriched.

Protein isolates were then precipitated using a modified chloroform and methanol protocol (Ferro et al. 2000) wherein the reagents were added to the protein samples in a 3:4:1 v/v/v ratio (protein/methanol/chloroform) and centrifuged at 13,000 rpm in a benchtop centrifuge (15,330 X g) at 4 °C. DTT was removed by resuspending the precipitated protein pellet in 10% SDS and undergoing a second round of precipitation. Once DTT was removed, pellets were resuspended in 1% SDS and protein quantification of replicate subsamples was performed using a BCA assay (G-Biosciences) in a microplate spectrophotometer (BioTek).

2.3 Nanospray-LC-MS/MS

4 ng of protein per replicate subsample was tryptically digested in solution following established protocols (Chakrabarty et al. 2016). In summary, protein isolates were incubated with 10mM DTT at 56 °C for 45 minutes under continuous agitation. Protein isolates were then incubated with 10mM iodoacetamide in the dark at room temperature for 30 minutes. 50mM ammonium bicarbonate was then added followed by trypsin in a 1:50 w/w ratio (trypsin/protein) and incubated overnight at 37 °C under continuous agitation. After tryptic digestion, 0.1% formic acid was added to neutralize the pH and protein isolates were then dehydrated in a speedvac (Vacufuge plus, Eppendorf). Once dehydrated, protein isolates were reconstituted in 0.1% formic and introduced to a Velos Pro Dual-Pressure Linear Ion Trap Mass Spectrometer

(TermoFisher Scientifc). Nanospray-LC-MS/MS was carried out using a data dependent protocol. Protein fragmentation was achieved by collision induced dissociation (CID).

Isolated protein sequences were identified from mass spectra using Proteome Discoverer software (ver. 2.0, TermoFisher Scientifc). Using the Sequest HT algorithm within the software, spectra were matched against a translated *Breviolum psygmophilum* transcriptome publicly available from Reef Genomics databases (Liew, Aranda & Voolstra 2016; Parkinson et al. 2016). Sequest HT criteria were as follows: the proteolytic enzyme was indicated as trypsin; two missed cleavages were allowed; precursor mass range of 350–5000Da; fragment mass tolerance of ± 2.5 and 0.6Da; peptide charges excluded +1 (Kamal et al. 2018).

2.4 Dataset Building

A decoy search strategy was employed in Proteome Discoverer software using a 5% False Discovery Rate (FDR)(Wilhelm et al. 2014). *Breviolum psygmophilum* proteins in replicate subsamples were considered identified with high confidence at ≤ 5% FDR if they met either of the following criteria: A) ≥ 2 peptides were detected in ≥ 2 replicates; or B) ≥ 1 peptide was detected in all three replicates (Kamal et al. 2018). Using these criteria, a dataset of 147 proteins was compiled (supplementary table S1). Proteome Discoverer utilizes the label-free method of spectral counting to quantify protein expression (peptide spectral matches; i.e., PSMs). PSMs of confidently identified proteins were normalized as % total PSMs per replicate subsample (Kamal et al. 2018).

To annotate the 147 proteins identified within the *B. psygmophilum* transcriptome, their sequences were BLASTed against the Uniprot KB Swiss-Prot database. An e value ≥ e^{-5} was considered a confident annotation (Mayfield et al. 2018). If a *B. psygmophilum* sequence could

not meet the criteria for confident annotation, it was BLASTed against the entire Uniprot KB database (i.e., Swiss-Prot and TrEMBL databases).

Once annotated, GO terms (Gene Ontology) and literature searches were utilized to categorize the proteins into functional groups based on their roles when expressed at the cell surface or secreted into the extracellular space. In instances where GO terms agreed with the known extracellular role, the GO term was used to group proteins of the same function. In all other instances, proteins were grouped according to known functions documented in the literature (supplementary table S2). Literature searches were conducted by providing the search term "extracellular", "secreted", or "cell surface" before the protein name, and only manuscripts found with these searches were used to determine if proteins possessed a cell surface or extracellular presence. Additionally, if these searches yielded proteins known to interact with a host immune system when present at the cell surface or in the extracellular space, then it was classified as either immune activating, regulating, or suppressing (e.g., cell surface heat shock protein 70 promotes phagocytosis and is therefore classified under immune activation). The regulatory category encompassed proteins with known regulatory roles or whose extracellular effects on a host immune system were conflicting.

These methods found 67 of the 147 proteins identified that have a documented extracellular function in the literature and 12 proteins with an extracellular presence but an unknown function. Statistical analyses were carried out on these proteins (79 in total) to determine how treatment and length of treatment affected the composition of proteins and protein function at the cell surface. 47 proteins were known chloroplast constituents and were therefore considered contamination. Chloroplast contamination is not uncommon in cell wall/cell surface studies in dinoflagellates (Li et al. 2012; Wang et al. 2004a). Chloroplast contamination

is likely due to the extreme peripheral position of the large dinoflagellate chloroplasts (Lee et al. 2014). Chloroplast constituents did not change with heat (supplementary figure S3) and were not considered further.

2.5 Validation of NodG homolog and Nod homolog searches among Symbiodiniaceae

A nod factor G (nodG) homolog was identified (comp8899_c0_seq1.p1) in *Breviolum psygmophilum* and classified under signal transduction (table 1). Because of its putative roles in symbiosis, special attention was paid to the validation of its presence within the *B. psygmophilum* transcriptome. The presence of nod factors in other Symbiodiniaceae was also investigated for this reason. A Pfam protein domain search was compared between the *B. psygmophilum* nodG and the reviewed uniprot nodG sequence it was matched to via BLAST (nodG, uniprot ID P72332 from from *Rhizobium sp.* strain N33). Additionally, an EMBL-EBI pairwise sequence alignment using the EMBOSS Water algorithm was conducted with the following criteria: EBLOSUM62 was used at the matrix, gap penalty was set to 10, and extend penalty was set to 0.5 (Madeira et al. 2019).

Investigations into nod factor presence in other Symbiodiniaceae were carried out on six species whose genomes or transcriptomes are publically available on Reef Genomics databases: *Breviolum aenigmaticum*, *B. minutum*, *B. pseudominutum*, *B. psygmophilum*, *Cladocopium* (species unknown), and *Fugacium kawagutii*. Symbiodiniaceae sequences were BLASTed against a databased composed of the 148 nod factor sequences available through the Uniprot KB database. An e value $\geq e^{-5}$ cutoff was imposed. The top ten strongest BLAST hits plus the sequence of the nodG homolog identified in this study were then phylogenetically compared

using the Clustal Omega algorithm and bacterial nodI as an outgroup (unprot ID Q39GT7, *Burkholderia lata*)(Madeira et al. 2019).

2.6 Statistical analysis

All statistical analyses were conducted using R statistical software (R Core Team, 2015). Identified proteins were divided into groups based on protein function (i.e., functional groups). Bray-Curtis distances were utilized by similarity percentages analysis (i.e., SIMPER analysis) to calculate the strongest drivers of differences observed between control and heat treated samples (Clarke 1993; Warton et al. 2012). From SIMPER analyses, the most influential functional groups and/or individual proteins within a functional group were determined. SIMPER was carried out using the 'simper' function in the R package 'vegan' (Oksanen et al. 2018). PCA was conducted on the cumulative protein abundance for functional groups of interest using the 'ggbiplot' function in the R package 'ggbiplot' (Vu 2011).

To address the possible correlation in protein expression within resampled experimental units, repeated measures MANOVA was conducted using the 'RM' function in the R package 'MANOVA.RM' (Friedrich, Konietschke & Pauly 2018). Non-parametric t-tests were then conducted on the cumulative protein abundance for influential functional groups (e.g., cumulative abundance of proteins with immune modulatory functions in control vs. heat treated samples). Within functional groups, non-parametric t-tests were also carried out on the abundance of individual proteins that were determined to be influential by SIMPER (e.g., abundance of the protein V-type H^+-ATPase in control vs. heat treated samples).

To quantify the biological significance of the differences observed in protein abundance observed, effect size was calculated using Cohen's *d* estimation (Cohen 1992a; Cohen1992b;

Rice & Harris 2005). Effect size is defined as the discrepancy between the null hypothesis and the alternate hypothesis (Cohen 1992a). The small sample size (n = 3 per treatment) in combination with the variability observed between replicates can potentially underinflate statistical significance at $\alpha = 0.05$. This can therefore obscure findings of biological importance. Effect size is thus reported in addition to p-values to provide more transparent and accurate statistical interpretation (Greenland et al. 2016; Wasserstein & Lazar 2016). Cohen's *d* was calculated using the 'cohen.d' function in the R package 'EffSize' (Torchiano 2018). A small effect size is a Cohen's *d* ~0.2, a medium effect size is a Cohen's *d* ~0.5, and a large effect size is a Cohen's *d* ~0.8 (values noticeably lower than 0.2 are considered negligible while values noticeably greater than 0.8 are considered very large effect sizes)(Rice & Harris 2005; Torchiano 2018).

RESULTS

Constitutive cell-surface protein composition of Breviolum psygmophilum

Control samples and heat samples at 0 hours of exposure to treatments are pooled and considered the constitutive state of the *Breviolum psygmophilum* cell surface. A total of 147 proteins were identified at ≤ 5% FDR (supplementary table S1). 79 of identified proteins are known to be either secreted or actively released into the extracellular space, or expressed at the cell surface in various prokaryotic and eukaryotic species (supplementary table S2). These 79 proteins were used in statistical analyses for this study. 12 proteins had either no literature documentation of cell surface presence or the literature concerning the protein was conflicting. These proteins were also considered contamination. Three proteins could not be identified by BLAST.

The 79 proteins known to occur at the cell surface or in the extracellular space encompassed nine functional groups: protein folding, cell structure, adhesion, CO_2 uptake, extracellular ATP synthase, extracellular redox, signal transduction, ion homeostasis, and an unknown category representing proteins whose function is unknown when expressed in the extracellular space (they will not be addressed further as a result; table 1). Adhesion proteins represent the most abundant functional group at the cell surface of *B. psygmophilum*, while proteins representing the ion homeostasis functional group were least abundant (figure 1).

Nodulation factors present in Breviolum psygmophilum *and other Symbiodiniaceae species*

The *B. psygmophilum* nodG identified is, indeed, a putative nodulation factor. Pairwise sequence alignment between *B. psygmophilum* nodG homolog and *Rhizobium sp.* strain N33 nodG (uniprot ID P72332) achieved a high sequence alignment: 48.4% identity match, 66.5% similarity, and 3.6% gaps (figure 2A). The overall alignment score was 547. Pfam searches between the *Breviolum psygmophilum* nodG homolog and the *Rhizobium sp.* strain N33 nodG also displayed identical protein domain structure (figure 2B).

Potential nodulation factors are ubiquitous in Symbiodiniaceae, with a total of 6,557 matches identified across the six Symbiodiniaceae species investigated (supplementary file 1). All six species were represented in the top ten strongest hits found via BLAST. Nod sequences investigated group by species (figure 2C).

Response of Breviolum psygmophilum *cell-surface proteins to heat*

Proteins at the cell surface were responsive to temperature stress, particularly when time is taken into account (table 2). One protein was identified as uniquely present in the control

samples (comp36516_c0_seq1.p1; ATP synthase subunit) and one protein was identified as uniquely present in the heat-treated samples (comp35699_c0_seq1.p1; calreticulin). The cumulative abundance of proteins found in both heat-treated and control samples (i.e., shared proteins) do not differ between treatments until after 24 hours of exposure to heat treatment ($p = 0.400$, Cohen's $d = -0.440$, figure 3A). Differences are primarily seen in the abundance between the proteins uniquely expressed in either the control or heat-treated samples: after 24 hours of exposure to heat treatment, abundance of the heat-treatment-unique protein was greater than that of the control treatment ($p = 0.176$, Cohen's $d = -0.894$, figure 3B). The control-treatment-unique protein was not present after 24 hours.

Total abundance of proteins within functional groups showed differences through time and by treatment (figure 4). The functional groups driving the differences observed between control and heat-treated samples were, in order of most influential: protein folding, cell structure, adhesion, CO_2 uptake, and extracellular ATP synthase (table 2). When the most influential functional groups were used to characterize the protein abundance data, only those samples that belong to the 24-hour heat treatment were distinct (figure 5). As such, only those differences at the 24-hour time point were considered in further analyses.

Protein responses in the most influential functional groups to heat

The protein folding functional group was represented by 14 unique proteins that represented five protein types (table 1). The top two most influential proteins in the protein folding group were heat shock protein (HSP) 70 and HSP 90 (table 3, SIMPER cumsum ~80%). After 24 hours of exposure to heat treatment, both proteins are in greater abundance when compared to control samples ($p = 0.400$ and Cohen's $d = -1.174$, $p = 0.100$ and Cohen's $d = -2.870$; respectively; table 3, figure 6A).

Cell structure was represented by nine unique proteins that represented four protein types (table 1). Tubulin and a major outer membrane lipoprotein were the two most influential proteins (table 3, SIMPER cumsum ~83%). After 24 hours of exposure to heat treatment, tubulin abundance decreases ($p = 0.400$ and Cohen's $d = 0.981$, table 3, figure 6B) while the abundance of the major outer membrane lipoprotein increases ($p = 0.100$ and Cohen's $d = -1.243$, table 3, figure 6B).

Adhesive proteins were represented by 14 unique proteins that encompassed six protein types (table 1) and were most influenced by enolase and triosephosphate isomerase (TPI)(table 3, SIMPER cumsum ~55%). After 24 hours of exposure to heat treatment, neither protein differed in abundance compared to control treatments ($p = 0.633$, Cohen's $d = -0.441$ and $p = 0.960$, Cohen's $d = 0.043$; respectively; table 3, figure 6C).

CO_2 uptake was represented by two unique proteins that were both identified as carbonic anhydrase by BLAST (table 1). Extracellular ATP synthase was similarly represented by four unique proteins that were all identified as ATP synthase subunits by BLAST (table 1). After 24 hours of exposure to heat treatment, carbonic anhydrase did not differ from control samples in abundance ($p = 0.931$, Cohen's $d = 0.078$, table 3, figure 6D), however, variation between samples was much higher for heat-treated samples vs. control samples. ATP synthase decreased in abundance in heat-treated samples compared to control samples ($p = 0.378$, Cohen's $d = 0.814$, table 3, figure 6E).

Responses of extracellular redox, signal transduction, and ion homeostasis proteins to heat

Extracellular redox was represented by 11 unique proteins that represented seven protein types (table 1). Fumarate reductase and cytochrome c were the most influential proteins within

the extracellular redox functional group (table 3, SIMPER cumsum ~64%). Fumarate reductase was found in greater abundance in heat-treated samples compared to control samples, while cytochrome c does not differ in abundance but was greater in between-sample variation ($p = 0.700$, Cohen's $d = -0.954$ and $p = 1.000$, Cohen's $d = 0.214$; respectively; table 3, figure 6F).

The signal transduction group was represented by nine unique proteins that represented eight protein types (table 1). The 14-3-3-like protein and calreticulin were the most influential proteins within this functional group (table 3, SIMPER cumsum ~40%). 14-3-3 increased in abundance after 24 hours of exposure to heat treatment while calreticulin was only found in heat treated samples ($p = 0.200$, Cohen's $d = -1.459$ and $p = 0.197$, Cohen's $d = -1.564$; respectively; table 3, figure 6G). Ion homeostasis was represented by a K^+-stimulated sodium pump and a V-type proton ATPase (table 1). Only the V-type proton ATPase was found in greater abundance after 24 hours of exposure to heat treatment ($p = 0.391$, Cohen's $d = -0.865$, table 3, figure 6H).

Immune modulatory proteins present at the Breviolum psygmophilum *cell surface and their response to heat*

Proteins known to modulate a host immune system via immune activation, suppression, or regulation were identified in cell-surface protein isolates (supplementary table S3). Proteins were assigned to each category based on information available within the literature (supplementary table S3). The regulatory category encompassed proteins with known regulatory roles or whose extracellular effects on a host immune system were conflicting.

Immune modulatory proteins were affected by both treatment and time (RM MANOVA, table 4). Differences only at the 24-hour time point are addressed: cumulative abundance of all immune-activating proteins increased in response to heat ($p = 0.1$, Cohen's $d = -2.131$, table 4,

figure 7) while the cumulative abundance of all immune-suppressing proteins decreased (p = 0.505, Cohen's *d* = 0.816, table 4, figure 7); immune regulatory proteins were not responsive to heat (p = 0.4, Cohen's *d* = 0.585, table 4, figure 7).

DISCUSSION

The nature of the coral-Symbiodiniaceae symbiosis implies an important role for the symbiont surface due to constant contact between the coral cell and the intracellular symbiont. As such, proteomic investigation at this locale is important in understanding potential mechanisms in partner dynamics. In this study, the *Breviolum psygmophilum* transcriptome developed by Parkinson et al. (2016) was used as a database to inform protein identification from cultured *B. psygmophilum*, and only proteins encoded within the *B. psygmophilum* genome are identified as a result.

The biotin probe utilized within this study ensures a cell-surface enriched protein fraction was analyzed due to the probe's hydrophobic nature (Elschenbroich et al. 2010). Identified proteins were further validated for cell surface presence or absence and classified into functional groups based on rigorous, non-biased literature searches. Our investigation reveals elements of host-specific interaction mechanisms and shows cell-surface proteins are responsive to heat stress. We also show that stress-mitigating mechanisms have the potential to influence a host immune system.

Despite the probe's hydrophobic properties, a large number of chloroplast constituents were isolated. Chloroplast contamination is not uncommon in cell wall/cell surface studies in dinoflagellates (Li et al. 2012; Wang et al. 2004a). While this may be the result of the probe entering the cell, this is unlikely as very little other specifically intracellular proteins were found

in this study. This can also potentially result from cell lysis during the experiment, as released proteins can adhere to the surface of intact cells. However, the thorough washings conducted during sample processing minimize this as a possibility. The chloroplast contamination therefore likely results from the extreme peripheral position of the large dinoflagellate chloroplasts (Lee et al. 2014) and subsequent co-isolation with proteins specifically bound by the cell surface probe. Because chloroplast constituents did not change with heat, they were considered random contamination and were not addressed further.

Constitutive cell-surface proteins of Breviolum psygmophilum *carry out essential functions*

The extracellular matrix and cell membrane carry out important functions. They are often viewed as a fist line of defense against assaults on cellular integrity (Deniaud-Bouët et al. 2017) and are also responsible for waste exchange and nutrient uptake (Hahn and Mendgen 2001). In addition, they are important for modulating osmotic pressure (Deniaud-Bouët et al. 2017) and sensing cues from the extracellular environment that lead to cell growth or differentiation (Deniaud-Bouët et al. 2017). Recent advances in cell-surface research are highlighting this dynamic nature across the tree of life (Shi et al. 2016; Lemmon et al. 2016). It is now clear that cells actively maintain the cell surface and the extracellular space directly adjacent to the cell surface to preserve homeostasis.

At the constitutive state, the adhesive functional group had the highest abundance at the *Breviolum psygmophilum* cell surface, followed closely by the cell structure and CO_2 uptake proteins. Adhesive proteins were primarily represented by glycolytic proteins which, when expressed at the cell surface, bind to plasminogen (Gancedo, Flores & Gancedo 2016) and laminin (Amblee & Jeffery 2015). CO_2 uptake was represented by two proteins identified as

carbonic anhydrase (CA). In the unicellular green alga *Dunaliella tertiolecta*, cell-surface CA assists in the uptake of CO_2 from the surrounding water (Aizawa & Miyachi 1984). The same role is carried out by cell-surface CA in various phytoplankton (Mustaffa, Striebel & Wurl 2017), including Symbiodiniaceae (Yellowlees et al. 1993; Karim et al. 2011). The identification of these at the cell surface of *B. psygmophilum* corroborates a growing body of literature demonstrating the ubiquity of proteins with pleiotropic (Orjalo et al. 2009; Ebnet 2017) and moonlighting (Jeffery 2015; Gancedo, Flores & Gancedo 2016) properties. This is with particular regard to extracellular protein function (Wang & Jeffery 2016).

Other emerging roles for the cell surface are extracellular ATP synthesis (Federica & Antonio 2018) and extracellular redox processes (Banerjee 2012). Extracellular ATP synthase (i.e., eATP synthase) has only recently been accepted as a truly functional complex when expressed at the cell surface (Federica & Antonio 2018) and, as such, is poorly understood. They do, however, have ion regulating properties that are believed to result from the movement of hydrogen ions into and out of the cell during the synthesis and hydrolysis of ATP (Federica & Antonio 2018). There may be as of yet unknown functions at the cell surface of *B. psygmophilum* that rely on eATP synthase or eATP. Extracellular redox, on the other hand, is known to be important in maintaining the intracellular redox environment (Banerjee 2012). Interestingly, extracellular redox modulation has roles in inflammatory processes (Carta et al. 2009) and may therefore be an important aspect governing symbiosis dynamics between corals and *B. psygmophilum*.

Nod factors are ubiquitous across Symbiodiniaceae species

Nod factors are secreted molecules that are primarily characterized in the plant endosymbiotic bacteria, *Rhizobium*. In the plant-rhizobia model, flavonoids are secreted by the host plant to attract bacteria (Hassan & Mathesius 2012). The detection of these flavonoids by the bacteria in turn produce Nod factors that are subsequently secreted by the bacteria (Oldroyd & Downie 2004). Perception of the bacteria-Nod factor combination by the plant tissues then cause the iconic root hair deformation and nodulation characteristic of a successful establishment of symbiosis (Oldroyd & Downie 2004). These Nod factors are host-specific molecules (Oldroyd & Downie 2004; Hassan & Mathesius 2012), and incompatible Nod factors will prevent a symbiosis from forming (Oldroyd & Downie 2004).

The presence of the nodG homolog in *Breviolum psygmophilum* corroborates previous reports of Nod factors present in Symbiodiniaceae (e.g. Lin et al. 2015; Weston et al. 2012). The nodG homolog identified at the *B. psygmophilum* cell surface shows high homology to the reviewed *Rhizobium sp.* nodG and is therefore likely a true Nod factor. Further, potential Nod factor homologs were ubiquitous across the six Symbiodiniaceae species investigated in this study, and the subset of sequences that were phylogenetically investigated show Nod factors grouping by species.

This has important implications for symbiosis establishment between Symbiodiniaceae and coral, as it was previously believed that lectin and glycan interactions between Symbiodiniaceae and the coral host were responsible for partner specificity (Logan et al. 2010; Wood-Charlson et al. 2006). Recent evidence may begin to shift this paradigm, as manipulation of Symbiodiniaceae glycans do not appear to alter host infection rates (Parkinson et al. 2018). The presence of Nod factor-like proteins at the *B. psygmophilum* cell surface, in addition to their

presence within multiple species of Symbiodiniaceae, may demonstrate an important role in partner selection.

The cell-surface of Breviolum psygmophilum *is responsive to heat stress over time*

Heat affects the *Breviolum psygmophilum* cell surface primarily after 24 hours of exposure to heat treatment. As such, comparisons were made at the 24-hour time point. Protein folding was the most influential functional group driving the differences between control and heat-treated samples. This resulted from an increase in heat shock protein (HSP) 70 and HSP 90 at the *B. psygmophilum* cell surface. HSPs are commonly upregulated in response to stress (Wiersma et al. 2015) and function to protect existing proteins from denaturing (Hasanuzzaman et al. 2013; Wang et al. 2004b). Here, we show that cell-surface HSPs are a key response to heat stress in *B. psygmophilum*. HSP action may be facilitated by eATP synthase, as both HSP 70 and HSP 90 require ATP to bind target proteins and carry out chaperone functions (Hasanuzzaman et al. 2013; Wang et al. 2004b). It may be of biological importance that eATP synthase decreases in response to heat while HSP proteins increase. Uncoupling of the two may reflect dysfunction brought on by heat stress. Regardless, the observation of increased HSPs demonstrate that stress experienced by *B. psygmophilum* under elevated temperatures manifests at the cell surface and has implications for an intracellular symbiosis *in hospite*.

Tubulin also decreased after 24 hours of exposure to heat. Dynamic tubulin modulation is important for cell wall remodeling (Chan et al. 2010; Ochs et al. 2014), and decreases observed in response to heat are somewhat paradoxical within the context of HSP increases. This is likely because remodeling to accommodate responses such as protein translocation and insertion took place prior to 24 hours. Cell wall remodeling in *B. psygmophilum* may therefore occur during

early responses to stress. Conversely, the abundance of a major outer membrane lipoprotein increases in response to heat after 24 hours of exposure. In the dinoflagellate cell wall, these proteins are important for protein binding, lipid anchoring, and calcium binding (Wang et al. 2011). It may be that these lipoproteins have roles in the attachment of other proteins to the *B. psygmophilum* cell wall.

Increases in extracellular redox demonstrates an increased need by *B. psygmophilum* to maintain their intracellular redox environment, and may result from an increased energy demand that can potentially fatigue redox gradients across the mitochondrial membrane (Banerjee 2012). Related is the increase in the V-type H^+-ATPase, a protein responsible for the transport of protons into and out of the cell (Miles et al. 2017). Responses by both the extracellular redox and ion homeostasis functional groups demonstrate the importance of the cell surface in maintaining the intracellular environment. Importantly, H^+-ATPase was thought to only be expressed by Symbiodiniaceae when in a symbiotic state (Bertucci et al. 2010; Miles et al. 2017). However, this was supported by gene expression alone. Using proteogenomic methods, we show that this protein is indeed found in a non-symbiotic Symbiodiniaceae species and that it is responsive to heat stress.

Proteins known to stimulate host immune responses are present at the cell surface of Breviolum psygmophilum *and increase with heat*

Proteins known to modulate a host immune system were present at the *Breviolum psygmophilum* cell surface. Within the 15 proteins detected, three categories could be identified based on literature searches: immune activation (i.e., eliciting an immune response from a host upon detection); immune regulation (i.e., roles in immune activation and resolution); and

immune suppression (i.e., preventing or hindering a host immune response). The majority of these proteins (11/15) are known to activate a host immune system. Three proteins, ubiquitin (Majetschak 2011), ATP synthase (Chivasa et al. 2009), and peptidyl-prolyl cis-trans isomerase (Ünal and Steinert 2014), have roles in immune regulation. One protein, nicotinamide phosphoribosyl transferase, is known to suppress a host immune system upon extracellular detection (Audrito et al. 2015).

Although the effect of specific proteins on the coral immune system was not itself investigated, it is a worthwhile consideration when addressing cell-surface proteins. For example, cell-surface heat shock protein 70 can promote phagocytosis (Zhu et al. 2016), and inflammatory cytokine production through interaction with TLR2 and TLR4 (Asea et al. 2002). Further, the existence and persistence of an intracellular symbiont ultimately involves the immune system as it inherently implies that the host is not clearing a foreign body.

In Symbiodiniaceae, persistence within the host is generally attributed to host immune suppression. This is evidenced by phenomena such as some corals displaying decreased disease susceptibility when bleached, or in other words, when corals have a lower symbiont load (Merselis, Liman & Rodriguez-Lanetty 2018) and the upregulation of immune suppressing TGF-β in the coral host during the onset of symbiosis (Berthelier et al. 2017). It may therefore be important that immune-activating proteins increase while regulating proteins decrease and immune-suppressing proteins virtually disappear after 24 hours of exposure to heat stress. Should such a pattern persist when in a symbiotic state, it would support the hypothesis that thermally-induced bleaching results from a host immune response against Symbiodiniaceae. It also supports the hypothesis that the immune response results from symbiont dysfunction.

Breviolum psygmophilum *present an "eat me" signal after experiencing heat stress*

Calreticulin was present at the *Breviolum psygmophilum* cell surface after 24 hours of exposure to heat stress. Calreticulin typically provides chaperone-like functions in the endoplasmic reticulum (Wang et al. 2004b), however, it is known to accumulate at the cell surface during stress events (Park & Kim 2017). In apoptotic cells this accumulation can promote cell clearance by serving as an "eat me" signal to phagocytic cells (Park & Kim 2017). Because the symbiosome is established as an arrested phagosome (Mohamed et al. 2016), one possibility is that cell surface calreticulin "re-activates" the fusion of the symbiosome to the previously inhibited lysosome. Calreticulin could therefore serve as a signal for dysfunction to the coral host and induce symbiophagic processes.

CONCLUSIONS

The coral-Symbiodiniaceae symbiosis is responsible for the persistence of coral reefs in tropical waters. Rising global temperatures are a primary threat to this symbiosis. This work joins an emerging body of research highlighting the importance of cell-surface modulation. Here, we present the first formal investigation into the response of cell-surface proteins to elevated temperatures in a Symbiodiniaceae species. We have identified a Nod factor-like protein at the cell surface of a Symbiodiniaceae species, and show that this locale is dynamically modified in response to heat. These data demonstrate that stress experienced within the cell is manifested at the cell surface, and that these proteins have the potential to influence host responses during temperature stress. As coral bleaching (i.e., symbiosis breakdown) continues to decimate reefs, continuing investigation into responsible mechanisms is of vital importance for informing conservation and management practices.

Acknowledgements

The authors would like to acknowledge funding from awards IOS-1831860 and OCE-1712134 from the National Science Foundation to LDM. This material is based upon work supported by the LSAMP bridge to doctorate fellowship programs under grant no.1026806 to CAR. We also acknowledge funding from the UT system Proteomics Core Facility Network for a mass spectrometer

Compliance with ethical standards

Conflict of interest The authors declare they have no conflict of interest.

Ethical approval All applicable international, national, and/or institutional guidelines for the care and use of animals were followed.

REFERENCES

Amblee V, Jeffery CJ (2015) Physical Features of Intracellular Proteins that Moonlight on the Cell Surface. PLoS ONE 10(6): e0130575. http://doi:10.1371/journal.pone.0130575

Aizawa K, Miyachi S (1984) Carbonic anhydrase located on cell surface increases the affinity for inorganic carbon in photosynthesis of *Dunaliella tertiolecta*. FEBS J 173:41 – 44

Asea A, Rehli M, Kabingu E, Boch JA, Bare O, Auron PE, Stevenson MA, Calderwood SK (2002) Novel signal transduction pathway utilized by extracellular HSP70: role of toll-like receptor (TLR) 2 and TLR4. J Biol Chem 277: 15028 - 15034

Audrito V, Serra S, Brusa D, Mazzola F, Arruga F, Vaisitti T, Coscia M, Maffei R, Rossi D, Wang T, Inghirami G, Rizzi M, Gaidano G, Garcia JG, Wolberger C, Raffaelli N, Deaglio

S. (2015) Extracellular nicotinamide phosphoribosyltransferase (NAMPT) promotes M2 macrophage polarization in chronic lymphocytic leukemia. Blood 125: 111 - 123

Baker A (2003) Flexibility and Specificity in Coral-Algal Symbiosis: Diversity, Ecology, and Biogeography of Symbiodinium. Annu Rev Ecol Evol Syst 34:661 – 689

Banerjee R (2012) Redox outside the box: linking extracellular redox remodeling with intracellular redox metabolism. J Biol Chem 287:4397-4402

Berthelier J, Schnitzler CE, Wood-Charlson EM, Poole AZ, Weis VM, Detournay O (2017) Implication of the host TGFβ pathway in the onset of symbiosis between larvae of the coral *Fungia scutaria* and the dinoflagellate *Symbiodinium* sp. (clade C1f). Coral Reefs 36: 1263 - 1268

Bertucci A, Tambutté E, Tambutté S, Allemand D, and Zoccola D (2010) Symbiosis-dependent gene expression in coral–dinoflagellate association: cloning and characterization of a P-type H+-ATPase gene Proc Biol Sci 277: 87 – 95

Chakrabarty J, Naik A, Fessler M, Munske G, Chowdhury S (2016) Differential tandem mass spectrometry-based cross-linker: a new approach for high confidence in identifying protein cross-linking. Anal Chem 18: 10215 - 10222.

Chan J, Crowell E, Eder M, Calder G, Bunnewell S, Findlay K, Vernhettes S, Höfte H, Lloyd C (2010) The rotation of cellulose synthase trajectories is microtubule dependent and influences the texture of epidermal cell walls in Arabidopsis hypocotyls. J Cell Sci 123:3490-3495

Chang SS, Prezelin BB, Trench RK (1983) Mechanisms of photoadaptation in three strains of the symbiotic dinoflagellate Symbiodinium microadriaticum. Mar Biol 76:219 – 229

Chivasa S, Murphy AM, Hamilton JM, Lindsey K, Carr JP, Slabas AR (2009) Extracellular ATP is a regulator of pathogen defence in plants. Plant J 60: 436 - 448

Clarke KR (1993) Non-parametric multivariate analyses of changes in community structure. Austral Ecol 18:117–143.

Cohen J(a) (1992) Statistical power analysis. Curr Dir Psychol Sci 1:98-101

Cohen J(b) (1992) A power primer. Psychol Bull 112:155-159

Colombo-Pallotta MF, Rodriguez-Roman A, Iglesias-Prieto R (2010) Calcification in bleached and unbleached Montastraea faveolata: evaluating the role of oxygen and glycerol. Coral reefs 29:899–907

Cvitanovic C, Wilson SK, Fulton CJ, Almany GR, Anderson P, Babcock RC, Ban NC, Beeden RJ, Beger M, Cinner J, Dobbs K, Evans LS, Farnham A, Friedman KJ, Gale K, Gladstone W, Grafton Q, Graham NAJ, Gudge S, Harrison PL, Holmes TH, Johnstone N, Jones GP, Jordan A, Kendrick AJ, Klein CJ, Little LR, Malcolm HA, Morris D, Possingham HP, Prescott J, Pressey RL, Skilleter GA, Simpson C, Waples K, Wilson D, Williamson DH (2013) Critical research needs for managing coral reef marine protected areas: Perspectives of academics and managers. J Environ Manage 114:84 - 91

Davy SK, Allemand D, Weis VM (2012) Cell Biology of Cnidarian-Dinoflagellate Symbiosis. Microbiol Mol Biol Rev 76: 229–261

Deniaud-Bouët E, Hardouina K, Potina P, Kloarega B, Hervé C (2017) A review about brown algal cell walls and fucose-containing sulfated polysaccharides: Cell wall context, biomedical properties and key research challenges. Carbohydr Polym 175: 395–408

Ebnet K (2017) Junctional Adhesion Molecules (JAMs): Cell Adhesion Receptors With Pleiotropic Functions in Cell Physiology and Development. Physiol Rev 97:1529 - 1554

Edmunds PJ, Spencer Davies P (1986) An energy budget for Porites porites (Scleractinia). Mar Biol 92:339 – 347

Elschenbroich S, Kim Y, Medin JA, Kislinger T (2010) Isolation of cell surface proteins for mass spectrometry-based proteomics Expert Rev Proteomics 7:141–154

Federica T, Antonio G (2018) Systematic review of plasma-membrane ecto-ATP synthase: A new player in health and disease. Exp Mol Pathol 104:59 – 70

Ferro M, Seigneurin-Berny D, Rolland N, Chapel A, Salvi D, Garin J, Joyard J (2000) Organic solvent extraction as a versatile procedure to identify hydrophobic chloroplast membrane proteins. Electrophoresis 21: 3517 - 3526

Friedrich S, Konietschke F, Pauly M (2018) MANOVA.RM: Analysis of Multivariate Data and Repeated Measures Designs. R package version 0.3.2. http://github.com/smn74/MANOVA.RM

Gancedo C, Flores CL, Gancedo JM (2016) The Expanding Landscape of Moonlighting Proteins in Yeasts. Microbiol Mol Biol Rev 80:765 - 777

Gates RD, Baghdasarian G, Muscatine L (1992) Temperature Stress Causes Host Cell Detachment in Symbiotic Cnidarians: Implications for. Biol Bull 182:324 - 332

Greenland S, Stephen J. Senn SJ, Rothman KJ, Carlin JB, Poole C, Goodman SN, Altman DG (2016) Statistical tests, P values, confidence intervals, and power: a guide to misinterpretations. Eur J Epidemiol 31:337–350

Hahn M, Mendgen K (2001) Signal and nutrient exchange at biotrophic plant-fungus interfaces. Curr Opin Plant Biol 4:322-7

Hasanuzzaman M, Nahar K, Alam MM, Roychowdhury R, Fujita M (2013) Physiological, Biochemical, and Molecular Mechanisms of Heat Stress Tolerance in Plants. Int J Mol Sci 14:9643 – 9684

Hassan S, Mathesius U (2012) The role of flavonoids in root-rhizosphere signalling: opportunities and challenges for improving plant-microbe interactions. J Exp Bot 63:3429 - 3444

Hoegh-Guldberg (1999) Climate change, coral bleaching and the future of the worldís coral reefs. Mar Freshwater Res 50:839 – 866

Hoegh-Guldberg O, Mumby PJ, Hooten AJ, Steneck RS, Greenfield P, Gomez E, Harvell CD, Sale PF, Edwards AJ, Caldeira K, Knowlton N, Eakin CM, Iglesias-Prieto R, Muthiga N, Bradbury RH, Dubi A, Hatziolos ME (2007) Coral Reefs Under Rapid Climate Change and Ocean Acidification. Science 318: 1737 – 1742

Howes MT, Kirkham M, Riches J, Cortese K, Walser PJ, Simpson F, Hill MM, Jones A, Lundmark R, Lindsay MR, Hernandez-Deviez DJ, Hadzic G, McCluskey A, Bashir R, Liu L, Pilch P, McMahon H, Robinson PJ, Hancock JF, Mayor S, Parton RG (2010) Clathrin-independent carriers form a high capacity endocytic sorting system at the leading edge of migrating cells. J Cell Biol 190:675 – 691

Jeffery CJ (2015) Why study moonlighting proteins?. Front genet 6:211 doi:10.3389/fgene.2015.00211

Jimbo M, Yamashita H, Koike K, Sakai R, Kamiya H (2010) Effects of lectin in the scleractinian coral *Ctenactis echinata* on symbiotic zooxanthellae. Fish Sci 76:355 - 363

Jo, Eastman, Webb, Stoletov, Klemke, Gonias (2010) Cell Signaling by Urokinase-type Plasminogen Activator Receptor Induces Stem Cell–like Properties in Breast Cancer Cells. Cancer Res 70:8948 - 8958.

Jones IV AR, Meshulam T, Oliveira MF, Burritt N, Corkey BE (2015) Extracellular Redox Regulation of Intracellular Reactive Oxygen Generation, Mitochondrial Function and Lipid Turnover in Cultured Human Adipocytes PLoS ONE 11(10): e0164011. doi:10.1371/journal. pone.0164011

Kamal AHM, Chakrabarty JK, Udden SMN, Zaki MdH, Chowdhury SM (2018) Infammatory Proteomic Network Analysis of Statin-treated and Lipopolysaccharide-activated Macrophages. Sci Rep 8:164 doi: 10.1038/s41598-017-18533-1

Karim W, Kaswadji R, Prartono T, Gorettipanggabean LM (2011) Growth and extracellular carbonic anhydrase activity of zooxanthellae Symbiodinium sp. in response of zinc enrichment. Hayati Journal of Biosciences. 18:157 – 163

Koike K, Jimbo M, Sakai R, Kaeriyama M, Muramoto K, Ogata T, Maruyama T, Kamiya H (2004) Octocoral chemical signaling selects and controls dinoflagellate symbionts. Biol Bull 207:80 - 86

LaJeunesse TC, Parkinson JE, Gabrielson PW, Jeong HJ, Reimer JD, Voolstra CR, Santos SR (2018) Systematic Revision of Symbiodiniaceae Highlights the Antiquity and Diversity of Coral Endosymbionts. Curr Biol 28:2570 – 2580

Lee SK, Kim Y, Kim SS, Lee JH, Cho K, Lee SS, Lee ZW, Kwon KH, Kim YH, Suh-Kim H, Yoo JS, Park YM (2009) Differential expression of cell surface proteins in human bone marrow mesenchymal stem cells cultured with or without basic fibroblast growth factor containing medium. Proteomics 9:4389 - 4405.

Lee SY, Jeong HJ, Kang MS, Jang TY, Jang SH, Lim AS (2014) Morphological characterization of *Symbiodinium minutum* and *S. psygmophilum* belonging to clade B. Algae.; 29:299 – 310

Lemmon MA, Freed DM, Schlessinger J, Kiyatkin A (2016) The Dark Side of Cell Signaling: Positive Roles for Negative Regulators. Cell 164:1172 - 1184

Liew YJ, Aranda M, Voolstra CR (2016) Reefgenomics.Org - a repository for marine genomics data. Database 2016 baw152: https://doi.org/10.1093/database/baw152

Li C, Wang , DaZhi , Dong H, Xie Z, Hong H (2012) Proteomics of a toxic dinoflagellate *Alexandrium catenella* DH01: detection and identification of cell surface proteins using fluroescent labeling. *Sci Bull* 57:3320 - 3327

Li H, Huang Z, Ye S, Lu C, Cheng P, Chen S, Chen C (2013) Membrane Labeling of Coral Gastrodermal Cells by Biotinylation: The Proteomic Identification of Surface Proteins Involving Cnidaria-Dinoflagellate Endosymbiosis. PLoS ONE 9(1): e85119. doi: 10.1371/journal.pone.0085119

Lin S, Cheng S, Song B, Zhong X, Lin X, Li W, Li L, Zhang Y, Zhang H, Ji Z, Cai M, Zhuang Y, Shi X, Lin L, Wang L, Wang Z, Liu X, Yu S, Zeng P, Hao H7, Zou Q, Chen C, Li Y, Wang Y, Xu C, Meng S, Xu X, Wang J, Yang H, Campbell DA, Sturm NR, Dagenais-Bellefeuille S, Morse D (2015) The Symbiodinium kawagutii genome illuminates dinoflagellate gene expression and coral symbiosis. Science 350:691-694

Little AF, van Oppen MJ, Willis BL (2004) Flexibility in algal endosymbioses shapes growth in reef corals. Science 304:1492 – 1494

Logan D, LaFlamme A, Weis V, Davy S (2010) Flow-Cytometric Characterization Of The Cell-Surface Glycans Of Symbiotic Dinoflagellates (Symbiodinium Spp.). J Phycol 46: 525 – 533

Madeira F, Park YM, Lee J, Buso N, Gur T, Madhusoodanan N, Basutkar P, Tivey ARN, Potter SC, Finn RD, Lopez R (2019) The EMBL-EBI search and sequence analysis tools APIs in 2019. Nucleic Acids Res pii: gkz268. doi: 10.1093/nar/gkz268

Majetschak M (2011) Extracellular ubiquitin: immune modulator and endogenous opponent of damage-associated molecular pattern molecules. J Leukoc Biol 89: 205 - 219

Mayfield AB, Chen Y-J, Lu C-Y, Chen C-S (2018) The proteomic response of the reef coral *Pocillopora acuta* to experimentally elevated temperatures. PLoS ONE 13(1): e0192001. https://doi.org/10.1371/journal.pone.0192001

McGinty E, Pieczonka J, Mydlarz L (2012) Variations in Reactive Oxygen Release and Antioxidant Activity in Multiple Symbiodinium Types in Response to Elevated Temperature. Microb Ecol 64:1000 – 1007

Merselis DG, Lirman D, Rodriguez-Lanetty M (2018) Symbiotic immuno-suppression: is disease susceptibility the price of bleaching resistance? PeerJ 6: e4494. doi: 10.7717/peerj.4494

Miles M, Voolstra CR, Castro CB, Pires DO, Calderon EN, Sumida PYG (2017) Expression of a symbiosis-specific gene in Symbiodinium type A1 associated with coral, nudibranch and giant clam larvae. R Soc Open Sci 4: 170253 doi: 10.1098/rsos.170253

Mohamed AR, Cumbo V, Harii S, Shinzato C, Chan CX, Ragan MA, Bourne DG, Willis BL, Ball EE, Satoh N, Miller DJ (2016) The transcriptomic response of the coral Acropora digitifera to a competent Symbiodinium strain: the symbiosome as an arrested early phagosome. Mol Ecol 25:3127 – 3141

Mustaffa NIH, Striebel M, Wurl O (2017) Enrichment of extracellular carbonic anhydrase in the sea surface microlayer and its effect on air-sea CO2 exchange. Geophys Res Lett 44: 324 – 330

Nielsen DA, Petrou K, Gates RD (2018) Coral bleaching from a single cell perspective. ISME J 12:1558–1567

Ochs J, LaRue T, Tinaz B, Yongue C, Domozych DS (2014) The cortical cytoskeletal network and cell-wall dynamics in the unicellular charophycean green alga Penium margaritaceum. Ann Bot 114:1237-1249

Oksanen J, Blanchet FG, Friendly M, Kindt R, Legendre P, McGlinn D, Minchin PR, O'Hara RB, Simpson GL, Solymos P, Stevens MHH, Szoecs E, Wagner H (2018) vegan: Community Ecology Package. R package version 2.5-3. https://CRAN.R-project.org/package=vegan

Oldroyd GE, Downie JA (2004) Calcium, kinases and nodulation signalling in legumes. Nat Rev Mol Cell Biol 5:566 – 76

Orjalo AV, Bhaumik D, Gengler BK, Scott GK, Campisi J (2009) Cell surface-bound IL-1alpha is an upstream regulator of the senescence-associated IL-6/IL-8 cytokine network. Proc Natl Acad Sci U S A. 106:17031-17036

Park SY, Kim IS (2017) Engulfment signals and the phagocytic machinery for apoptotic cell clearance. Exp Mol Med 49:e331

Parkinson JE, Baumgarten S, Michell CT, Baums IB, LaJeunesse TC, Voolstra CR (2016) Gene Expression Variation Resolves Species and Individual Strains among Coral-Associated Dinoflagellates within the Genus Symbiodinium. Genome Biol Evol 8:665 – 680

Parkinson JE, Tivey TR, Mandelare PE, Adpressa DA, Loesgen S, Weis VM (2018) Subtle Differences in Symbiont Cell Surface Glycan Profiles Do Not Explain Species-Specific Colonization Rates in a Model Cnidarian-Algal Symbiosis. Front Microbiol 9:842. doi: 10.3389/fmicb.2018.00842

Pelz T, Drose DR, Fleck D, Henkel B, Ackels T, Spehr M, Neuhaus EM (2018) An ancestral TMEM16 homolog from *Dictyostelium discoideum* forms a scramblase. PLoS ONE 13(2): e0191219. https://doi.org/10.1371/journal.pone.0191219

Rice ME, Harris GT (2005) Comparing Effect Sizes in Follow-Up Studies: ROC Area, Cohen's d, and r. Law Hum Behav 5:615-20

Shi L, Dong H, Reguera G, Beyenal H, Lu A, Liu J, Yu HQ, Fredrickson JK (2016) Extracellular electron transfer mechanisms between microorganisms and minerals. Nat Rev Microbiol 1:651 – 62

Shimus, Levy, Herman (1985) A chemically cleavable biotinylated nucleotide: Usefulness in the recovery of protein-DNA complexes from avidin affinity columns. Proc Natl Acad Sci 82:2593 - 2597.

Shomer, Novacky, Pike, Yermiyahu, Kinraide (2003) Electrical potentials of plant cell walls in response to the ionic environment. Plant Physiol 133:411 - 422

Spalding M, Burke L, Wood SA, Ashpole J, Hutchison J, zu Ermgassen P (2017) Mapping the global value and distribution of coral reef tourism. Mar Policy 82:104 - 113

Suzuki M, Van Paesschen W, Stalmans I, Horita S, Yamada H, Bergmans BA, Legius E, Riant F, De Jonghe P, Lia Y, Sekine T, Igarashi T, Fujimoto I, Mikoshiba K, Shimadzu M, Shiohara M, Braverman N, Al-Gazali L, Fujita T, Seki G (2010) Defective membrane expression of the Na + -HCO 3 − cotransporter NBCe1 is associated with familial migraine. Proc Natl Acad Sci 107:15963 - 15968.

Torchiano M (2018) Efficient Effect Size Computation. R package version 0.7.4. http://github.com/mtorchiano/effsize/

Ünal CM1, Steinert M (2014) Microbial peptidyl-prolyl cis/trans isomerases (PPIases): virulence factors and potential alternative drug targets. Microbiol Mol Biol Rev 78: 544 - 571

Vu V (2011) A ggplot2 based biplot. R package version 0.55. http://github.com/vqv/ggbiplot

Wang SB, Hu Q, Sommerfeld M, Chen F (2004a) Cell wall proteomics of the green alga Haematococcus pluvialis (Chlorophyceae). Proteomics 4:692 – 708

Wang W, Vinocur B, Shoseyov O, Altman A (2004b) Role of plant heat-shock proteins and molecular chaperones in the abiotic stress response. Trends Plant Sci 9:244 – 52

Wang DZ, Dong HP, Li C, Xie ZX, Lin L, Hong HS (2011) Identification and Characterization of Cell Wall Proteins of a Toxic Dinoflagellate Alexandrium catenella Using 2-D DIGE and MALDI TOF-TOF Mass Spectrometry. Evid Based Complement Alternat Med 2011:984080. doi: 10.1155/2011/984080

Wang W, Jeffery CJ (2016) An analysis of surface proteomics results reveals novel candidates for intracellular/surface moonlighting proteins in bacteria. Mol Biosyst 12:1420-1431

Warton DI, Wright ST, Wang Y (2012) Distance-based multivariate analyses confound location and dispersion effects. Methods Ecol Evol 3:89–101

Wasserstein RL and Lazar NA (2016) ASA Statement on Statistical Significance and P-Values. Am Stat 70:129-133

Weis V (2008) Cellular mechanisms of Cnidarian bleaching: stress causes the collapse of symbiosis. J Exp Biol 211:3059 – 3066

Weston AJ, Dunlap WC, Shick JM, Klueter A, Iglic K, Vukelic A, Starcevic A, Ward M, Wells ML, Trick CG, Long PF (2012) A profile of an endosymbiont-enriched fraction of the coral Stylophora pistillata reveals proteins relevant to microbial-host interactions. Mol Cell Proteomics 11:M111.015487. doi: 10.1074/mcp.M111.015487

Wiersma VR, Michalak M, Abdullah TM, Bremer E, Eggleton P (2015) Mechanisms of Translocation of ER Chaperones to the Cell Surface and Immunomodulatory Roles in Cancer and Autoimmunity. Front Oncol 5:7. doi: 10.3389/fonc.2015.00007

Wilhelm M, Schlegl J, Hahne JH, Gholami AM, Lieberenz M, Savitski MM, Ziegler E, Butzmann L, Gessulat S, Marx H, Mathieson T, Lemeer S, Schnatbaum K, Reimer U, Wenschuh H, Mollenhauer M, Slotta-Huspenina J, Boese JH, Bantscheff M, Gerstmair A, Faerber F, Kuster B. 2014. Mass-spectrometry-based draft of the human proteome. Nature 509: 582–587

Wood-Charlson E, Hollingworth L, Krupp D, Weis V (2006) Lectin/glycan interactions play a role in recognition in a coral/dinoflagellate symbiosis. Cell Microbiol 8: 1985–1993

Yellowlees D, Dionisio-Sese ML, Masuda K, Maruyama T, Abe T, Baillie B, Tsuzuki M, Miyachi S (1993) Role of carbonic anhydrase in the supply of inorganic carbon to the giant clam—zooxanthellate symbiosis. Mar Biol 115: 605 – 611

Zhu H, Fang X, Zhang D, Wu W, Shao M, Wang L, Gu J (2016) Membrane-bound heat shock proteins facilitate the uptake of dying cells and cross-presentation of cellular antigen. Apoptosis 21: 96 – 109

Figure captions

Fig1 Stacked plot depicting relative abundance of functional groups. Percentages reported are based on the average abundance of each functional group between treatment replicates. Y-axis represents percent normalized PSMs

Fig2 Validation of nodG in Breviolum psygmophilum A) sequence alignment between B. psygmophilum nodG homolog and Rhizobium sp. nodG (uniprot ID P72332); B) Pfam protein domains present in B. psygmophilum nodG homolog and Rhizobium sp. nodG; C) Phylogenetic analysis of top ten strongest BLAST hits for nod factors across Symbiodiniaceae species. (*) denotes B. psygmophilum nodG identified in the current study

Fig3 Total abundance of proteins found in each treatment A) total abundance of proteins for sequences found only in either control or heat-treated samples. B) total abundance of proteins for sequences found in both control or heat-treated samples. Blue lines with circles represent control treatment; red lines with triangles represent heat treatment. At 24 hours of exposure, shared proteins do not differ in abundance ($p = 0.400$, Cohen's $d = -0.440$) but unique proteins do ($p = 0.176$, Cohen's $d = -0.894$). Y-axis represents normalized PSMs

Fig4 Total abundance of proteins found in each treatment A) total abundance of proteins for sequences found only in either control or heat-treated samples. B) total abundance of proteins for sequences found in both control or heat-treated samples. Blue hues represent control treatments; red hues represent heat treatments. Y-axis represents normalized PSM.

Fig5 PCA plot comparing treatments to functional groups.

Fig6 Top two most influential proteins for each functional group according to simper. A) Protein folding; B) Adhesion; C) CO_2 uptake; D) Extracellular ATP; E) Extracellular redox; F) Signal transduction; G) Ion homeostasis. (*) represent those differences between treatment

that are stastically significant; (a) represent those differences with large effect sizes. Effect size was calculated using Cohen's d estimation. Y-axis represents normalized PSMs.

Fig7 Comparison of total abundance of each immune modulation category and its response to heat after 24 h. A) Constitutive abundance of proteins in immune activation (salmon), regulation (regulation), or suppression categories (light blue); B) Response of immune modulation proteins after 24 h exposure to heat. Blue boxes represent control treatments; red boxes represent heat treatments (*) represent those differences between treatment that are stastically significant; (a) represent those differences with large effect sizes. Effect size was calculated using Cohen's d estimation. Y-axis represents normalized PSMs.

Appendix 2A: Tables and Figures

TABLES

Table 1. Protein functional groups. List of proteins isolated from the *Breviolum Psigmophilum* cell surface, categorized into functional groups based on roles at the cell surface

Functional Group	*B. psygmophilum* transcriptome sequence	Protein Name
Adhesion	comp36757_c0_seq1.p1	Elongation factor 1-alpha
	comp11356_c0_seq1.p1	Enolase
	comp18414_c0_seq5.p1	Enolase
	comp29485_c0_seq1.p1	Enolase
	comp29838_c0_seq2.p1	Enolase
	comp33094_c0_seq4.p1	Glutamine synthetase
	comp36464_c0_seq1.p1	Glutamine synthetase
	comp37011_c1_seq2.p1	Glutamine synthetase
	comp37015_c0_seq2.p1	Glyceraldehyde-3-phosphate dehydrogenase
	comp37083_c0_seq2.p1	Glyceraldehyde-3-phosphate dehydrogenase
	comp34391_c0_seq1.p1	Phosphoglycerate kinase
	comp33801_c0_seq4.p1	Triosephosphate isomerase
	comp37351_c0_seq1.p2	Triosephosphate isomerase
	comp37849_c0_seq1.p1	Triosephosphate isomerase
Cell structure	comp1748_c0_seq1.p2	Actin
	comp35046_c0_seq3.p2	Actin
	comp33420_c0_seq2.p1	Collagen alpha-1(XVII) chain
	comp37901_c0_seq1.p1	Collagen alpha-1(XVII) chain
	comp61911_c0_seq1.p1	Major outer membrane lipoprotein
	comp24819_c0_seq1.p1	Tubulin
	comp36850_c0_seq5.p1	Tubulin
	comp37027_c0_seq2.p1	Tubulin
	comp37107_c0_seq1.p1	Tubulin
CO2 uptake	comp35964_c0_seq3.p1	Carbonic anhydrase
	comp36098_c0_seq3.p1	Carbonic anhydrase
Extracellular ATP	comp36516_c0_seq2.p1	ATP synthase gamma chain
	comp36952_c0_seq2.p1	ATP synthase gamma chain
	comp38541_c0_seq1.p1	ATP synthase subunit alpha
	comp25655_c0_seq1.p1	ATP synthase subunit beta

	comp27837_c0_seq1.p1	ATP synthase subunit beta
	comp34697_c0_seq1.p1	ATP synthase subunit beta
	comp37979_c0_seq1.p1	ATP synthase subunit beta
Extracellular redox	comp33468_c0_seq1.p1	Acyl-CoA dehydrogenase
	comp35869_c0_seq6.p2	Cytochrome c-550
	comp35093_c0_seq2.p2	Cytochrome c6
	comp39261_c0_seq1.p1	Dihydrolipoyl dehydrogenase
	comp18413_c0_seq1.p1	Fumarate reductase
	comp22274_c0_seq2.p1	Fumarate reductase
	comp36145_c0_seq1.p1	Fumarate reductase
	comp36488_c0_seq5.p1	Fumarate reductase
	comp36454_c0_seq1.p1	Glutathione S-transferase
	comp33055_c0_seq2.p1	L-lactate dehydrogenase
	comp37134_c0_seq1.p1	Pyruvate dehydrogenase
Signal transduction	comp11845_c0_seq1.p1	14-3-3-like protein
	comp36800_c0_seq1.p1	14-3-3-like protein
	comp35699_c0_seq1.p1	Calreticulin
	comp35990_c0_seq1.p1	Cell division cycle protein 48 homolog
	comp29762_c0_seq1.p1	Developmentally-regulated G-protein 2
	comp14901_c0_seq1.p1	Nicotinamide phosphoribosyltransferase
	comp8899_c0_seq1.p1	Nodulation protein G
	comp36444_c0_seq1.p2	Serine/threonine-protein phosphatase
	comp33615_c1_seq2.p1	Ubiquitin
Ion homeostasis	comp37477_c0_seq1.p1	V-type proton ATPase catalytic subunit A
	comp18453_c0_seq2.p1	Putative K(+)-stimulated pyrophosphate-energized sodium pump
Protein folding	comp8280_c0_seq1.p1	Chaperonin CPN60
	comp23514_c0_seq4.p1	Heat shock 70 protein
	comp33298_c0_seq4.p1	Heat shock 70 protein
	comp36948_c0_seq1.p1	Heat shock 70 protein
	comp36974_c0_seq1.p1	Heat shock 70 protein
	comp7486_c0_seq1.p1	Heat shock 70 protein
	comp24965_c0_seq1.p1	Heat shock 90 protein
	comp36621_c0_seq5.p1	Heat shock 90 protein
	comp36855_c0_seq1.p1	Heat shock 90 protein
	comp37297_c0_seq1.p1	Heat shock 90 protein

	comp16455_c0_seq1.p2	Peptidyl-prolyl cis-trans isomerase
	comp36920_c0_seq4.p1	Peptidyl-prolyl cis-trans isomerase
	comp38944_c0_seq1.p1	Peptidyl-prolyl cis-trans isomerase
	comp18648_c0_seq1.p1	Protein disulfide-isomerase
Unknown	comp8484_c0_seq1.p2	3-ketoacyl-CoA thiolase
	comp31713_c0_seq1.p1	3-ketoacyl-CoA thiolase
	comp22970_c0_seq1.p1	ATP-citrate synthase
	comp30984_c0_seq1.p1	ATP-citrate synthase
	comp35289_c0_seq2.p1	Elongation factor 2
	comp34171_c0_seq1.p1	Isocitrate lyase
	comp30131_c0_seq1.p1	Phosphoenolpyruvate carboxykinase
	comp38011_c0_seq1.p1	Phosphoenolpyruvate carboxykinase
	comp18185_c0_seq1.p1	Phosphoenolpyruvate carboxylase
	comp31985_c0_seq1.p2	S-adenosylmethionine synthase
	comp37675_c0_seq1.p1	Succinate dehydrogenase flavoprotein subunit
	comp38376_c0_seq1.p1	Succinate-CoA ligase subunit beta

Proteins categorized via GO terms (Gene Ontology databases) and literature searches

Table 2. Statistical comparison of treatment on all response variables. Repeated measures MANOVA outcome and SIMPER post hoc tests to determine largest drivers of difference between treatments

Whole model RM MANOVA	
Effect	*p-value*
Treatment	0.7
Time	0.189
Treatment * Time	0.132
Functional Group	**<0.001**
Treatment * Functional Group	0.398
Time * Functional Group	**0.002**
Treatment * Time * Functional Group	**0.017**

Post hoc SIMPER analysis		
Functional Group	*Average*	*Cumsum*
Protein Folding	0.054	0.217
Cell Structure	0.039	0.372
Adhesion	0.032	0.503
CO2 Uptake	0.032	0.632
Extracellular ATP	0.027	0.739
Unknown	0.023	0.832
Extracellular Redox	0.022	0.922
Signal Transduction	0.011	0.964
Ion Homeostasis	0.009	1

Bold P-values represent significant effects ($P \leq 0.05$). SIMPER conducted on protein abundance for sequences found within each functional group. "Average" represents average contribution to overall dissimilarity. "Cumsum" represents cumulative contribution to overall dissimilarity.

Table 3: Statistical comparison of two most influential proteins within each functional group. Based on SIMPER analysis on proteins contributing to the differences observed within functional group in response to treatment. Effect size was calculated by Cohen's d estimation.

Most Influential Functional Groups				
Functional Group	*Average*	*Cumsum*	*P-value*	*Effect Size*
Protein Folding				
HSP 70	0.206	0.438	0.400	**-1.174**
HSP 90	0.168	0.795	0.100	**-2.870**
Cell Structure				
Tubulin	0.304	0.652	0.400	**0.981**
Major outer membrane lipoprotein	0.083	0.830	0.100	**-1.243**
Adhesion				
Enolase	0.073	0.230	0.700	0.441
Triosephosphate Isomerase	0.069	0.546	1.000	0.043
CO2 Uptake				
Carbonic Anhydrase	0.263	1	0.700	0.079
Extracellular ATP				
ATP Synthase	0.263	1	0.400	**0.814**
Others				
Extracellular Redox				
Fumarate Reductase	0.239	0.474	0.700	**-0.954**
Cytochrome C	0.082	0.637	1.000	0.214
Signal Transduction				
14-3-3-like Protein	0.085	0.200	0.200	**-1.459**
Calreticulin	0.083	0.395	0.197	**-1.564**
Ion Homeostasis				
V-type H+ ATPase	0.259	0.746	0.507	**-0.865**
Putative K+ stimulated pyrophosphate energized sodium pump	0.088	1	1.000	0.040

Bold P-values represent significant effect for non-parametric t-tests ($P \leq 0.05$). Bold effect sizes represent large effect size values. SIMPER conducted on protein abundance for sequences found within each functional group. "Average" represents average contribution to overall dissimilarity. "Cumsum" represent cumulative contribution to overall dissimilarity. Unknown functional category not reported

Table 4. Statistical comparison of treatment on immune modulating proteins. Repeated measures MANOVA outcome and post hoc tests. Effect size was calculated by Cohen's d estimation.

Whole model RM MANOVA	
Effect	*p-value*
Treatment	0.437
Time	**0.02**
Treatment * Time	0.076
Interaction with Immune System	**<0.001**
Treatment * Interaction with Immune System	**0.009**
Time * Interaction with Immune System	**0.04**
Treatment * Time * Interaction with Immune System	0.081

Post hoc non-parametric t-test		
Immune modulation	*p-value*	*Effect Size*
Activation	0.1	**-2.131**
Regulation	0.4	0.585
Suppression	0.505	**0.816**

Bold P-values represent significant effects ($P \leq 0.05$). Bold effect sizes represent large effect size values.

FIGURES

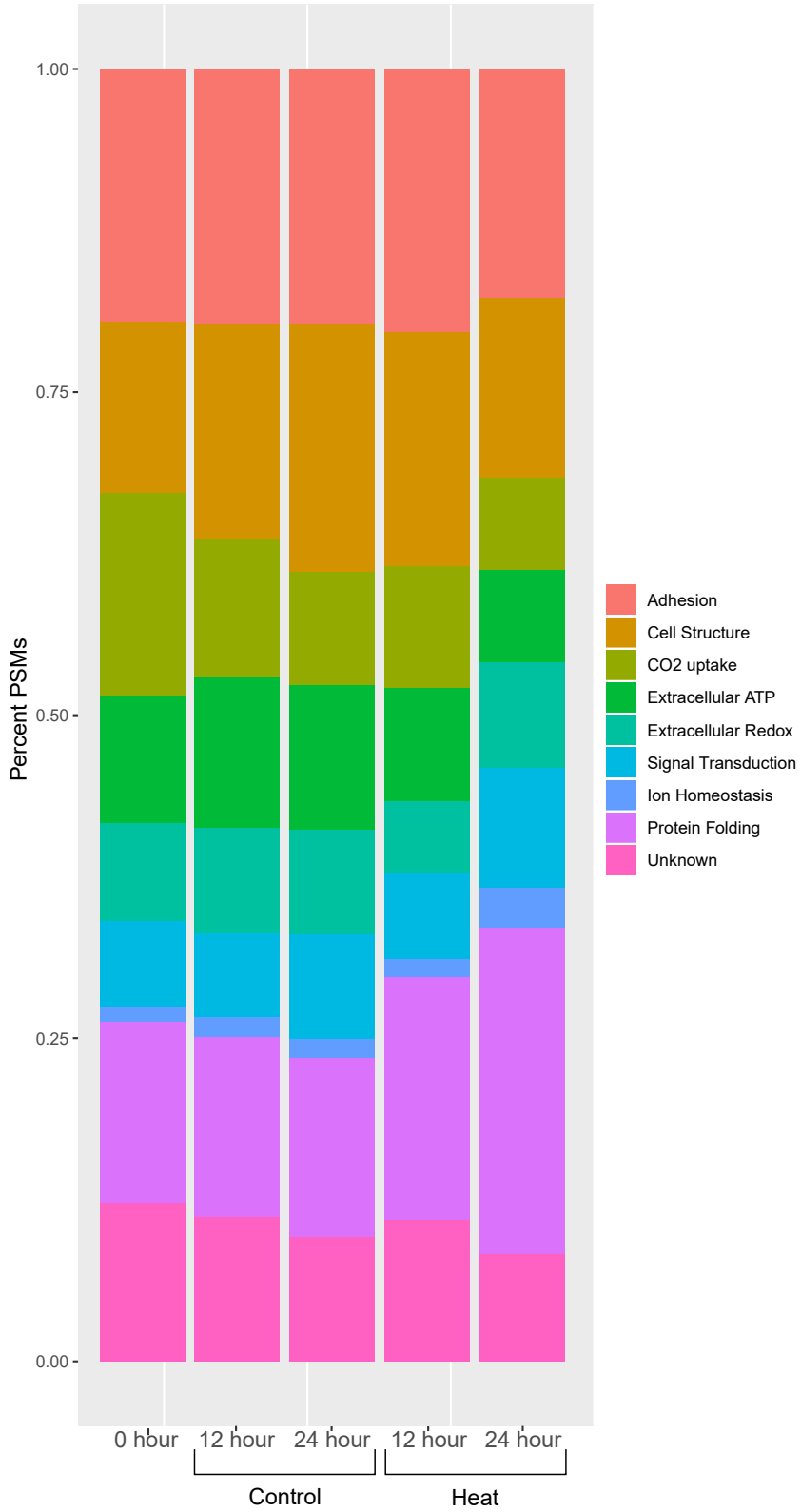

Fig 1 ***Stacked plot depicting relative abundance of functional groups.*** *Percentages reported are based on the average abundance of each functional group between treatment replicates. Y-axis represents percent normalized PSMs*

A)

```
EMBOSS_001          2 FELTGRKALVTGASGGIGEAIARVLHAQGAIVGLHGTRVEKLETLAAELG     51
                      |:|:|:.|||||||.|||.|||..|...||.|....|.....|.::|.:|
EMBOSS_001         98 FDLSGKVALVTGASRGIGAAIADTLAKAGATVVGTATSDAGAEAISARMG    147

EMBOSS_001         52 DR----VKLFPANLSNRDE-VKALGQKAEADLEGVDILVNNAGITKDGLF     96
                      ::    :||...:..|.:| |||:.:|..|.    ||||||||||||.|.
EMBOSS_001        148 EQWGQGIKLDVTDSKNVEEVVKAVTEKYGAP----DILVNNAGITKDTLM    193

EMBOSS_001         97 VRMSDADWDTVLEVNLTAVFRLTRELTHPMMRRRHGRIINITSVVGVTGN    146
                      :||.:..|..|:..||.:|||:|:..|..|.::|.||:|:|:||||..||
EMBOSS_001        194 MRMKEDQWLDVINTNLNSVFRMTKAATKGMTKKRWGRVISISSVVGSMGN    243

EMBOSS_001        147 PGQTNYCASKAGMIGFSKSLAQEIATRNITVNCVAPGFIESAMTDKLNDK    196
                      .||:||.|:||||.|:::::|:||.:|.||||.||||||::.||..|.|.
EMBOSS_001        244 VGQSNYAAAKAGMDGWTRAMAREIGSRGITVNSVAPGFIDTDMTADLPDD    293

EMBOSS_001        197 QKEAIMAAIPTRRMGTSVEVASAVAYLASNEAAYVTGQTIHVNGGLAM    244
                      .|:.::..:|.:|:|...|||.||.:|||..|.|:||.|:|||||:.|
EMBOSS_001        294 WKDKLLENVPAKRLGQPSEVAEAVLFLASPAAGYITGHTLHVNGGMYM    341
```

B)

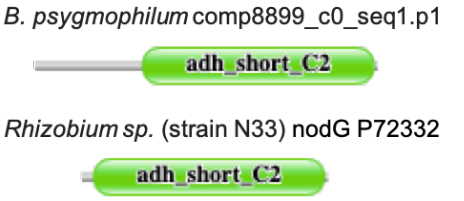

C)

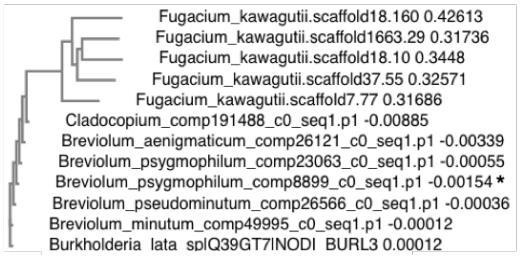

Fig 2 ***Validation of nodG in*** **Breviolum psygmophilum** *A) sequence alignment between* B. psygmophilum *nodG homolog and* Rhizobium sp. *nodG (uniprot ID P72332); B) Pfam protein domains present in* B. psygmophilum *nodG homolog and* Rhizobium sp. *nodG; C) Phylogenetic analysis of top ten strongest BLAST hits for nod factors across Symbiodiniaceae species. (*) denotes* B. psygmophilum *nodG identified in the current study*

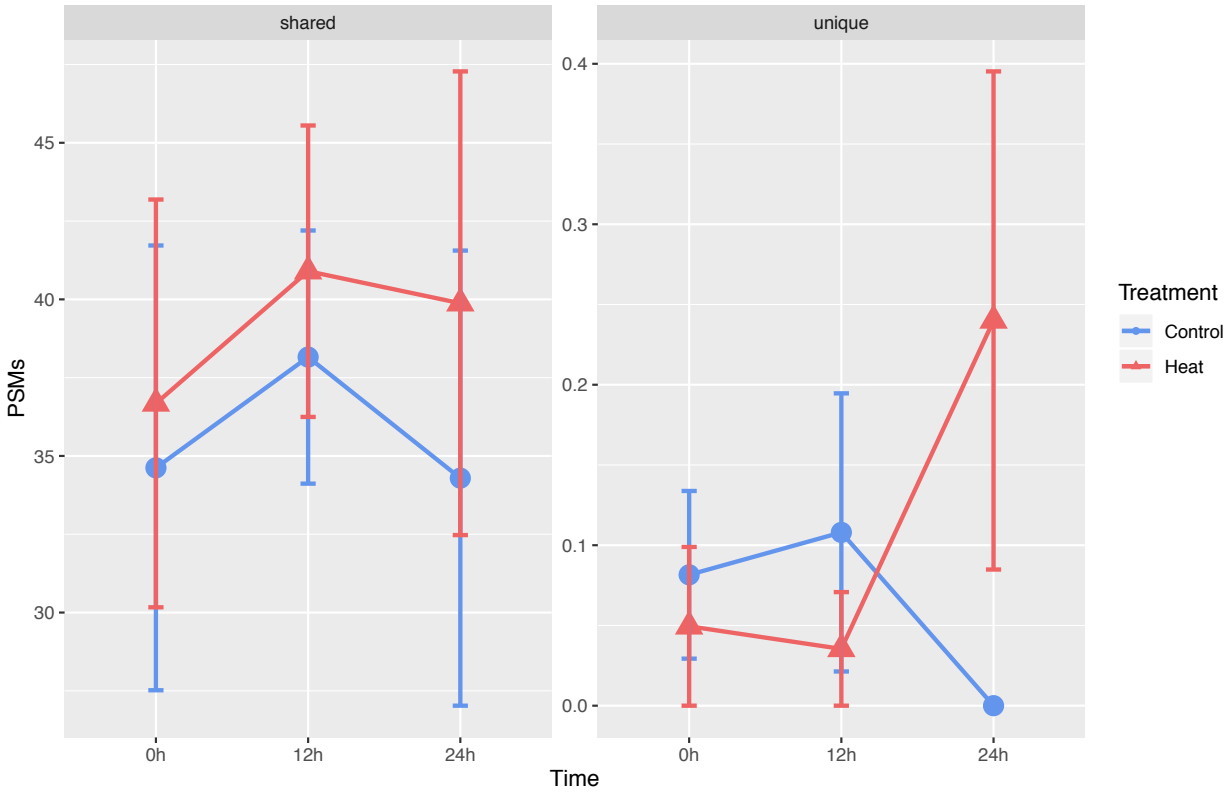

Fig 3 ***Total abundance of proteins found in each treatment*** *A) total abundance of proteins for sequences found only in either control or heat-treated samples. B) total abundance of proteins for sequences found in both control or heat-treated samples. Blue lines with circles represent control treatment; red lines with triangles represent heat treatment. At 24 hours of exposure, shared proteins do not differ in abundance (p = 0.400, Cohen's* d *= -0.440) but unique proteins do (p = 0.176, Cohen's* d *= -0.894). Y-axis represents normalized PSMs*

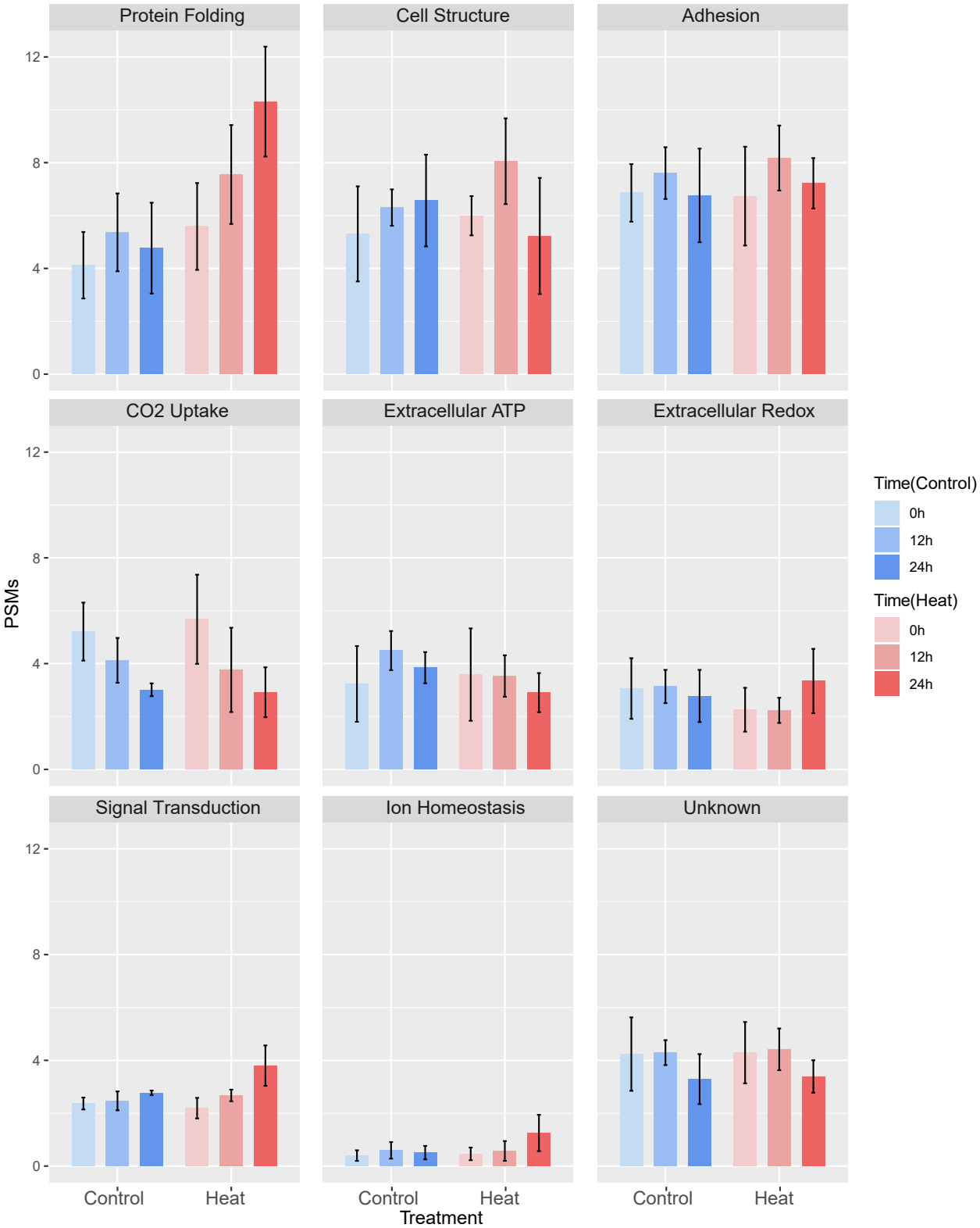

Fig 4 ***Total abundance of proteins found in each treatment*** *A) total abundance of proteins for sequences found only in either control or heat-treated samples. B) total abundance of proteins for sequences found in both control or heat-treated samples. Blue hues represent control treatments; red hues represent heat treatments. Y-axis represents normalized PSM.*

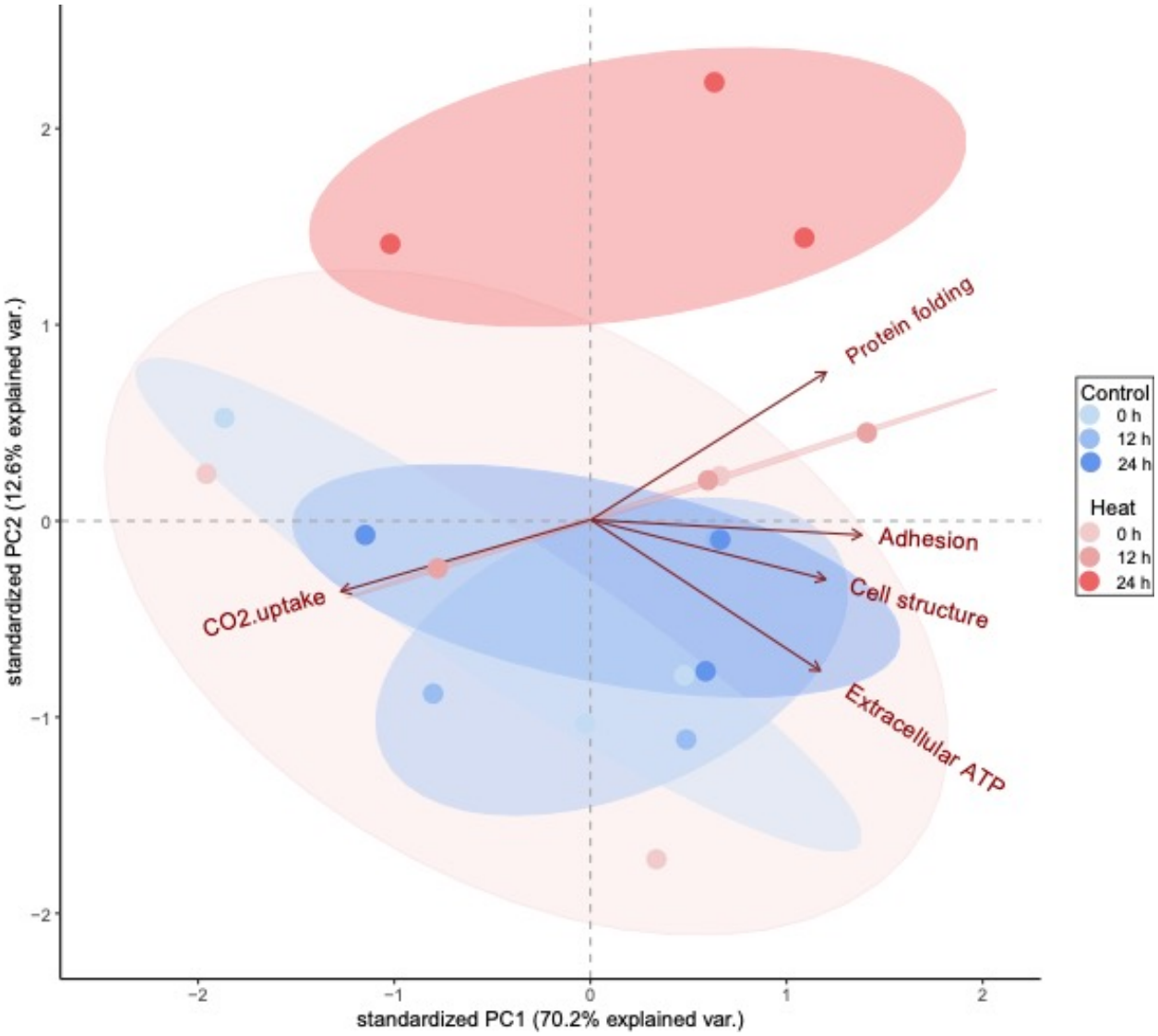

Fig 5 PCA plot comparing treatments to functional groups.

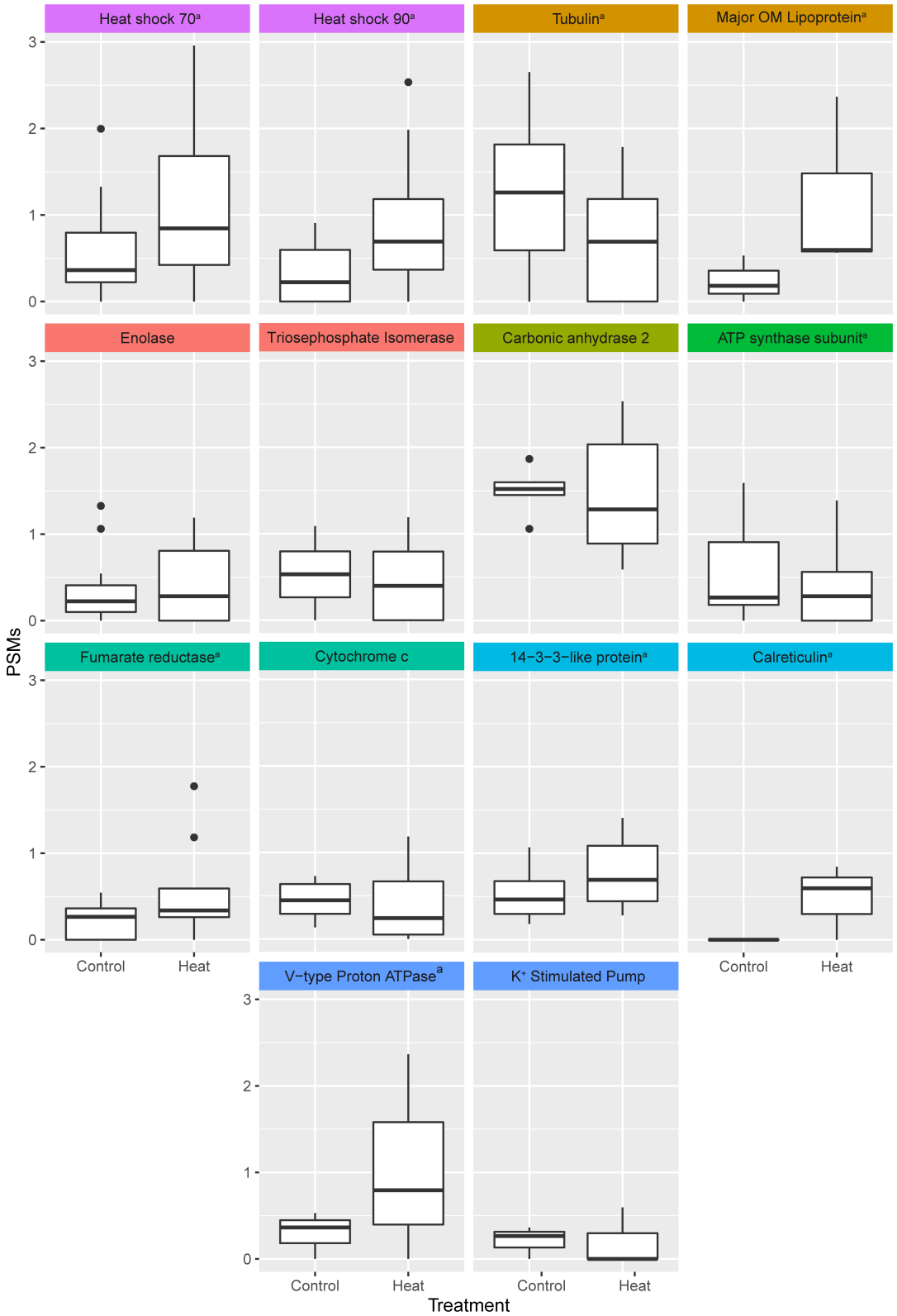

Fig 6 ***Top two most influential proteins for each functional group according to simper.*** *A) Protein folding; B) Adhesion; C) CO_2 uptake; D) Extracellular ATP; E) Extracellular redox; F) Signal transduction; G) Ion homeostasis. (*) represent those differences between treatment that are stastically significant; (a) represent those differences with large effect sizes. Effect size was calculated using Cohen's d estimation. Y-axis represents normalized PSMs.*

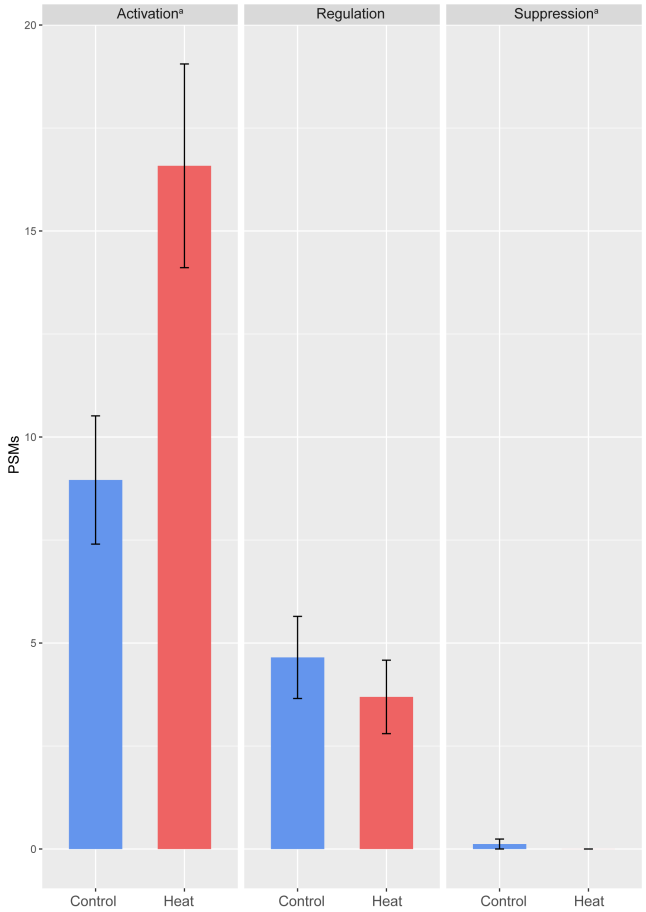

Fig 7 Comparison of total abundance of each immune modulation category and its response to heat after 24 h. A) Constitutive abundance of proteins in immune activation (salmon), regulation (regulation), or suppression categories (light blue); B) Response of immune modulation proteins after 24 h exposure to heat. Blue boxes represent control treatments; red boxes represent heat treatments ***(*) represent those differences between treatment that are stastically significant; (a) represent those differences with large effect sizes. Effect size was calculated using Cohen's d estimation.*** *Y-axis represents normalized PSMs.*

Appendix 2B: Supplementary Material

TABLES

Table S1. List of all proteins identified by nanospray LC-MS/MS. Proteins meeting criteria for high confidence at ≤ 5 % FDR.

sequence ID'd	Uniprot accesion	protein name	species	e value	score
comp11356_c0_seq1.p1	Q42971	Enolase	Oryza sativa	0	577
comp11845_c0_seq1.p1	P42644	14-3-3-like protein GF14 psi	Arabidopsis thaliana	2.00E-94	278
comp14901_c0_seq1.p1	Q52I78	Nicotinamide phosphoribosyltransferase	Sus scrofa	2.00E-154	460
comp16455_c0_seq1.p2	Q39613	Peptidyl-prolyl cis-trans isomerase	Catharanthus roseus	6.00E-104	299
comp1748_c0_seq1.p2	P02576	Actin	Physarum polycephalum	6.00E-158	444
comp18185_c0_seq1.p1	Q02909	Phosphoenolpyruvate carboxylase, housekeeping isozyme	Glycine max	0	684
comp18413_c0_seq1.p1	O13755	Fumarate reductase	Schizosaccharomyces pombe	4.00E-48	179
comp18414_c0_seq5.p1	Q9BPL7	Enolase 2	Toxoplasma gondii	4.00E-110	350
comp18453_c0_seq2.p1	Q8F641	Putative K(+)-stimulated pyrophosphate-energized sodium pump	Leptospira interrogans	0	684
comp18648_c0_seq1.p1	A0A1Q9D1J9	Protein disulfide-isomerase	Symbiodinium microadriaticum	4.70E-113	945
comp22274_c0_seq2.p1	O13755	Fumarate reductase	Schizosaccharomyces pombe	3.00E-97	302
comp22970_c0_seq1.p1	Q91V92	ATP-citrate synthase	Mus musculus	0	1303
comp23514_c0_seq4.p1	Q6Z7B0	Heat shock 70 kDa protein	Oryza sativa	9.00E-137	403
comp24819_c0_seq1.p1	P33188	Tubulin beta chain	Paramecium tetraurelia	0	757
comp24965_c0_seq1.p1	P54651	Heat shock cognate 90 kDa protein	Dictyostelium discoideum	0	538
comp25655_c0_seq1.p1	Q25117	ATP synthase subunit beta	Hemicentrotus pulcherrimus	0	759

Summary	
147	total proteins identified
65	non-cell surface proteins
47	chloroplast-related proteins
0.72	fraction of non-cell surface proteins belonging to chloroplast constituents
79	confirmed cell surface proteins
3	unidentified proteins
82	total

Could not be identified by homology

May be found on cell surface but literature was conflicting/unclear

Chloroplast constituent

Other non-cell surface protein

Confirmed cell surface protein

comp29485_c0_seq1.p1	Q9PVK2	Alpha-enolase	Alligator mississippiensis	0	550
comp29762_c0_seq1.p1	A0A1Q9EEJ5_SYMMI	Developmentally-regulated G-protein 2	Symbiodinium microadriaticum	7.30E-45	425
comp29838_c0_seq2.p1	Q8IJN7	Enolase	Plasmodium falciparum	0	652
comp30131_c0_seq1.p1	Q75JD5	Phosphoenolpyruvate carboxykinase (ATP)	Dictyostelium discoideum	0	734
comp30984_c0_seq1.p1	Q91V92	ATP-citrate synthase	Mus musculus	0	1318
comp31713_c0_seq1.p1	Q8VCH0	3-ketoacyl-CoA thiolase B, peroxisomal	Mus musculus	6.00E-150	436
comp31985_c0_seq1.p2	Q6SYB9	S-adenosylmethionine synthase 2	Nicotiana tabacum	8.00E-156	450
comp33055_c0_seq2.p1	Q6DAY3	L-lactate dehydrogenase	Pectobacterium atrosepticum	2.00E-51	183
comp33094_c0_seq4.p1	P15623	Glutamine synthetase	Bacteroides fragilis	3.00E-130	405
comp33298_c0_seq4.p1	P19208	Heat shock 70 kDa protein C	Caenorhabditis briggsae	0	883
comp33420_c0_seq2.p1	A0A1Q9E298_SYMMI	Collagen alpha-1(XVII) chain	Symbiodinium microadriaticum	1.50E-35	347
comp33468_c0_seq1.p1	Q5ATG5	Acyl-CoA dehydrogenase apdG	Emericella nidulans	1.00E-108	332
comp33615_c1_seq2.p1	P19848	Ubiquitin	Coprinellus congregatus	5.00E-48	155
comp33801_c0_seq4.p1	P48495	Triosephosphate isomerase	Petunia hybrida	7.00E-93	293
comp34171_c0_seq1.p1	P25248	Isocitrate lyase	Brassica napus	6.00E-161	469
comp34391_c0_seq1.p1	P51903	Phosphoglycerate kinase	Gallus gallus	0	538
comp34697_c0_seq1.p1	Q06J29	ATP synthase subunit beta	Bigelowiella natans	2.00E-150	434
comp35046_c0_seq3.p2	P26182	Actin	Achlya bisexualis	0	720
comp35093_c0_seq2.p2	Q3MDW2	Cytochrome c6	Anabaena variabilis	1.00E-29	107
comp35289_c0_seq2.p1	Q23716	Elongation factor 2	Cryptosporidium parvum	0	1257
comp35699_c0_seq1.p1	Q9STD3	Calreticulin	Chlamydomonas reinhardtii	1.00E-123	366
comp35869_c0_seq6.p2	A0T0C6	Cytochrome c-550	Phaeodactylum tricornutum	5.00E-52	168
comp35964_c0_seq3.p1	P9WPJ9	Carbonic anhydrase 2	Mycobacterium tuberculosis	5.00E-22	97.8

comp35990_c0_seq1.p1	P54774	Cell division cycle protein 48 homolog	Glycine max	0	1161
comp36098_c0_seq3.p1	P9WPJ9	Carbonic anhydrase 2	Mycobacterium tuberculosis	7.00E-25	106
comp36145_c0_seq1.p1	O13755	Fumarate reductase	Schizosaccharomyces pombe	1.00E-133	400
comp36444_c0_seq1.p2	A0A1Q9EHJ8	Serine/threonine-protein phosphatase	Symbiodinium microadriaticum	3.40E-22	259
comp36454_c0_seq1.p1	P46436	Glutathione S-transferase	Ascaris suum	6.00E-28	108
comp36464_c0_seq1.p1	P15623	Glutamine synthetase	Bacteroides fragilis	7.00E-125	389
comp36488_c0_seq5.p1	O13755	Fumarate reductase	Schizosaccharomyces pombe	1.00E-119	378
comp36516_c0_seq2.p1	B1XHY7	ATP synthase gamma chain	Synechococcus sp.	1.00E-92	286
comp36621_c0_seq5.p1	O44001	Heat shock protein 90	Eimeria tenella	0	1045
comp36757_c0_seq1.p1	P90519	Elongation factor 1-alpha	Cryptosporidium parvum	3.00E-122	367
comp36800_c0_seq1.p1	P42644	14-3-3-like protein GF14 psi	Arabidopsis thaliana	7.00E-111	322
comp36850_c0_seq5.p1	P41352	Tubulin beta chain	Tetrahymena thermophila	0	565
comp36855_c0_seq1.p1	Q90474	Heat shock protein HSP 90-alpha 1	Danio rerio	0	655
comp36920_c0_seq4.p1	A0A1Q9EKM5	Peptidyl-prolyl cis-trans isomerase	Symbiodinium microadriaticum	2.10E-131	1,057
comp36948_c0_seq1.p1	P11144	Heat shock 70 kDa protein	Plasmodium falciparum	0	1006
comp36952_c0_seq2.p1	A0A1Q9DKL5_SYMMI	ATP synthase gamma chain	Symbiodinium microadriaticum	5.10E-120	1,011
comp36974_c0_seq1.p1	Q9LTX9	Heat shock 70 kDa protein 7	Arabidopsis thaliana	0	872
comp37011_c1_seq2.p1	Q12613	Glutamine synthetase	Colletotrichum gloeosporioides	5.00E-128	389
comp37015_c0_seq2.p1	P22513	Glyceraldehyde-3-phosphate dehydrogenase, glycosomal OS=T...	Trypanosoma cruzi	0	534
comp37027_c0_seq2.p1	P33188	Tubulin beta chain	Paramecium tetraurelia	0	842
comp37083_c0_seq2.p1	O59841	Glyceraldehyde-3-phosphate dehydrogenase	Ogataea parapolymorpha	3.00E-141	410
comp37107_c0_seq1.p1	P11481	Tubulin alpha-1/alpha-2 chain	Volvox carteri	0	618
comp37134_c0_seq1.p1	Q968X7	Pyruvate dehydrogenase [NADP(+)]	Cryptosporidium parvum	0	1537

comp37297 c0 seq1.p1	P24724	Heat shock protein 90	Theileria parva	2.00E-119	358
comp37351 c0 seq1.p2	O77458	Triosephosphate isomerase	Drosophila yakuba	1.00E-78	245
comp37477 c0 seq1.p1	Q03498	V-type proton ATPase catalytic subunit A	Plasmodium falciparum	0	836
comp37675_c0_seq1.p1	Q6ZDY8	Succinate dehydrogenase [ubiquinone] flavoprotein subunit	Oryza sativa	0	838
comp37849 c0 seq1.p1	P30741	Triosephosphate isomerase	Culex tarsalis	9.00E-80	243
comp37901_c0_seq1.p1	A0A1Q9E298	Collagen alpha-1(XVII) chain	Symbiodinium microadriaticum	2.30E-34	340
comp37979_c0_seq1.p1	P10719	ATP synthase subunit beta	Rattus norvegicus	0	751
comp38011 c0 seq1.p1	Q75JD5	Phosphoenolpyruvate carboxykinase (ATP)	Dictyostelium discoideum	0	731
comp38376 c0 seq1.p1	Q84LB6	Succinate--CoA ligase [ADP-forming] subunit beta	Solanum lycopersicum	4.00E-140	410
comp38541_c0_seq1.p1	P19483	ATP synthase subunit alpha, mitochondrial	Bos taurus	0	741
comp38944_c0_seq1.p1	P42693	Peptidyl-prolyl cis-trans isomerase	Acinetobacter baylyi	1.00E-31	118
comp39261 c0 seq1.p1	P09622	Dihydrolipoyl dehydrogenase	Homo sapiens	0	535
comp61911_c0_seq1.p1	H8WB07	Major outer membrane lipoprotein	Marinobacter hydrocarbonoclasticus	7.80E-44	370
comp7486_c0_seq1.p1	P37900	Heat shock 70 kDa protein	Pisum sativum	0	853
comp8280_c0_seq1.p1	Q05046	Chaperonin CPN60-2, mitochondrial	Cucurbita maxima	0	668
comp8484_c0_seq1.p2	P09110	3-ketoacyl-CoA thiolase	Homo sapiens	3.00E-47	160
comp8899_c0_seq1.p1	P72332	Nodulation protein G	Rhizobium sp. (strain N33)	3.00E-68	217
comp33009 c0 seq6.p1	Q6NYL3	Peroxisomal bifunctional enzyme	Danio rerio	6.00E-148	452
comp35530_c0_seq1.p2	A0A1Q9E998	Chaperone protein DnaJ	Magnetospirillum magneticum	1.70E-113	870
comp36825 c0 seq2.p1	A6NE01	Protein FAM186A	Homo sapiens	2.00E-21	104
comp37246 c0 seq1.p2	A0A1Q9F3H6	Putative vacuolar protein sorting-associated protein 13A	Symbiodinium microadriaticum	5.10E-84	704
comp39601_c0_seq1.p1	Q9SGC1	Probable phosphoglucomutase	Arabidopsis thaliana	0	671
comp20593_c0_seq1.p1	-	-	-	-	-
comp23259_c0_seq2.p1	-	-	-	-	-

comp36691_c1_seq3.p1	-	-	-	-	-
comp10960_c0_seq1.p1	Q40300	Fucoxanthin-chlorophyll a-c binding protein F	Macrocystis pyrifera	5.00E-20	84.3
comp16298_c0_seq1.p1	A0T0T0	Photosystem II D2 protein	Thalassiosira pseudonana	0	592
comp17885_c0_seq1.p1	Q40296	Fucoxanthin-chlorophyll a-c binding protein B	Macrocystis pyrifera	9.00E-26	102
comp22880_c0_seq1.p1	Q40301	Fucoxanthin-chlorophyll a-c binding protein E	Macrocystis pyrifera	1.00E-26	106
comp24214_c0_seq1.p1	P49472	Photosystem II CP43 reaction center protein	Trieres chinensis	0	588
comp25457_c0_seq1.p1	P55738	Caroteno-chlorophyll a-c-binding protein (Fragment)	Amphidinium carterae	3.00E-24	94.4
comp26413_c0_seq1.p1	P46285	Sedoheptulose-1,7-bisphosphatase, chloroplastic OS=Tritic...	Triticum aestivum	6.00E-73	237
comp26421_c0_seq1.p1	P0C8N4	Cytochrome f	Synechococcus elongatus	1.00E-46	157
comp28892_c0_seq1.p1	A2Y8E0	Ferredoxin--NADP reductase, leaf isozyme 1, chloroplastic...	Oryza sativa subsp. indica	3.00E-105	319
comp28937_c0_seq1.p1	Q40297	Fucoxanthin-chlorophyll a-c binding protein A	Macrocystis pyrifera	1.00E-37	137
comp29553_c0_seq2.p1	A0A1Q9EDY9	Pentatricopeptide repeat-containing protein	Symbiodinium microadriaticum	1.80E-37	365
comp29702_c0_seq1.p1	Q40297	Fucoxanthin-chlorophyll a-c binding protein A	Macrocystis pyrifera	3.00E-35	133
comp29994_c0_seq1.p1	P49471	Photosystem II CP47 reaction center protein	Trieres chinensis	0	528
comp31424_c0_seq2.p1	P08976	Light-harvesting complex I LH38 proteins	Euglena gracilis	5.00E-14	79.3
comp31588_c0_seq1.p1	Q40300	Fucoxanthin-chlorophyll a-c binding protein F	Macrocystis pyrifera	5.00E-38	143
comp31665_c0_seq1.p1	Q40297	Fucoxanthin-chlorophyll a-c binding protein A	Macrocystis pyrifera	6.00E-16	77.8
comp32919_c0_seq1.p1	Q03965	Chlorophyll a-b binding protein L1818, chloroplastic	Chlamydomonas moewusii	4.00E-11	65.5
comp33020_c0_seq1.p1	P55738	Caroteno-chlorophyll a-c-binding protein (Fragment)	Amphidinium carterae	1.00E-23	92.8
comp33347_c0_seq1.p1	Q9XQV3	Photosystem I P700 chlorophyll a apoprotein A1	Heterocapsa triquetra	0	808
comp34403_c0_seq9.p1	A0A1Q9DEP8	Pentatricopeptide repeat-containing protein	Symbiodinium microadriaticum	1.90E-99	811
comp34508_c0_seq1.p1	Q40296	Fucoxanthin-chlorophyll a-c binding protein B	Macrocystis pyrifera	3.00E-37	136

comp34988_c0_seq4.p1	Q9XQV2	Photosystem I P700 chlorophyll a apoprotein A2	Heterocapsa triquetra	0	758
comp35082_c0_seq2.p1	Q85FP8	Photosystem I reaction center subunit XI	Cyanidioschyzon merolae	8.00E-25	101
comp35507_c1_seq1.p1	Q40300	Fucoxanthin-chlorophyll a-c binding protein F	Macrocystis pyrifera	5.00E-39	137
comp36223_c0_seq1.p2	P49481	Photosystem I reaction center subunit II	Trieres chinensis	7.00E-44	149
comp36254_c0_seq1.p1	Q40301	Fucoxanthin-chlorophyll a-c binding protein E	Macrocystis pyrifera	4.00E-27	112
comp36318_c0_seq10.p1	Q40300	Fucoxanthin-chlorophyll a-c binding protein F	Macrocystis pyrifera	1.00E-34	131
comp36452_c0_seq1.p1	Q41093	Fucoxanthin-chlorophyll a-c binding protein E	Phaeodactylum tricornutum	2.00E-10	62.4
comp36527_c0_seq1.p1	Q9SYW8	Photosystem I chlorophyll a/b-binding protein 2	Arabidopsis thaliana	7.00E-13	72
comp36596_c0_seq2.p1	Q40300	Fucoxanthin-chlorophyll a-c binding protein F	Macrocystis pyrifera	4.00E-34	125
comp36606_c0_seq1.p1	Q95AG0	Cytochrome f	Chlamydomonas subcaudata	4.00E-102	309
comp36624_c1_seq8.p1	Q40300	Fucoxanthin-chlorophyll a-c binding protein F	Macrocystis pyrifera	4.00E-39	140
comp36753_c0_seq4.p1	P85194	Oxygen-evolving enhancer protein 1, chloroplastic	Helianthus annuus	2.00E-64	210
comp36951_c0_seq2.p1	P51874	Peridinin-chlorophyll a-binding protein, chloroplastic	Symbiodinium sp.	0	540
comp36965_c0_seq1.p1	Q40297	Fucoxanthin-chlorophyll a-c binding protein A	Macrocystis pyrifera	8.00E-21	91.3
comp36978_c0_seq1.p1	P51874	Peridinin-chlorophyll a-binding protein, chloroplastic	Symbiodinium sp.	0	542
comp37113_c0_seq2.p1	Q41406	Ribulose bisphosphate carboxylase (Fragment)	Symbiodinium sp.	0	1067
comp37163_c0_seq1.p2	Q40300	Fucoxanthin-chlorophyll a-c binding protein F	Macrocystis pyrifera	2.00E-31	116
comp37683_c0_seq1.p2	Q40297	Fucoxanthin-chlorophyll a-c binding protein A	Macrocystis pyrifera	1.00E-36	129
comp37712_c0_seq1.p1	P13869	Chlorophyll a-b binding protein, chloroplastic	Petunia hybrida	6.00E-13	72
comp37993_c0_seq1.p1	Q40300	Fucoxanthin-chlorophyll a-c binding protein F	Macrocystis pyrifera	2.00E-18	81.6
comp38528_c0_seq1.p1	Q00610	Clathrin heavy chain 1	Homo sapiens	0	1753
comp39453_c0_seq1.p1	Q00598	Ferredoxin--NADP reductase, cyanelle	Cyanophora paradoxa	3.00E-63	207

comp39674_c0_seq1.p1	A0A1Q9EFI4	Light-harvesting complex I LH38 protein	Symbiodinium microadriaticum	6.40E-82	693
comp41757_c0_seq1.p1	P55738	Caroteno-chlorophyll a-c-binding protein (Fragment)	Amphidinium carterae	2.00E-26	99
comp45326_c0_seq1.p1	Q40297	Fucoxanthin-chlorophyll a-c binding protein A	Macrocystis pyrifera	2.00E-34	126
comp8282_c0_seq1.p1	Q41093	Fucoxanthin-chlorophyll a-c binding protein E	Phaeodactylum tricornutum	4.00E-15	73.9
comp10356_c0_seq1.p1	A0A1Q9EML6	TBC domain-containing protein C4G8.04	Symbiodinium microadriaticum	0	2,264
comp18766_c0_seq1.p2	A0A1Q9E982	Kinase D-interacting substrate of 220 kDa	Symbiodinium microadriaticum	3.00E-27	289
comp26217_c0_seq4.p1	A0A1Q9CKC1	Bifunctional lysine-specific demethylase and histidyl-hydroxylase NO66	Symbiodinium microadriaticum	9.30E-47	438
comp26771_c0_seq1.p1	P83373	Malate dehydrogenase, mitochondrial	Fragaria ananassa	4.00E-111	330
comp27837_c0_seq1.p1	P06541	ATP synthase subunit beta	Chlamydomonas reinhardtii	9.00E-123	361
comp29404_c0_seq1.p1	Q9EPH8	Polyadenylate-binding protein 1	Rattus norvegicus	6.00E-140	423
comp30829_c0_seq1.p1	Q9C5M0	Mitochondrial dicarboxylate/tricarboxylate transporter DTC	Arabidopsis thaliana	1.00E-95	288
comp31051_c0_seq1.p1	Q9I2V5	Aconitate hydratase B	Pseudomonas aeruginosa	0	1220
comp32089_c0_seq1.p3	Q01238	Major basic nuclear protein 2	Crypthecodinium cohnii	1.00E-20	82.4
comp34766_c0_seq1.p1	L7HV32	Urea amidolyase	Magnaporthe oryzae	3.40E-12	204
comp34939_c0_seq2.p1	Q54E49	Probable ATP-dependent RNA helicase ddx6	Dictyostelium discoideum	0	652
comp35538_c0_seq1.p1	O02494	Eukaryotic initiation factor 4A	Cryptosporidium parvum	0	564
comp8310_c0_seq1.p1	Q9EPH8	Polyadenylate-binding protein 1	Rattus norvegicus	1.00E-165	489

Proteins characterized via the NCBI-BLAST algorithm against the Uniprot KB Swiss-Prot database. In instances where an annotation could not be achieved using the Swill-Prot database, the protein sequence was BLASTed against the entire Uniprot KB database (i.e., Swiss-Prot and TrEMBL)

Table S2. List of proteins, GO terms, and functional groups used for analyses.

sequence ID'd	Uniprot accesion	species	protein name	GO term	GO ID	Functional group	Immune modulatory?
comp11356_c0_seq1.p1	Q42971	Oryza sativa	Enolase	glycolytic process	GO:0006096	Adhesion	✓
comp18414_c0_seq5.p1	Q9BPL7	Toxoplasma gondii	Enolase 2	glycolytic process	GO:0006096	Adhesion	✓
comp29485_c0_seq1.p1	Q9PVK2	Alligator mississippiensis	Alpha-enolase	glycolytic process	GO:0006096	Adhesion	✓
comp29838_c0_seq2.p1	Q8IJN7	Plasmodium falciparum	Enolase	glycolytic process	GO:0006096	Adhesion	✓
comp33094_c0_seq4.p1	P15623	Bacteroides fragilis	Glutamine synthetase	nitrogen compound metabolic process	GO:0006807	Adhesion	✘
comp33801_c0_seq4.p1	P48495	Petunia hybrida	Triosephosphate isomerase	glycolytic process	GO:0006096	Adhesion	✘
comp34391_c0_seq1.p1	P51903	Gallus gallus	Phosphoglycerate kinase	glycolytic process	GO:0006096	Adhesion	✘
comp36464_c0_seq1.p1	P15623	Bacteroides fragilis	Glutamine synthetase	nitrogen compound metabolic process	GO:0006807	Adhesion	✘
comp36757_c0_seq1.p1	P90519	Cryptosporidium parvum	Elongation factor 1-alpha	translational elongation	GO:0006414	Adhesion	✘
comp37011_c1_seq2.p1	Q12613	Colletotrichum gloeosporioides	Glutamine synthetase	nitrogen compound metabolic process	GO:0006807	Adhesion	✘
comp37015_c0_seq2.p1	P22513	Trypanosoma cruzi	Glyceraldehyde-3-phosphate dehydrogenase, glycosomal	glycolytic process	GO:0006096	Adhesion	✘
comp37083_c0_seq2.p1	O59841	Ogataea parapolymorpha	Glyceraldehyde-3-phosphate dehydrogenase	glycolytic process	GO:0006096	Adhesion	✘
comp37351_c0_seq1.p2	O77458	Drosophila yakuba	Triosephosphate isomerase	glycolytic process	GO:0006096	Adhesion	✘
comp37849_c0_seq1.p1	P30741	Culex tarsalis	Triosephosphate isomerase	glycolytic process	GO:0006096	Adhesion	✘
comp61911_c0_seq1.p1	H8WB07	Marinobacter hydrocarbonoclasticus	Major outer membrane lipoprotein	lipid modification	GO:0030258	Cell structure	✓
comp1748_c0_seq1.p2	P02576	Physarum polycephalum	Actin	cytoskeleton	GO:0005856	Cell structure	✘
comp24819_c0_seq1.p1	P33188	Paramecium tetraurelia	Tubulin beta chain	structural constituent of cytoskeleton	GO:0005200	Cell structure	✘
comp33420_c0_seq2.p1	A0A1Q9E298	Symbiodinium microadriaticum	Collagen alpha-1(XVII) chain	cell-matrix adhesion	GO:0007160	Cell structure	✘

comp35046_c0_seq3.p2	P26182	Achlya bisexualis	Actin	cytoskeleton	GO:0005856	Cell structure	✘
comp36850_c0_seq5.p1	P41352	Tetrahymena thermophila	Tubulin beta chain	structural constituent of cytoskeleton	GO:0005200	Cell structure	✘
comp37027_c0_seq2.p1	P33188	Paramecium tetraurelia	Tubulin beta chain	structural constituent of cytoskeleton	GO:0005200	Cell structure	✘
comp37107_c0_seq1.p1	P11481	Volvox carteri	Tubulin alpha-1/alpha-2 chain	structural constituent of cytoskeleton	GO:0005200	Cell structure	✘
comp37901_c0_seq1.p1	A0A1Q9E298	Symbiodinium microadriaticum	Collagen alpha-1(XVII) chain	cell-matrix adhesion	GO:0007160	Cell structure	✘
comp35964_c0_seq3.p1	P9WPJ9	Mycobacterium tuberculosis	Carbonic anhydrase 2	carbon utilization	GO:0015976	CO2 uptake	✘
comp36098_c0_seq3.p1	P9WPJ9	Mycobacterium tuberculosis	Carbonic anhydrase 2	carbon utilization	GO:0015976	CO2 uptake	✘
comp25655_c0_seq1.p1	Q25117	Hemicentrotus pulcherrimus	ATP synthase subunit beta	ATP synthesis coupled proton transport	GO:0015986	Extracellular ATP	✓
comp27837_c0_seq1.p1	P06541	Chlamydomonas reinhardtii	ATP synthase subunit beta	ATP synthesis coupled proton transport	GO:0015986	Extracellular ATP	✓
comp34697_c0_seq1.p1	Q06J29	Bigelowiella natans	ATP synthase subunit beta	ATP synthesis coupled proton transport	GO:0015986	Extracellular ATP	✓
comp36516_c0_seq2.p1	B1XHY7	Synechococcus sp.	ATP synthase gamma chain	ATP synthesis coupled proton transport	GO:0015986	Extracellular ATP	✓
comp36952_c0_seq2.p1	A0A1Q9DKL5	Symbiodinium microadriaticum	ATP synthase gamma chain	ATP synthesis coupled proton transport	GO:0015986	Extracellular ATP	✓
comp37979_c0_seq1.p1	P10719	Rattus norvegicus	ATP synthase subunit beta	ATP synthesis coupled proton transport	GO:0015986	Extracellular ATP	✓
comp38541_c0_seq1.p1	P19483	Bos taurus	ATP synthase subunit alpha, mitochondrial	ATP synthesis coupled proton transport	GO:0015986	Extracellular ATP	✓
comp35093_c0_seq2.p2	Q3MDW2	Anabaena variabilis	Cytochrome c6	electron transport chain	GO:0022900	Extracellular redox	✓
comp35869_c0_seq6.p2	A0T0C6	Phaeodactylum tricornutum	Cytochrome c-550	respiratory electron transport chain	GO:0022904	Extracellular redox	✓
comp39261_c0_seq1.p1	P09622	Homo sapiens	Dihydrolipoyl dehydrogenase	regulation of membrane potential	GO:0042391	Extracellular redox	✘

comp18413_c0_seq1.p1	O13755	Schizosaccharomyces pombe	Fumarate reductase	oxidation-reduction process	GO:0055114	Extracellular redox	✘
comp22274_c0_seq2.p1	O13755	Schizosaccharomyces pombe	Fumarate reductase	oxidation-reduction process	GO:0055114	Extracellular redox	✘
comp33055_c0_seq2.p1	Q6DAY3	Pectobacterium atrosepticum	L-lactate dehydrogenase	oxidation-reduction process	GO:0055114	Extracellular redox	✘
comp33468_c0_seq1.p1	Q5ATG5	Emericella nidulans	Acyl-CoA dehydrogenase apdG	oxidation-reduction process	GO:0055114	Extracellular redox	✘
comp36145_c0_seq1.p1	O13755	Schizosaccharomyces pombe	Fumarate reductase	oxidation-reduction process	GO:0055114	Extracellular redox	✘
comp36454_c0_seq1.p1	P46436	Ascaris suum	Glutathione S-transferase	oxidation-reduction process	GO:0055114	Extracellular redox	✘
comp36488_c0_seq5.p1	O13755	Schizosaccharomyces pombe	Fumarate reductase	oxidation-reduction process	GO:0055114	Extracellular redox	✘
comp37134_c0_seq1.p1	Q968X7	Cryptosporidium parvum	Pyruvate dehydrogenase [NADP(+)]	oxidation-reduction process	GO:0055114	Extracellular redox	✘
comp11845_c0_seq1.p1	P42644	Arabidopsis thaliana	14-3-3-like protein GF14 psi	protein binding	GO:0005515	Extracellular signal transduction	✓
comp14901_c0_seq1.p1	Q52I78	Sus scrofa	Nicotinamide phosphoribosyltransferase	NAD biosynthetic process	GO:0009435	Extracellular signal transduction	✓
comp33615_c1_seq2.p1	P19848	Coprinellus congregatus	Ubiquitin	protein ubiquitination	GO:0016567	Extracellular signal transduction	✓
comp35699_c0_seq1.p1	Q9STD3	Chlamydomonas reinhardtii	Calreticulin	protein folding	GO:0006457	Extracellular signal transduction	✓
comp36800_c0_seq1.p1	P42644	Arabidopsis thaliana	14-3-3-like protein GF14 psi	protein binding	GO:0005515	Extracellular signal transduction	✓
comp8899_c0_seq1.p1	P72332	Rhizobium sp. (strain N33)	Nodulation protein G	nodulation	GO:0009877	Extracellular signal transduction	✓
comp29762_c0_seq1.p1	A0A1Q9EEJ5	Symbiodinium microadriaticum	Developmentally-regulated G-protein 2	GTPase activity	GO:0003924	Extracellular signal transduction	✘

comp35990_c0_seq1.p1	P54774	Glycine max	Cell division cycle protein 48 homolog	cell cycle	GO:0007049	Extracellular signal transduction	✘
comp36444_c0_seq1.p2	A0A1Q9EHJ8	Symbiodinium microadriaticum	Serine/threonine-protein phosphatase	protein dephosphorylation	GO:0006470	Extracellular signal transduction	✘
comp37477_c0_seq1.p1	Q03498	Plasmodium falciparum	V-type proton ATPase catalytic subunit A	proton transmembrane transport	GO:1902600	Ion homeostasis	✓
comp18453_c0_seq2.p1	Q8F641	Leptospira interrogans	Putative K(+)-stimulated pyrophosphate-energized sodium pump	proton transmembrane transport	GO:1902600	Ion homeostasis	✘
comp16455_c0_seq1.p2	Q39613	Catharanthus roseus	Peptidyl-prolyl cis-trans isomerase	protein folding	GO:0006457	protein folding	✓
comp18648_c0_seq1.p1	A0A1Q9D1J9	Symbiodinium microadriaticum	Protein disulfide-isomerase	isomerase activity	GO:0016853	protein folding	✓
comp23514_c0_seq4.p1	Q6Z7B0	Oryza sativa	Heat shock 70 kDa protein	cellular response to unfolded protein	GO:0034620	protein folding	✓
comp24965_c0_seq1.p1	P54651	Dictyostelium discoideum	Heat shock cognate 90 kDa protein	protein folding	GO:0006457	protein folding	✓
comp33298_c0_seq4.p1	P19208	Caenorhabditis briggsae	Heat shock 70 kDa protein C	cellular response to unfolded protein	GO:0034620	protein folding	✓
comp36621_c0_seq5.p1	O44001	Eimeria tenella	Heat shock protein 90	protein folding	GO:0006457	protein folding	✓
comp36855_c0_seq1.p1	Q90474	Danio rerio	Heat shock protein HSP 90-alpha 1	protein folding	GO:0006457	protein folding	✓
comp36920_c0_seq4.p1	A0A1Q9EKM5	Symbiodinium microadriaticum	Peptidyl-prolyl cis-trans isomerase	protein folding	GO:0006457	protein folding	✓
comp36948_c0_seq1.p1	P11144	Plasmodium falciparum	Heat shock 70 kDa protein	cellular response to unfolded protein	GO:0034620	protein folding	✓
comp36974_c0_seq1.p1	Q9LTX9	Arabidopsis thaliana	Heat shock 70 kDa protein 7	cellular response to unfolded protein	GO:0034620	protein folding	✓
comp37297_c0_seq1.p1	P24724	Theileria parva	Heat shock protein 90	protein folding	GO:0006457	protein folding	✓
comp38944_c0_seq1.p1	P42693	Acinetobacter baylyi	Peptidyl-prolyl cis-trans isomerase	protein folding	GO:0006457	protein folding	✓
comp7486_c0_seq1.p1	P37900	Pisum sativum	Heat shock 70 kDa protein	cellular response to unfolded protein	GO:0034620	protein folding	✓
comp8280_c0_seq1.p1	Q05046	Cucurbita maxima	Chaperonin CPN60-2, mitochondrial	protein folding	GO:0006457	protein folding	✓
comp34171_c0_seq1.p1	P25248	Brassica napus	Isocitrate lyase	glyoxylate cycle	GO:0006097	Unknown	✘

comp18185_c0_seq1.p1	Q02909	Glycine max	Phosphoenolpyruvate carboxylase, housekeeping isozyme	tricarboxylic acid cycle	GO:0006099	Unknown	✘
comp22970_c0_seq1.p1	Q91V92	Mus musculus	ATP-citrate synthase	fatty acid biosynthetic process	GO:0006633	unknown	✘
comp30131_c0_seq1.p1	Q75JD5	Dictyostelium discoideum	Phosphoenolpyruvate carboxykinase (ATP)	tricarboxylic acid cycle	GO:0006099	Unknown	✘
comp30984_c0_seq1.p1	Q91V92	Mus musculus	ATP-citrate synthase	fatty acid biosynthetic process	GO:0006633	unknown	✘
comp31713_c0_seq1.p1	Q8VCH0	Mus musculus	3-ketoacyl-CoA thiolase B, peroxisomal	fatty acid metabolic process	GO:0006631	unknown	✘
comp31985_c0_seq1.p2	Q6SYB9	Nicotiana tabacum	S-adenosylmethionine synthase 2	S-adenosylmethionine biosynthetic process	GO:0006556	Unknown	✘
comp35289_c0_seq2.p1	Q23716	Cryptosporidium parvum	Elongation factor 2	translational elongation	GO:0006414	Unknown	✘
comp37675_c0_seq1.p1	Q6ZDY8	Oryza sativa	Succinate dehydrogenase [ubiquinone] flavoprotein subunit	tricarboxylic acid cycle	GO:0006099	Unknown	✘
comp38011_c0_seq1.p1	Q75JD5	Dictyostelium discoideum	Phosphoenolpyruvate carboxykinase (ATP)	tricarboxylic acid cycle	GO:0006099	Unknown	✘
comp38376_c0_seq1.p1	Q84LB6	Solanum lycopersicum	Succinate--CoA ligase [ADP-forming] subunit beta	tricarboxylic acid cycle	GO:0006099	Unknown	✘
comp8484_c0_seq1.p2	P09110	Homo sapiens	3-ketoacyl-CoA thiolase	fatty acid metabolic process	GO:0006631	unknown	✘

GO terms obtained from Gene Ontology databases. Literature searches were conducted by providing the search term, "extracellular", "secreted", or "cell surface" before the protein name.

Table S3. List of proteins, GO terms, mechanism, and references for immune modulatory proteins.

Immune modulation	*B. psyg* sequence	protein name	GO term	GO ID	Immune modulation Mechanism	Reference
Activation	comp11845_c0_seq1.p1	14-3-3-like protein GF14 psi	protein binding	GO:0005515	Promotes phagocytosis/inflammation	Ulvila J, Vanha-aho LM, Kleino A, Va¨ha¨-Ma¨kila¨ M,Vuoksio M, Eskelinen S, Hultmark D, Kocks C, Hallman M, Parikka M, Ra¨met M (2011) Cofilin regulator 14-3-3 is an evolutionarily conserved protein required for phagocytosis and microbial resistance. J Leukoc Biol 89: 649 - 659 Schuster TB, Costina V, Findeisen P, Neumaier M, Ahmad-Nejad P (2011) Identification and Functional Characterization of 14-3-3 in TLR2 Signaling. J Proteome Res 10: 4661 - 4670
	comp36800_c0_seq1.p1	14-3-3-like protein GF14 psi	protein binding	GO:0005515	Promotes phagocytosis/inflammation	Ulvila J, Vanha-aho LM, Kleino A, Va¨ha¨-Ma¨kila¨ M,Vuoksio M, Eskelinen S, Hultmark D, Kocks C, Hallman M, Parikka M, Ra¨met M (2011) Cofilin regulator 14-3-3**ζ** is an evolutionarily conserved protein required for phagocytosis and microbial resistance. J Leukoc Biol 89: 649 - 659 Schuster TB, Costina V, Findeisen P, Neumaier M, Ahmad-Nejad P (2011) Identification and Functional Characterization of 14-3-3 in TLR2 Signaling. J Proteome Res 10: 4661 - 4670
	comp29485_c0_seq1.p1	Alpha-enolase	glycolytic process	GO:0006096	Promotes inflammation	Sawhney S, Hood K, Shaw A, Braithwaite AW, Stubbs R, Hung NA, Royds JA, Slatter TL (2015) Alpha-Enolase Is Upregulated on the Cell Surface and Responds to Plasminogen Activation in Mice Expressing a Δ133p53α Mimic. PLoS ONE 10(2): e0116270. doi:10.1371/journal.pone.0116270

comp35699_c0_seq1.p1	Calreticulin	protein folding	GO:0006457	DAMP/promotes phagocytosis	Tufi R, Panaretakis T, Bianchi K, Criollo A, Fazi B, Di Sano F, Tesniere A, Kepp O, Paterlini-Brechot P, Zitvogel L, Piacentini M, Szabadkai G, Kroemer G (2008) Reduction of endoplasmic reticulum Ca2+ levels favors plasma membrane surface exposure of calreticulin. Cell Death Differ 15: 274 - 282
comp8280_c0_seq1.p1	Chaperonin CPN60-2, mitochondrial	protein folding	GO:0006457	Promotes inflammation	Hu Y, Henderson B, Lund PA, Tormay P, Ahmed MT, Gurcha SS, Besra GS, Coates AR (2008) A Mycobacterium tuberculosis mutant lacking the groEL homologue cpn60.1 is viable but fails to induce an inflammatory response in animal models of infection. Infect Immun 76: 1535 - 1546
comp35869_c0_seq6.p2	Cytochrome c-550	respiratory electron transport chain	GO:0022904	DAMP/promotes apoptosis/promotes ROS production/promotes inflammation	Renz A, Berdel WE, Kreuter M, Belka C, Schulze-Osthoff K, Los M (2001) Rapid extracellular release of cytochrome c is specific for apoptosis and marks cell death in vivo. Blood 98: 1542 - 1548
comp35093_c0_seq2.p2	Cytochrome c6	electron transport chain	GO:0022900	DAMP/promotes apoptosis/promotes ROS production/promotes inflammation	Renz A, Berdel WE, Kreuter M, Belka C, Schulze-Osthoff K, Los M (2001) Rapid extracellular release of cytochrome c is specific for apoptosis and marks cell death in vivo. Blood 98: 1542 - 1548
comp11356_c0_seq1.p1	Enolase	glycolytic process	GO:0006096	Promotes inflammation	Sawhney S, Hood K, Shaw A, Braithwaite AW, Stubbs R, Hung NA, Royds JA, Slatter TL (2015) Alpha-Enolase Is Upregulated on the Cell Surface and Responds to Plasminogen Activation in Mice Expressing a Δ133p53α Mimic. PLoS ONE 10(2): e0116270. doi:10.1371/journal.pone.0116270

comp29838_c0_seq2.p1	Enolase	glycolytic process	GO:0006096	Promotes inflammation	Sawhney S, Hood K, Shaw A, Braithwaite AW, Stubbs R, Hung NA, Royds JA, Slatter TL (2015) Alpha-Enolase Is Upregulated on the Cell Surface and Responds to Plasminogen Activation in Mice Expressing a Δ133p53α Mimic. PLoS ONE 10(2): e0116270. doi:10.1371/journal.pone.0116270
comp18414_c0_seq5.p1	Enolase 2	glycolytic process	GO:0006096	Promotes inflammation	Sawhney S, Hood K, Shaw A, Braithwaite AW, Stubbs R, Hung NA, Royds JA, Slatter TL (2015) Alpha-Enolase Is Upregulated on the Cell Surface and Responds to Plasminogen Activation in Mice Expressing a Δ133p53α Mimic. PLoS ONE 10(2): e0116270. doi:10.1371/journal.pone.0116270
comp23514_c0_seq4.p1	Heat shock 70 kDa protein	cellular response to unfolded protein	GO:0034620	Promotes phagocytosis	Fredly H, Ersvær E, Gjertsen BT, Bruserud O (2011) Immunogenic apoptosis in human acute myeloid leukemia (AML): primary human AML cells expose calreticulin and release heat shock protein (HSP) 70 and HSP90 during apoptosis. Oncol Rep 25: 1549 - 1556
comp36948_c0_seq1.p1	Heat shock 70 kDa protein	cellular response to unfolded protein	GO:0034620	Promotes phagocytosis	Fredly H, Ersvær E, Gjertsen BT, Bruserud O (2011) Immunogenic apoptosis in human acute myeloid leukemia (AML): primary human AML cells expose calreticulin and release heat shock protein (HSP) 70 and HSP90 during apoptosis. Oncol Rep 25: 1549 - 1556
comp7486_c0_seq1.p1	Heat shock 70 kDa protein	cellular response to unfolded protein	GO:0034620	Promotes phagocytosis	Fredly H, Ersvær E, Gjertsen BT, Bruserud O (2011) Immunogenic apoptosis in human acute myeloid leukemia (AML): primary human AML cells expose calreticulin and release heat shock protein (HSP) 70 and HSP90 during apoptosis. Oncol Rep 25: 1549 - 1556

comp36974_c0_seq1.p1	Heat shock 70 kDa protein 7	cellular response to unfolded protein	GO:0034620	Promotes phagocytosis	Fredly H, Ersvær E, Gjertsen BT, Bruserud O (2011) Immunogenic apoptosis in human acute myeloid leukemia (AML): primary human AML cells expose calreticulin and release heat shock protein (HSP) 70 and HSP90 during apoptosis. Oncol Rep 25: 1549 - 1556
comp33298_c0_seq4.p1	Heat shock 70 kDa protein C	cellular response to unfolded protein	GO:0034620	Promotes phagocytosis	Fredly H, Ersvær E, Gjertsen BT, Bruserud O (2011) Immunogenic apoptosis in human acute myeloid leukemia (AML): primary human AML cells expose calreticulin and release heat shock protein (HSP) 70 and HSP90 during apoptosis. Oncol Rep 25: 1549 - 1556
comp24965_c0_seq1.p1	Heat shock cognate 90 kDa protein	protein folding	GO:0006457	Promotes phagocytosis	Fredly H, Ersvær E, Gjertsen BT, Bruserud O (2011) Immunogenic apoptosis in human acute myeloid leukemia (AML): primary human AML cells expose calreticulin and release heat shock protein (HSP) 70 and HSP90 during apoptosis. Oncol Rep 25: 1549 - 1556
comp36621_c0_seq5.p1	Heat shock protein 90	protein folding	GO:0006457	Promotes phagocytosis	Fredly H, Ersvær E, Gjertsen BT, Bruserud O (2011) Immunogenic apoptosis in human acute myeloid leukemia (AML): primary human AML cells expose calreticulin and release heat shock protein (HSP) 70 and HSP90 during apoptosis. Oncol Rep 25: 1549 - 1556
comp37297_c0_seq1.p1	Heat shock protein 90	protein folding	GO:0006457	Promotes phagocytosis	Fredly H, Ersvær E, Gjertsen BT, Bruserud O (2011) Immunogenic apoptosis in human acute myeloid leukemia (AML): primary human AML cells expose calreticulin and release heat shock protein (HSP) 70 and HSP90 during apoptosis. Oncol Rep 25: 1549 - 1556

	comp36855_c0_seq1.p1	Heat shock protein HSP 90-alpha 1	protein folding	GO:0006457	Promotes phagocytosis	Fredly H, Ersvær E, Gjertsen BT, Bruserud O (2011) Immunogenic apoptosis in human acute myeloid leukemia (AML): primary human AML cells expose calreticulin and release heat shock protein (HSP) 70 and HSP90 during apoptosis. Oncol Rep 25: 1549 - 1556
	comp61911_c0_seq1.p1	Major outer membrane lipoprotein	lipid modification	GO:0030258	Promotes inflammation	Vidal V, Scragg IG, Cutler SJ, Rockett KA, Fekade D, Warrell DA, Wright DJ, Kwiatkowski D (1998) Variable major lipoprotein is a principal TNF-inducing factor of louse-borne relapsing fever. Nat Med. 4: 1416 - 1420
	comp8899_c0_seq1.p1	Nodulation protein G	nodulation	GO:0009877	Promotes phagocytosis	Oldroyd GE, Downie JA (2004) Calcium, kinases and nodulation signalling in legumes. Nat Rev Mol Cell Biol 5:566 – 76
	comp18648_c0_seq1.p1	Protein disulfide-isomerase	isomerase activity	GO:0016853	Promotes phagocytosis	Stolf BS, Smyrnias I, Lopes LR, Vendramin A, Goto H, Laurindo FR, Shah AM, Santos CX (2011) Protein disulfide isomerase and host-pathogen interaction. ScientificWorldJournal 11: 1749 - 1761
Regulation	comp36516_c0_seq2.p1	ATP synthase gamma chain	ATP synthesis coupled proton transport	GO:0015986	Promotes inflammation or suppresses immunity	Idzko M, Hammad H, van Nimwegen M, Kool M, Willart MA, Muskens F, Hoogsteden HC, Luttmann W, Ferrari D, Di Virgilio F, Virchow JC, Lambrecht BN (2007) Extracellular ATP triggers and maintains asthmatic airway inflammation by activating dendritic cells. Nat Med 13: 913 - 919 Chivasa S, Murphy AM, Hamilton JM, Lindsey K, Carr JP, Slabas AR (2009) Extracellular ATP is a regulator of pathogen defence in plants. Plant J. 60: 436 - 448

comp36952_c0_seq2.p1	ATP synthase gamma chain	ATP synthesis coupled proton transport	GO:0015986	Promotes inflammation or suppresses immunity	Idzko M, Hammad H, van Nimwegen M, Kool M, Willart MA, Muskens F, Hoogsteden HC, Luttmann W, Ferrari D, Di Virgilio F, Virchow JC, Lambrecht BN (2007) Extracellular ATP triggers and maintains asthmatic airway inflammation by activating dendritic cells. Nat Med 13: 913 - 919 Chivasa S, Murphy AM, Hamilton JM, Lindsey K, Carr JP, Slabas AR (2009) Extracellular ATP is a regulator of pathogen defence in plants. Plant J. 60: 436 - 448
comp38541_c0_seq1.p1	ATP synthase subunit alpha, mitochondrial	ATP synthesis coupled proton transport	GO:0015986	Promotes inflammation or suppresses immunity	Idzko M, Hammad H, van Nimwegen M, Kool M, Willart MA, Muskens F, Hoogsteden HC, Luttmann W, Ferrari D, Di Virgilio F, Virchow JC, Lambrecht BN (2007) Extracellular ATP triggers and maintains asthmatic airway inflammation by activating dendritic cells. Nat Med 13: 913 - 919 Chivasa S, Murphy AM, Hamilton JM, Lindsey K, Carr JP, Slabas AR (2009) Extracellular ATP is a regulator of pathogen defence in plants. Plant J. 60: 436 - 448
comp25655_c0_seq1.p1	ATP synthase subunit beta	ATP synthesis coupled proton transport	GO:0015986	Promotes inflammation or suppresses immunity	Idzko M, Hammad H, van Nimwegen M, Kool M, Willart MA, Muskens F, Hoogsteden HC, Luttmann W, Ferrari D, Di Virgilio F, Virchow JC, Lambrecht BN (2007) Extracellular ATP triggers and maintains asthmatic airway inflammation by activating dendritic cells. Nat Med 13: 913 - 919 Chivasa S, Murphy AM, Hamilton JM, Lindsey K, Carr JP, Slabas AR (2009) Extracellular ATP is a regulator of pathogen defence in plants. Plant J. 60: 436 - 448

comp27837_c0_seq1.p1	ATP synthase subunit beta	ATP synthesis coupled proton transport	GO:0015986	Promotes inflammation or suppresses immunity	Idzko M, Hammad H, van Nimwegen M, Kool M, Willart MA, Muskens F, Hoogsteden HC, Luttmann W, Ferrari D, Di Virgilio F, Virchow JC, Lambrecht BN (2007) Extracellular ATP triggers and maintains asthmatic airway inflammation by activating dendritic cells. Nat Med 13: 913 - 919 Chivasa S, Murphy AM, Hamilton JM, Lindsey K, Carr JP, Slabas AR (2009) Extracellular ATP is a regulator of pathogen defence in plants. Plant J. 60: 436 - 448
comp34697_c0_seq1.p1	ATP synthase subunit beta	ATP synthesis coupled proton transport	GO:0015986	Promotes inflammation or suppresses immunity	Idzko M, Hammad H, van Nimwegen M, Kool M, Willart MA, Muskens F, Hoogsteden HC, Luttmann W, Ferrari D, Di Virgilio F, Virchow JC, Lambrecht BN (2007) Extracellular ATP triggers and maintains asthmatic airway inflammation by activating dendritic cells. Nat Med 13: 913 - 919 Chivasa S, Murphy AM, Hamilton JM, Lindsey K, Carr JP, Slabas AR (2009) Extracellular ATP is a regulator of pathogen defence in plants. Plant J. 60: 436 - 448
comp37979_c0_seq1.p1	ATP synthase subunit beta	ATP synthesis coupled proton transport	GO:0015986	Promotes inflammation or suppresses immunity	Idzko M, Hammad H, van Nimwegen M, Kool M, Willart MA, Muskens F, Hoogsteden HC, Luttmann W, Ferrari D, Di Virgilio F, Virchow JC, Lambrecht BN (2007) Extracellular ATP triggers and maintains asthmatic airway inflammation by activating dendritic cells. Nat Med 13: 913 - 919 Chivasa S, Murphy AM, Hamilton JM, Lindsey K, Carr JP, Slabas AR (2009) Extracellular ATP is a regulator of pathogen defence in plants. Plant J. 60: 436 - 448
comp36920_c0_seq4.p1	Peptidyl-prolyl cis-trans isomerase	protein folding	GO:0006457	Context-dependent	Ünal CM, Steinert M (2014) Microbial peptidyl-prolyl cis/trans isomerases (PPIases): virulence factors and potential alternative drug targets. Microbiol Mol Biol Rev. 78: 544 - 571

	comp16455_c0_seq1.p2	Peptidyl-prolyl cis-trans isomerase	protein folding	GO:0006457	Context-dependent	Ünal CM, Steinert M (2014) Microbial peptidyl-prolyl cis/trans isomerases (PPIases): virulence factors and potential alternative drug targets. Microbiol Mol Biol Rev. 78: 544 - 571
	comp38944_c0_seq1.p1	Peptidyl-prolyl cis-trans isomerase	protein folding	GO:0006457	Context-dependent	Ünal CM, Steinert M (2014) Microbial peptidyl-prolyl cis/trans isomerases (PPIases): virulence factors and potential alternative drug targets. Microbiol Mol Biol Rev. 78: 544 - 571
	comp33615_c1_seq2.p1	Ubiquitin	protein ubiquitination	GO:0016567	modulatory roles	Majetschak M (2011) Extracellular ubiquitin: immune modulator and endogenous opponent of damage-associated molecular pattern molecules. J Leukoc Biol 89: 205 - 219
Suppression	comp14901_c0_seq1.p1	Nicotinamide phosphoribosyltransferase	NAD biosynthetic process	GO:0009435	Suprress effector responses	Audrito V, Serra S, Brusa D, Mazzola F, Arruga F, Vaisitti T, Coscia M, Maffei R, Rossi D, Wang T, Inghirami G, Rizzi M, Gaidano G, Garcia JG, Wolberger C, Raffaelli N, Deaglio S. (2015) Extracellular nicotinamide phosphoribosyltransferase (NAMPT) promotes M2 macrophage polarization in chronic lymphocytic leukemia. Blood 125: 111 - 123

GO terms obtained from Gene Ontology databases. Literature searches were conducted by providing the search term, "extracellular", "secreted", or "cell surface" before the protein name.

FIGURES

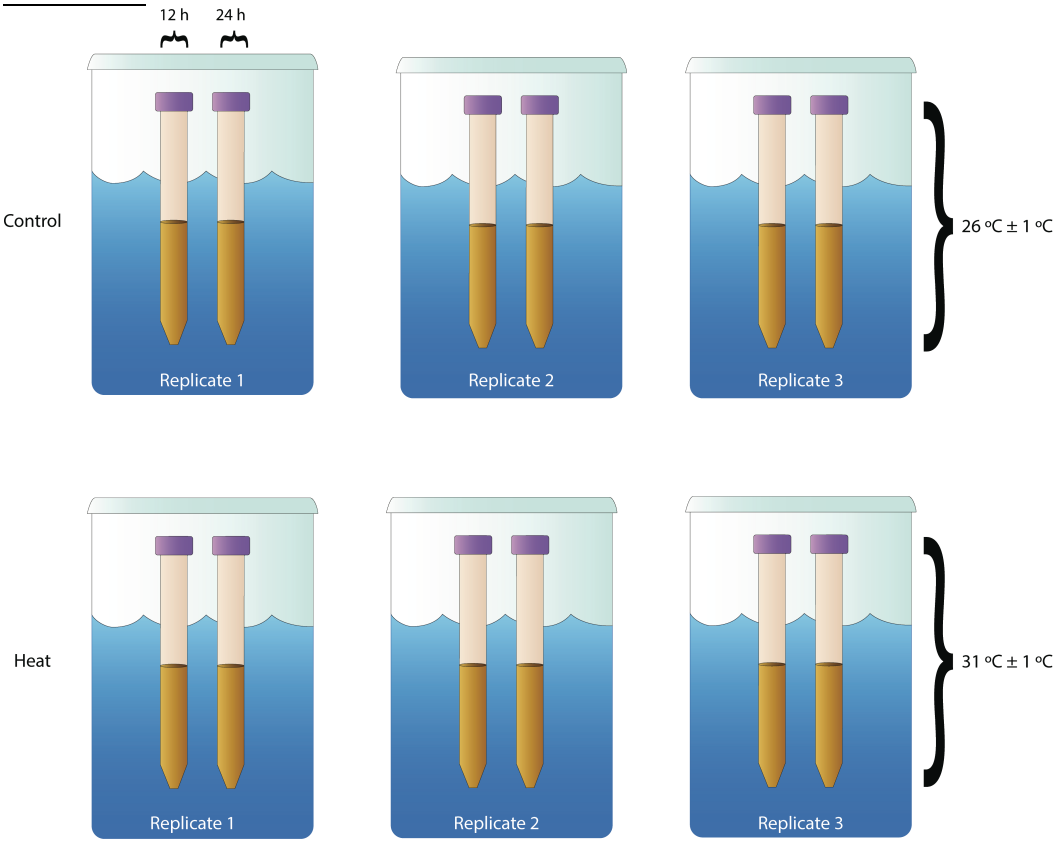

Fig S1 *Diagram illustrating experimental setup. 3 replicate cultures were exposed to control temperatures (26 ± 1 °C) for 24 h and three replicate cultures were exposed to 32 ± 1 °C for 24 h to simulate bleaching conditions. Each replicate was aliquoted into three subsamples that were collected and processed at 0 h, 12 h, and 24 h exposure to treatment.*

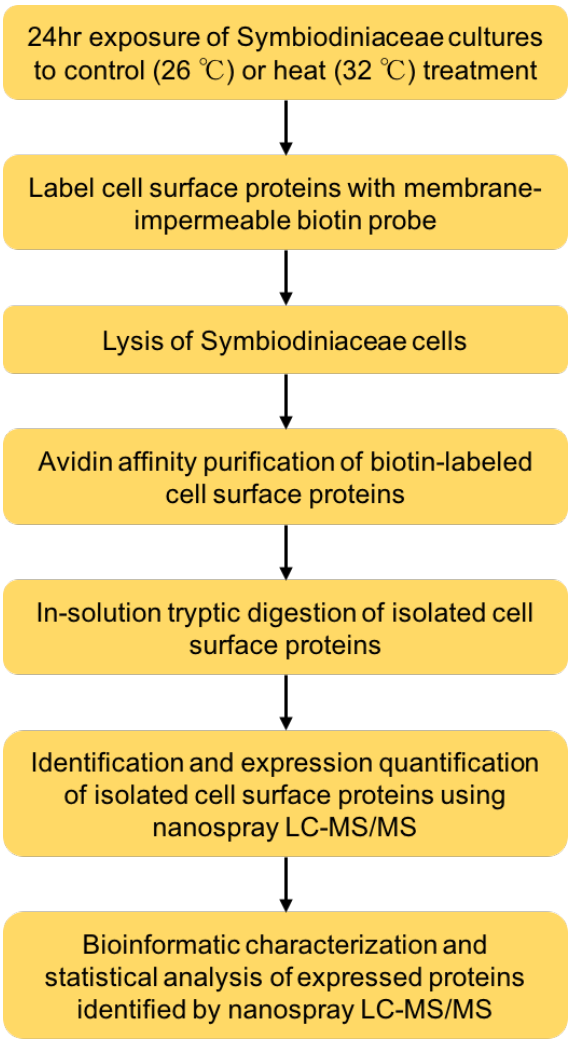

Fig S2 Diagram illustrating methods of the present study. Breviolum psygmophilum *cultures were exposed to respective treatments for 24 h. At designated time points, replicate subsamples were removed. In-tact cells were thoroughly washed using sterile PBS and then incubated with a membrane-impermeable biotin probe to label exposed proteins at the* B. psygmophilum *cell surface. Cells were then incubated with 25 mM tris to quench biotinylation, washed thoroughly using sterile PBS, and lysed. Labeled proteins were isolated via avidin affinity purification. Isolated proteins were then identified via nanospray LC-MS/MS. Identified proteins were characterized via the NCBI BLAST algorithm. Statistical analyses were carried out using R statistical software.*

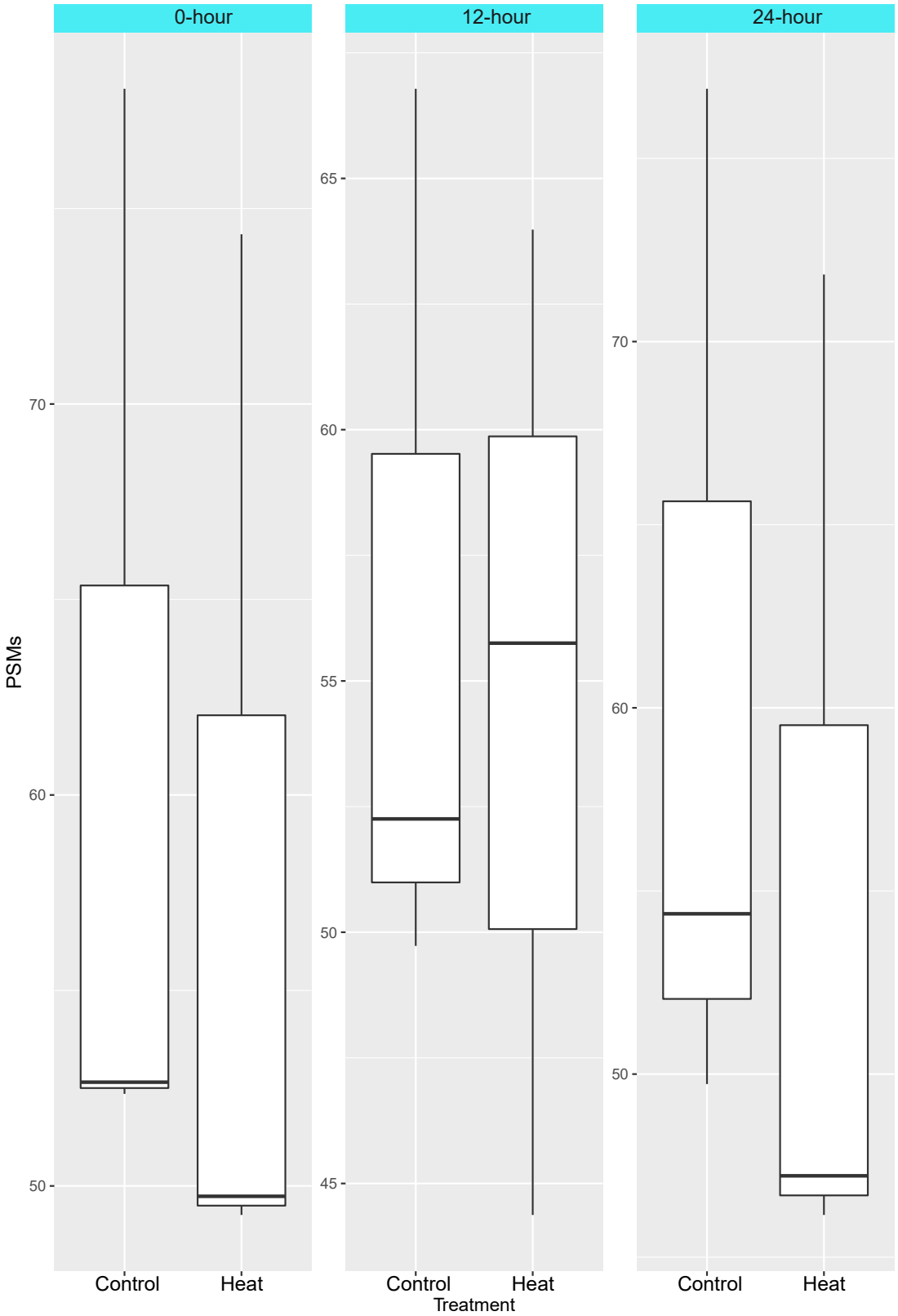

Fig S3 Abundance of chloroplasts constituents isolated over time. Y-axis represents normalized PSMs

Chapter 3

Proteomic investigation of a diseased gorgonian coral indicates disruption of essential cell function and investment in inflammatory and other immune processes

Contessa A. Ricci, Abu Hena Mostafa Kamal, Jayanta Kishor Chakrabarty, Lauren E. Fuess, Whitney T. Mann, Lea R. Jinks, Vanessa Brinkhuis, Saiful M. Chowdhury, Laura D. Mydlarz

Citation:

Ricci CA, Kamal AHM, Chakrabarty JK, Fuess LE, Mann WT, Jinks LR, Brinkhuis V, Chowdhury SM, Mydlarz LD (2019) Proteomic investigation of a diseased gorgonian coral indicates disruption of essential cell function and investment in inflammatory and other immune processes. Integr Comp Biol pii: icz107. doi: 10.1093/icb/icz107

ABSTRACT

As scleractinian coral cover declines in the face of increased frequency in disease outbreaks, future reefs may become dominated by octocorals. Understanding octocoral disease responses and consequences is therefore necessary if we are to gain insight into the future of ecosystem services provided by coral reefs. In Florida, populations of the octocoral *Eunicea calyculata* infected with Eunicea Black Disease (EBD) were observed in the field in the fall of 2011. This disease was recognized by a stark, black pigmentation caused by heavy melanization. Histological preparations of *E. calyculata* infected with EBD demonstrated granular amoebocyte (GA) mobilization, melanin granules in much of the GA population, and the presence of fungal hyphae penetrating coral tissue. Previous transcriptomic analysis also identified immune trade-offs evidenced by increased immune investment at the expense of growth. Our investigation utilized proteogenomic techniques to reveal decreased investment in general cell signaling while increasing energy production for immune responses. Inflammation was also prominent in diseased *E. calyculata* and sheds light on factors driving the extreme phenotype observed with EBD. With disease outbreaks continuing to increase in frequency, our results highlight new targets within the cnidarian immune system and provide a framework for understanding transcriptomics in the context of an organismal disease phenotype and its protein expression.

INTRODUCTION

Corals have been experiencing increased frequency in disease outbreaks in recent decades (Bruno et al. 2007). This has led to a subsequent decline in scleractinian coral over the past 40 years (Jackson et al. 2014) and some reefs have inversely seen an increase in octocoral cover due to their relative robustness to stressors (Lenz et al. 2015; Ruzicka et al. 2013). It is therefore possible that octocorals will become a dominant reef component as scleractinian coral abundance continues to decline. Understanding octocoral responses to disease and the long-term effects of those responses is therefore necessary if we are to gain insight into the future of ecosystem services provided by coral reefs.

The octocoral immune repertoire, like most corals, utilizes both chemical and cellular defense mechanisms (Ellner et al. 2007; Mydlarz et al. 2016). For example, natural and/or lab infection studies of the sea fan *Gorgonia ventalina* demonstrate chitinolytic enzyme activity (Douglas et al. 2007), general antifungal/antibacterial compounds (Burge et al. 2013; Couch et al. 2008; Kim et al. 2000), pattern recognition receptors (Burge et al. 2013), and the generation of antioxidative enzymes (Couch et al. 2008; Mydlarz and Harvell 2007). Of particular note is the dramatic invasion of *G. ventalina* granular amoebocytes (GAs) into fungal-infected tissue (Ellner et al. 2007; Mydlarz et al. 2008) and pronounced melanin barriers (Ellner et al. 2007; Mydlarz et al. 2008). GAs are putative immunocytes (Menzel and Bigger 2015) and are present in multiple octocoral species (Fuess et al. 2018; Menzel and Bigger 2015). They are believed to release cytotoxic compounds when a pathogen is too large for phagocytosis (Mydlarz et al. 2008) but are not believed to be a homogenous cell type (Menzel and Bigger 2015). Some GA cell types may even be putative melanocytes (Fuess et al. 2018; Mydlarz et al. 2008).

Transcriptomic analyses have provided substantial information as proxies for protein expression as it relates to coral biology and physiology (e.g., Barshis et al. 2012; DeSalvo et al. 2010; Leggat et al. 2011). As such, they have allowed sensitive, high-throughput data analysis that has advanced our understanding on scales not previously available at the protein level (Hegde et al. 2003). Indeed, the bulk of coral studies to date involving protein investigation have been represented by relatively low-throughput techniques such as 2D gels (Mayfield et al. 2018; Ricaurte et al. 2016) and/or biochemical assays (Koike et al. 2004; Logan et al. 2010; Kvennefors 2008). Mass spectrometry has advanced protein investigation throughput, and the combination of this with nucleotide databases to predict protein identification (termed proteogenomics) has promoted such studies in non-model organisms (Nesvizhskii 2014; Khudyakov et al. 2018; Gochfeld, Ankisetty and Slattery 2015). Although this combination allows high-throughput proteomic data generation, transcriptomics remain the more sensitive techniques. However, one drawback of relying solely on transcriptomic analysis for expression is that transcription does not guarantee protein expression (Proffitt et al. 2017). Layering different forms of data is therefore beneficial in that it compensates for shortcomings inherent in different analyses.

The purpose of this study was to examine the protein response of an octocoral, *Eunicea calyculata*, naturally infected with Eunicea Black Disease (EBD). This disease was observed for the first time off the Florida coast in the fall of 2011 and was easily recognized by a stark, black pigmentation caused by heavy melanization. It had been documented along the Florida Reef Tract with 12-86% prevalence across multiple *Eunicea* species (Fuess et al. 2018). The disease is a chronic infection associated with reduced feeding and polyp extension in infected corals (VB 2015 personal observation). Previous transcriptomic analysis also identified evidence of immune

trade-offs due to increased immune investment at the expense of growth and, likely, fecundity (Fuess et al. 2018).

In this study, we describe the proteome of healthy and diseased *E. calyculata*. We layer these data over previous histological and transcriptomic data to characterize late stage physiological and immune responses to EBD. This approach facilitates the analysis of EBD from the genetic aspect to phenotype and provides a unique understanding of the physiology of corals to prolonged infection.

METHODS

Sample collection

Samples were collected near Miami, FL (25° 50.526′ −80° 05.286′) following methods previously described in detail by Fuess et al. (2018) and in compliance with Chapter 68B-8.016 of the Marine Special Activity License program. A subset of the same samples used by Fuess et al. were utilized in this study. In short, diseased *Eunicea calyculata* were visually identified by black pigmentation. Because corals were infected for an unknown length of time before collection, diseased corals were considered infected for a prolonged period. Corals were considered healthy if they lacked any black pigmentation and had no visual appearance of disease. Healthy and diseased fragments were collected and immediately frozen in liquid nitrogen upon return to the surface and shipped back to the University of Texas at Arlington on dry ice and stored at −80°C until processing. Three fragments from healthy, and three fragments from diseased *E. calyculata* were utilized for the present study.

Histological preparation

For histological analysis, coral samples were immediately placed in a fixative of 1 part buffered zinc-formalin concentrate (Zfix TM, Anatech, Battle Creek, MI) and 4 parts filtered sea water for at least 24 hours and then decalcified in an aqueous solution of calcium citrate and formic acid. Histological samples were embedded in paraffin, sectioned at 4 mm, and stained with hematoxylin and eosin (H&E) or the Fontana-Masson silver stain protocol (ammoniacal silver nitrate stains melanin with nuclear fast red (Kernechtrot) counterstain) at the histology lab at the Florida Fish and Wildlife Research Institute. Histological images are presented here for descriptive reference only.

Transcriptome assembly

Transcriptome assembly was previously reported (Fuess et al. 2018). Full reads are available for download from NCBI (SRA PRJNA407366).

Protein extraction

Coral samples were ground in liquid nitrogen using a mortar and pestle. Proteins were then extracted for 45 minutes on ice by first adding approximately 2 ml of 100 mM sodium phosphate-buffered saline (pH 7.8) and centrifuging for 10 minutes at 4°C at 3500 rpm (Eppendorf centrifuge 5810R). Proteins in the supernatant were then collected through acetone precipitation.

Nanospray-LC-MS/MS

Proteins were first prepared for SDS-PAGE by boiling in DTT and Laemmli buffer (Cold Spring Harbor protocols) at 95°C for 20 minutes. 15µg of protein was then loaded on a 12%

SDS-PAGE gel and ran at 184 volts for two hours. Whole lanes were excised and coral proteins were tryptically digested in gel after reduction and alkylation following established protocols (Chakrabarty et al. 2016). Peptides were extracted using 50% acetonitrile, dehydrated in a speedvac (Vacufuge plus, Eppendorf), and reconstituted in 5% acetonitrile/0.1% formic acid in ultrapure water. Reconstituted peptides were introduced via nanospray to a Velos Pro Dual-Pressure Linear Ion Trap Mass Spectrometer (ThermoFisher Scientifc) for analysis using a data-dependent protocol. Protein fragmentation was achieved by collision induced dissociation (CID).

Isolated protein sequences were identified from mass spectra using Proteome Discoverer software (ver. 2.1, ThermoFisher Scientifc). Spectra were matched against an *in silico* theoretical digestion of the *Eunicea calyculata* transcriptome generated by Fuess et al. (2018) using the Sequest HT algorithm within the software. Sequest HT criteria were as follows: the proteolytic enzyme was indicated as trypsin; two missed cleavages were allowed; precursor mass range of 350–3500Da; fragment mass tolerance of ±2.5 and 0.6Da; peptide charges excluded +1 (Kamal et al. 2018). Protein abundance was quantified within the software by the label-free method of spectral counting and is reported as peptide spectral matches (i.e., PSMs).

Dataset Building

A decoy search strategy was employed in Proteome Discoverer software (ver. 2.1, ThermoFisher Scientifc) using a 5% False Discovery Rate (FDR) (Wilhelm et al. 2014). Protein sequences were considered identified with high confidence if they met either of the following criteria: A) ≥ 2 peptides were detected in ≥ 2 replicates; or B) ≥ 1 peptide was detected in all three replicates (Kamal et al. 2018). Using these criteria, a dataset of 148 proteins was compiled

(supplementary table S1). PSMs of confidently identified proteins were normalized as % total PSMs per sample (Kamal et al. 2018).

To annotate the 148 proteins identified within the *Eunicea calyculata* transcriptome, their sequences were BLASTed against the Uniprot KB Swiss-Prot database. An e value $\geq e^{-5}$ was considered a confident annotation (Mayfield et al. 2018). If an *E. calyculata* sequence could not meet the criteria for confident annotation, it was BLASTed against the entire Uniprot KB database (i.e., Swiss-Prot and TrEMBL databases). Proteins were grouped according to GO terms (Gene Ontology) and groupings were supported by literature searches (supplementary table S1).

Statistical analysis

Identified proteins were divided into groups based on protein function (i.e., functional groups). Principal Component Analysis (PCA) was conducted on cumulative protein abundance for each functional group using the 'ggbiplot' function in the R package 'ggbiplot' (Vu 2011). Bray-Curtis distances were utilized by similarity percentages analysis (i.e., SIMPER analysis) to calculate the strongest drivers of differences observed between healthy and diseased corals (Clarke 1993; Warton et al. 2012). From SIMPER analyses, the most influential functional groups and/or individual proteins within a functional group were determined. SIMPER was carried out using the 'simper' function in the R package 'vegan' (Oksanen et al. 2018). Non-parametric t-tests were then conducted on the cumulative protein abundance (i.e., PSMs) for influential functional groups (e.g., cumulative abundance of proteins with immune functions in healthy vs. diseased corals). Within functional groups, non-parametric t-tests were also carried

out on the abundance of individual proteins that were determined to be influential by SIMPER (e.g., abundance of the protein arachidonate 5-lipoxygenase in healthy vs. diseased corals).

The small sample size (n = 3 per disease state), in combination with the variability observed between replicates, can potentially underinflate statistical significance at $\alpha = 0.05$. This can therefore obscure findings of biological importance. To provide more transparent and accurate statistical interpretation, effect size is reported in addition to p-values to provide context for biological significance (Greenland et al. 2016; Wasserstein & Lazar 2016). Effect size is defined as the discrepancy between the null hypothesis and the alternate hypothesis being tested (Cohen 1992a). In this study, effect size represents the differences observed in protein abundance between healthy and diseased coral with the null hypothesis as not different. Effect size was calculated using Cohen's *d* estimation (Cohen 1992a; Cohen1992b; Rice & Harris 2005). Cohen's *d* was calculated using the 'cohen.d' function in the R package 'EffSize' (Torchiano 2018). A small effect size is a Cohen's *d* ~0.2, a medium effect size is a Cohen's *d* ~0.5, and a large effect size is a Cohen's *d* ~0.8 (values noticeably lower than 0.2 are considered negligible while values noticeably greater than 0.8 are considered very large effect sizes)(Rice and Harris 2005; Torchiano 2018).

RESULTS

Eunicea black disease (EBD) was recognized by black pigmentation caused by melanin deposition (figure 1A). Histological preparations of *Eunicea calyculata* infected with EBD demonstrated granular amoebocyte (GA) mobilization, melanin granules in much of the GA population, and the presence of fungal hyphae penetrating coral tissue (figure 1B – D). 148 unique proteins were identified using a 5% FDR cutoff. These proteins were separated into 11

categories based on function (supplementary table S1). 12 proteins could not be identified by homology. One protein was uniquely expressed in healthy corals (*E. calyculata* transcript sequence comp40437_c0_seq1.p1, annotated as uromodulin), while three proteins were uniquely expressed in diseased corals (*E. calyculata* transcript sequences comp41681_c0_seq1.p1, comp40293_c0_seq1.p1, and comp44698_c0_seq1.p1; comp40293_c0_seq1.p1 was annotated as a C-type lectin while comp41681_c0_seq1.p1 and comp44698_c0_seq1.p1 could not be identified by homology). The most abundant protein class belonged to the cell structure and remodeling proteins (figure 2).

Eight proteins matched those found in the differentially expressed genes identified during transcriptomic analysis (table 1, Fuess et al. 2018). For the eight proteins found, four possessed large effect sizes (comp40293_c0_seq1.p1, C-type lectin, Cohen's $d = 1.22$; comp41554_c0_seq1.p1, histone, Cohen's $d = 0.90$; comp47621_c0_seq1.p1, heat shock protein 70, Cohen's $d = 0.94$; comp54096_c0_seq2.p1, carbonic anhydrase, Cohen's $d = 1.25$), indicating biological significance congruent with transcriptomic differential expression (supplementary figure S1).

Protein Abundance in Healthy and Diseased *Eunicea calyculata*

Diseased corals had higher abundance of unique proteins than healthy corals (three proteins vs. one protein; respectively). The combined abundance of the three unique proteins in diseased corals was also greater than the total abundance of the single unique protein in healthy corals ($p = 0.05$, Cohen's $d = 3.18$, figure 3A). Conversely, the cumulative abundance of proteins found in both healthy and diseased corals (i.e., shared proteins) was lower in diseased corals ($p = 0.05$, Cohen's $d = -3.18$, figure 3B).

In multivariate space, protein abundance for healthy and diseased corals showed a clear distinction (PCA, figure 4). PC1 and PC2 account for 76.6% of the total variation observed within the dataset. There were no significant differences ($p > 0.05$) in total protein abundance for individual functional categories (supplementary table S2). Biological significance, indicated by high Cohen's *d* values, was shown for every group with the exception of the chaperone, miscellaneous, unknown, and vesicle associated categories (supplementary table S2).

Drivers of difference between healthy and diseased corals

Differences between healthy and diseased corals were driven by, in order of most influential: reproduction, cell structure/remodeling, unknown proteins, immunity, and energy and metabolism (SIMPER, ~82% cumulative contribution, table 2). The unknown proteins were influenced primarily by three proteins (table 3) but because they could not be identified they will not be discussed further.

The reproduction category was driven by vitellogenin (SIMPER, ~97.7% cumulative contribution, table 3). There were no significant differences ($p > 0.05$) in the abundance of vitellogenin between healthy and diseased corals ($p = 0.23$, table 5), but Cohen's *d* was 1.28, demonstrating a large effect size (table 5, figure 5A). This may be an artifact of sex, as *E. calyculata* are gonochoric (Prada and Hellberg 2013). To address this, histological preparations were examined. Two of the three samples per disease condition were able to be sexed based on the presence of spermaries or eggs. Two males were used in the healthy samples, and one male and one female were used in the diseased samples. Neither spermaries nor eggs were present in the two samples that were not sexed.

The cell structure/remodeling category was driven by five protein types: collagen, a tetratricopeptide repeat-containing protein, actin, filamin-A, and tubulin (SIMPER, ~82.6% cumulative contribution, table 3). Collagen and filamin-A had large effect sizes with higher abundance in the diseased corals ($p = 0.51$, Cohen's $d = -1.24$ and $p = 0.13$, Cohen's $d = -1.17$; respectively; table 4, figure 5B).

The energy and metabolism category was driven by eight distinct proteins: acidic amino acid decarboxylase, phosphoenolpyruvate carboxykinase, a transketolase-type protein, fructose bisphosphate aldolase, an ATP synthase subunit, 6-phosphogluconate dehydrogenase, a choline transporter-like protein, and pyruvate carboxylase (SIMPER, ~82.8% cumulative contribution, table 3). The biological significance of the choline transporter-like protein, ATP synthase subunit, and pyruvate carboxylase proteins was large due to large effect sizes (Cohen's $d = -1.18$, Cohen's $d = 2.79$, Cohen's $d = 0.85$; respectively; table 4). Statistical significance ($p < 0.05$) was not observed ($p = 0.16$, $p = 0.06$, $p = 0.35$; respectively; table 4). The choline transporter-like protein and the ATP synthase subunit were more abundant in the diseased corals, while the pyruvate carboxylase had higher abundance in the healthy corals (figure 5C).

Immunity in late-stage EBD

Because the present study describes a disease phenotype, special attention was paid to the immunity functional group, which consisted of 28 unique proteins. Differences between healthy and diseased corals were mainly driven by eight proteins: arachidonate 5-lipoxygenase, quinone oxidoreductase, mucin, cytosolic non-specific dipeptidase, dual oxidase, galectin, and C-type lectin (SIMPER, ~81.8% cumulative contribution, table 3). C-type lectin was absent in all healthy coral replicates.

Immunity proteins were separated into seven categories based on their roles within the immune system: antioxidants, inflammation, lectin, antimicrobial, apoptosis, melanin synthesis, and the "first-line defense" proteins (supplementary table S3). The first-line defense category was comprised of mucin and the most influential proteins in the cell structure/remodeling and the miscellaneous categories: collagen and a cilia- and flagella-associated protein (SIMPER, top ~23.1% and top ~26.7% cumulative contributions; respectively; table 3). Although not traditionally classified as immune proteins, these were of interest because of their possible roles in the prevention of microbial adhesion and/or penetration.

The total abundance of proteins in the inflammation, antimicrobial, lectins, and first-line defense categories were not significantly different ($p > 0.05$) between healthy and diseased corals ($p = 0.28$, $p = 0.13$, $p = 0.28$, $p = 0.05$; respectively; table 5). However, they were deemed biologically significant due to large effect sizes (Cohen's $d = 1.13$, Cohen's $d = 1.31$, Cohen's $d = -1.39$, Cohen's $d = 1.74$; respectively; table 5). All other immune categories were not significantly different ($p > 0.05$) between healthy and diseased corals, and were not biologically significant due to small effect sizes (supplementary table S3). Inflammatory proteins were primarily represented by arachidonate 5-lipoxygenase and were more abundant in diseased corals ($p = 0.127$, Cohen's $d = -1.37$, figure 6A). Lectin proteins were represented by: C-type lectins, which were found only in diseased corals ($p = 0.04$, Cohen's $d = -1.22$); and galectin proteins which were in greater abundance in healthy corals ($p = 0.05$, Cohen's $d = 2.27$, table 5, figure 6B). The only protein representing the antimicrobial category was chitinase, which was in greater abundance in the diseased corals ($p = 0.1266$, Cohen's $d = -1.32$, table 5, figure 6C). The abundance of all first-line defense proteins was greater in diseased corals (figure 6E).

Laccase was identified as a component of the melanin synthesis pathway (table 5). Laccase did not differ in abundance between disease states ($p = 0.83$, Cohen's $d = -0.18$, figure 6D).

DISCUSSION

The layering of transcriptomic, proteomic, and histological analyses has provided a unique perspective on the effects of prolonged *Eunicea* Black Disease (EBD) infection. Using this approach, we link protein expression and cellular responses to late stage EBD and identified signatures of a specific pathogen within *Eunicea calyculata*. The responses of *E. calyculata* to EBD infection may, in fact, give this disease its unique phenotype and is expanded upon later.

The *E. calyculata* transcriptome developed by Fuess et al. (2018) was used as a database to inform proteomic identification via proteogenomic methods. By using the theoretical *in silico* digestion of the transcriptome, we identified 148 discrete proteins. This is comparable to a study by Kelkar et al. (2014) which identified 157 discrete proteins from whole cell lysates of the zebra fish, *Danio rerio*, using its own transcriptome. In *E. calyculata*, only four sequences were differentially abundant in both transcriptomic analyses (i.e., were differentially expressed genes; Fuess et al. 2018) and proteomic analyses (i.e., demonstrated differential abundance via large effect sizes). These were a C-type lectin, a histone, a heat shock cognate 70 protein, and a carbonic anhydrase.

While only four proteins were similar between transcriptomic and proteomic analyses, it may be informative because it points to a smaller pool of vital responses. Protein life cycle (i.e., translation and degradation) is important in later phases of a response (Jovanovic et al. 2015) and are likely influential forces in late-stage EBD. The apparent active transcription and translation

of these four proteins thus suggests that they were being constantly used and replenished at time of collection. Antimicrobial responses via the C-type lectin (Drummond and Brown 2013; Lehotzky et al. 2010) and stress responses via the heat shock 70 protein (Hasanuzzaman et al., 2014) are good examples of vital processes during infection. Further, increased levels of carbonic anhydrase are associated with inflammatory responses (Henry et al. 2016). Corals appear to be actively regulating these responses during disease as indicated by increased histones (Greer and Shi 2012).

Both the transcriptomic and proteomic data show tradeoffs when increasing immune traits in diseased corals. For example, transcriptomic analysis found increased immunity at the cost of cell division and growth (Fuess et al. 2018), and was hypothesized to ultimately result in reduced fecundity. In *E. calyculata*, proteins found in healthy and diseased (i.e., shared proteins) corals were in lower abundance while proteins unique to diseased corals were in greater total abundance (compared to those proteins unique to healthy corals). Organisms have a finite amount of energy and must allocate it appropriately in response to environmental change (French, Moore, and Demas 2009). The abundance of specialized proteins in diseased corals suggests a diversion of energy away from homeostasis and toward specialized disease responses. Further, evidence of increased energy demands when infected with EBD were observed, as diseased corals displayed greater abundance of the ATP synthase subunit ORF 7-like protein (this putatively shows an increase in the ATP synthase complex; Tybulewicz et al. 1984). In summary, these reflect the energetic cost of immunity.

Reproduction was the most influential functional group driving the differences between disease states. This was due to vitellogenin, a highly conserved protein for yolk development (Kelkar et al. 2014; Shikina et al. 2013). Vitellogenin abundance was higher in healthy corals.

Differences in abundance are not likely to be driven by sex based on the four samples where spermaries or eggs were present. Although vitellogenin is typically expressed in females (Hara, Hiramatsu and Fujita 2016) there are at least two coral species, *Euphyllia ancora* (Shikina et al. 2013) and *Galaxea fascicularis* (Hayakawa et al. 2005), that express vitellogenin at low levels in males. It is therefore not unlikely that vitellogenin would occur in male *E. calyculata*. However, without a healthy female colony to control for the levels of vitellogenin, it is difficult to speculate the significance of the presence of this protein in these samples any further.

FIRST-LINE DEFENSES ARE FORTIFIED AFTER INVASION

First line-defense proteins, represented by collagen, mucin, and a cilia- and flagella-associated protein, were found in greater abundance in EBD-infected corals. The external mucus layer of corals is widely recognized as a first line of defense, as it prevents the adherence and penetration of microbes (Shnit-Orland and Kushmaro 2008). Further, resident commensal and/or beneficial microbes in the mucus layer provide a competition barrier, whereby such microbes prevent the establishment of pathogens via mechanisms such as the production of antibacterial compounds (Piexoto et al. 2017). The increased abundance of first-line defense proteins in EBD-infected corals demonstrates continued investment in preventing pathogenic microbes from adhering to the coral epidermis and subsequent penetration into coral cells despite previous tissue invasion by the responsible pathogen.

Epidermal cilia are responsible for periodically shedding the mucus layer into the surrounding waters (Shnit-Orland and Kushmaro 2008). Mucin is a primary constituent of mucus layers (Tailford et al. 2015) while cilia- and flagella-associated proteins are associated with ciliary development (Maia et al. 2013). This suggests an increased investment in the mucosal layer of diseased *E. calyculata*, while increased cilia suggest an increased need to shed the

mucosal layer (perhaps at a greater frequency). Finally, an increase in collagen suggests an increased investment in the extracellular matrix (Chernousov and Carey 2000). This may serve as a mechanism to reinforce the cell's structural integrity (Sethi et al. 1999), mitigating cellular penetration by the responsible pathogen. Conversely, it may be a signature of an increased need for tissue repair (Weiskirchena , Weiskirchena and Tacke 2019) resulting from tissue penetration by the pathogen.

INFLAMMATORY RESPONSES MOBILIZE MELANIN-CONTAINING GRANULAR AMOEBOCYTES

Inflammatory proteins were primarily represented by arachidonate 5-lypoxygenase (5-LOX). This enzyme is responsible for the biosynthesis of eicosanoids from arachidonic acid and/or polyunsaturated fatty acids (Dennis and Norris 2015; Stanley 2006; Yuan et al. 2013). These important signaling molecules have regulatory roles in the initiation and resolution of immune processes (Dennis and Norris 2015; Stanley 2006; Yuan et al. 2013). Arachidonic acid metabolism and eicosanoid signaling have been implicated in *Acropora cervicornis* (Libro et al. 2013; Hemond and Vollmer 2015) and its response to disease (Libro et al. 2013). Importantly, eicosanoids synthesized by the 5-LOX pathway are specifically active during inflammation and promote leukocyte recruitment to sites of tissue damage in mammals (Dennis and Norris 2015; Lõhelaid and Samel 2018). While corals do not possess leukocytes specifically, they do possess an array of amoeboid immunocytes (Menzel and Bigger 2015) that may respond similarly to 5-LOX-induced eicosanoids.

Further, inflammatory responses can recruit melanocytes to a site of injury and induce melanization (Lévesque et al. 2012). Between disease states, there was greater 5-LOX abundance

in diseased *E. calyculata*. Histology demonstrated the mobilization of a large number of granular amoebocytes (GAs) with melanin granules in addition to the melanized disease phenotype (Fuess et al. 2018). Filamin-A was also found in greater abundance in diseased corals and is known to facilitate cell motility (Feng and Walsh 2004). Taken together, these data show a signature of cellular mobilization in the protein data for diseased corals that corroborate histological data. This provides evidence of a pronounced inflammatory component in the *E. calyculata* immune system that may be driving the extreme pigmented phenotype observed with EBD.

Melanin synthesis is initiated by the hydroxylation of monophenols and diphenols to dopaquinone by phenoloxidases (POs)(Nappi and Christensen 2005; Suguraman 2002). POs are generally categorized as either tyrosinase-type or laccase-type (Palmer et al. 2012) and invoke different pathways leading to melanin pigment production (Nappi and Christensen 2005). Both the transcriptomic analysis (Fuess et al. 2018) and the proteomic analysis presented in the current study only identified laccase-type PO in *E. calyculata*. Enzymatic assays showed greater PO activity in healthy *E. calyculata* (Fuess et al. 2018), but neither transcript or protein abundance for laccase differed between disease states. One hypothesis is that signatures from protein abundance are no longer detectable because melanin has already been deposited. It is also possible that POs in diseased corals either lack a sufficient cellular environment for optimum activity, or that diseased coral POs have lost some integrity. In either case, the melanin synthesis cascade appears to be exhausted in diseased *E. calyculata*.

The absence of a tyrosinase-type PO in the transcriptomic and proteomic analyses is significant. Although many organisms, including corals, possess both PO types (Baldrian 2005; Mydlarz and Palmer 2011; Palmer et al. 2012), it may be the case that *E. calyculata* rely primarily on a laccase-type pathway for melanin synthesis. It may also be that tyrosinase-type

POs were active during the initial stages of infection, as tyrosinase-type POs are known to exist in a latent form (i.e., prophenoloxidases) that must be enzymatically cleaved for activation (Mydlarz and Palmer 2011). Indeed, there is some evidence that melanin synthesis and deposition may be an initial response to stress in some corals (Wall et al. 2016). Because the extent of melanin deposition initiated by tyrosinase-type POs would primarily be determined by latent PO levels prior to infection, this type of PO is not expected to be detected using transcriptomic techniques and may have been depleted to undetectable levels for proteomic analysis. Late-stage disease dynamics may therefore be characterized by a separate process initiated by laccase-type POs: sclerotization (Suguraman 2002).

ANTIMICROBIAL RESPONSES REFLECT THE PRESENCE OF FUNGUS

Antimicrobial responses of EBD-infected *E. calyculata* reflect that corals were fighting off a pathogen at the time of collection (either a continued response to the etiological pathogen or a response to a secondary infection caused by opportunistic microbes). Transcriptomic analysis showed the upregulation of multiple transcripts with antimicrobial functions (Fuess et al. 2018). Similarly, three proteins were identified with antimicrobial functions in the present study: C-type lectin (Drummond and Brown 2013; Lehotzky et al. 2010), galectin (Cao and Guo 2016; Kohatsu et al. 2006), and chitinase (Douglas et al. 2007). With the exception of galectin, each of these proteins were found in greater abundance in diseased corals. Galectin was in greater abundance in healthy corals. However, given the multiple roles of this protein in normal cell function (Dumic et al. 2006), this is likely an artifact of energetic shifts toward immune responses in diseased corals.

C-type lectins and chitinases possess more specific roles in immunity and are most thoroughly studied in their action against fungi (Dambuza and Brown 2015; Drummond and Brown 2013; Fesel and Zuccaro 2015; Shiokawa et al. 2017). In addition, chitinases are primarily antifungal compounds (Di Rosa, Maria Brundo and Malaguarnera 2016). Chitinolytic (Douglas et al. 2007) and general antifungal activity (Kim et al. 2000) have been observed in *Gorgonia ventalina*. The higher abundance of C-type lectins and chitinase proteins in EBD-infected *E. calyculata*, in conjunction with the presence of fungal hyphae in histological preparations, suggests that the etiological agent of EBD is likely to be a fungal pathogen.

CONCLUSIONS

We provide a framework for understanding transcriptomics in the context of an organismal disease phenotype and protein expression. By doing so, we have shed light on targets (e.g., eicosanoids) for further investigation into cnidarian immunity. In the face of scleractinian coral decline, octocorals are likely to become the dominant cnidarian presence on future reefs. It is therefore necessary to understand the effects of stressors like disease in these corals if we are to understand potential changes in ecosystem services. With disease outbreaks increasing in high-profile regions like Florida and the Great Barrier Reef, it is increasingly important that we combine the types of data available to expand our knowledgebase surrounding coral disease.

Acknowledgements The authors would like to acknowledge funding from awards IOS-1831860 and OCE-1712134 from the National Science Foundation to LDM. The authors would like to thank the organizers of Symposia 9 at the 2019 Annual SICB meeting and would like to thank Esther Peters, Jan Landsberg, Yasu Kiryu, Noretta Perry and Yvonne Waters for assistance in

obtaining the histopathology pictures. This material is based upon work supported by the LSAMP bridge to doctorate fellowship programs under grant no.1026806 to CAR and National Science Foundation Graduate Research Fellowship under grant no. 1144240 to LEF.

REFERENCES

Baldrian P. 2005. Fungal laccases - occurrence and properties. FEMS Microbiol Rev 30:215–242

Barshis DJ, Ladner JT, Oliver TA, Seneca FO, Traylor-Knowles N, Palumbi SR. 2013. Genomic basis for coral resilience to climate change. PNAS 110: 1387 - 1392

Bruno JF, Selig ER, Casey KS, Page CA, Willis BL, Harvell CD, Sweatman H, Melendy AM. 2007. PLoS BIOLOGY Thermal Stress and Coral Cover as Drivers of Coral Disease Outbreaks. PLoS Biol 5(6): e124. doi:10.1371/ journal.pbio.0050124

Burge CA, Mouchka ME, Harvell CD, Roberts S. 2013. Immune response of the Caribbean sea fan, Gorgonia ventalina, exposed to an Aplanochytrium parasite as revealed by transcriptome sequencing. Front Physiol doi: 10.3389/fphys.2013.00180

Chakrabarty JK, Naik AG, Fessler MB, Munske GR, Chowdhury SM. 2016. Differential Tandem Mass Spectrometry-Based Cross-Linker: A New Approach for High Confidence in Identifying Protein Cross-Linking. Anal Chem 18;88(20):10215-10222

Chernousov MA and Carey DJ. 2000. Schwanncell extracellular matrix moleculesand their receptors. Histol Histopathol 15: 593-601

Clarke KR. 1993. Non-parametric multivariate analyses of changes in community structure. Austral Ecol 18:117–143.

Cohen J(a). 1992. Statistical power analysis. Curr Dir Psychol Sci 1:98-101

Cohen J(b). 1992. A power primer. Psychol Bull 112:155-159

Couch CS, Mydlarz LD, Harvell CD, Douglas NL. 2008. Variation in measures of immunocompetence of sea fan coral, Gorgonia ventalina, in the Florida Keys. Mar Biol 155:281–292

Dambuza IM and Brown GD. 2015. C-type lectins in immunity: recent developments. Curr Opin Immunol. 32:21–27

Dennis EA and Norris PC. 2015. Eicosanoid Storm in Infection and Inflammation. Nat Rev Immunol 15: 511–523

DeSalvo MK, Sunagawa S, Voolstra CR, Medina M. 2010. Transcriptomic responses to heat stress and bleaching in the elk horn coral *Acropora palmata*. Mar Ecol Prog Ser 402: 97 – 113

Di Rosa M, Brundo VM, Malaguarnera L. 2016. New insights on chitinases immunologic activities. World J Immunol 6: 96 - 104

Douglas NL, Mullen KM, Talmage SC, Harvell CD. 2007. Exploring the role of chitinolytic enzymes in the sea fan coral, Gorgonia ventalina. Mar. Biol. 150:1137–1144

Drummond RA, Brown GD. 2013. Signalling C-Type Lectins in Antimicrobial Immunity. PLoS Pathog 9: e1003417. doi:10.1371/journal. ppat.1003417

Dumic J, Dabelic S, Flögel M. 2006. Galectin-3: An open-ended story. Biochim Biophys Acta 1760: 616–635

Ellner SP, Jones LE, Mydlarz LD, Harvell CD. 2007. Am. Nat. 170:E143–E00

Feng Y and Walsh CA. 2004. The many faces of filamin: A versatile molecular scaffold for cell motility and signalling. Nat Cell Bio 6:1034-1038

Fesel PH and Zuccaro A. 2015. b-glucan: Crucial component of the fungal cell wall and elusive MAMP in plants. Fungal Genet Biol 90:53–60

French SS, Moore MC, Demas GE. 2009. Ecological immunology: the organism in context. Integr Comp Biol 49: 246 - 253

Fuess LE, Mann WT, Jinks LR, Brinkhuis V, Mydlarz LD. 2018. Transcriptional analyses provide new insight into the late-stage immune response of a diseased Caribbean coral. R. Soc. open sci. 5: 172062

Gochfeld DJ, Ankisetty S, Slattery M. 2015. Proteomic profiling of healthy and diseased hybrid soft corals *Sinularia maxima* and *S. polydactyla.* Dis Aquat Organ 116: 133 – 141

Greenland S, Stephen J. Senn SJ, Rothman KJ, Carlin JB, Poole C, Goodman SN, Altman DG. 2016. Statistical tests, P values, confidence intervals, and power: a guide to misinterpretations. Eur J Epidemiol 31:337–350

Greer EL, Shi Y. 2012. Histone methylation: a dynamic mark in health, disease and inheritance. Nat Rev Genet 13: 343 - 357

Hasanuzzaman M, Nahar K, Mahabub Alam M, Roychowdhury R, Fujita M. 2013. Physiological, biochemical, and molecular mechanisms of heat stress tolerance in plants. Int J Mol Sci. 14: 9643 – 9684

Hayakawa H, Nagano Y, Andoh T, Watanabe T. 2005. Sex-dependent expression of mRNA encoding a major egg protein in the gonochoric coral *Galaxea fascicularis.* Coral Reefs 24: 488 - 494

Hegde P, White I, and Debouck C. 2003. Interplay of transcriptomics and proteomics. Curr Opin Biotechnol. 6" 647 – 651

Hemond E and Vollmer S. 2015. Diurnal and nocturnal transcriptomic variation in the Caribbean staghorn coral, Acropora cervicornis. Mol Ecol 24: 4460–4473

Henry EK, Sy CB, Inclan-Rico JM, Espinosa V, Channy SS, Dwyer DF, Soteropoulos P, Rivera A, Siracusa MC. 2016. Carbonic anhydrase enzymes regulate mast cell-mediated inflammation. J Exp Med 213: 1663 - 1673

Kamal AHM, Chakrabarty JK, Udden SMN, Zaki MdH, Chowdhury SM. 2018. Infammatory Proteomic Network Analysis of Statin-treated and Lipopolysaccharide-activated Macrophages. 8:164 doi:10.1038/s41598-017-18533-1

Jackson J, Donovan M, Cramer K, Lam V. 2014. Status and Trends of Caribbean Coral Reefs: 1970-2012. Global Coral Reef Monitoring Network, IUCN, Gland, Switzerland.

Javanovic M, Rooney MS, Mertins P, Przybylski D, Chevrier N, Satija R, Rodriguez EH, Fields AP, Schwartz S, Raychowdhury R, Mumbach MR, Eisenhoure T, Rabani M, Gennert D, Lu D, Delorey T, Weissman JS, Carr SA, Hacohen N, Regev A. 2015. Dynamic profiling of the protein life cycle in response too pathogens. Science 347: DOI: 10.1126/science.1259038

Kelkar DS, Provost E, Chaerkady R, Muthusamy B, Manda SS , Subbannayya T, Selvan LDN, Wang CH, Datta KK, Woo S, Dwivedi SB, Renuse S, Getnet D, Huang TC, Kim MS, Pinto SM, Mitchell CJ, Madugundu AK, Kumar P, Sharma J, Advani J, Dey G, Balakrishnan L, Syed N, Nanjappa V, Subbannayya Y, Goel R, Prasad TSK , Bafna V, Sirdeshmukh R, Gowda H, Wang C, Leach SD, Pandey A. 2014. Annotation of the Zebrafish Genome through an Integrated Transcriptomic and Proteomic Analysis. Mol Cell Proteomics 11:3184-3198

Kohatsu L, Hsu DK, Jegalian AG, Liu FT, Baum LG. 2006. Galectin-3 induces death of Candida species expressing specific beta-1,2-linked mannans. J Immunol 177: 4718 - 4726

Khudyakov J, Deyarmin J, Hekman R, Pujade B, Maan R, Mody M, Banerjee R, Crocker D, Champagne C. A sample preparation workflow for adipose tissue shotgun proteomics and proteogenomics. Biol Open 7: bio036731 doi: 10.1242/bio.036731

Kim K, Harvell CD, Kim PD, Smith GW, Merkel SM. 2000. Fungal disease resistance of Caribbean sea fan corals (Gorgonia spp.). Mar Biol 136: 259-267

Koike K, Jimbo M, Sakai R, Kaeriyama M, Muramoto K, Ogata T, Maruyama T, Kamiya H. 2004. Octocoral Chemical Signaling Selects and Controls Dinoflagellate Symbionts. Bio Bull 207:80-86

Kvennefors EC, Leggat W, Hoegh-Guldberg O, Degnan BM, Barnes AC. 2008. An ancient and variable mannose-binding lectin from the coral Acropora millepora binds both pathogens and symbionts. Dev Comp Immunol 32:1582–1592

Leggat W, Seneca F, Wasmund K, Ukani L, Yellowlees D, Ainsworth TD. 2011. Differential Responses of the Coral Host and Their Algal Symbiont to Thermal Stress. PLoS ONE 6: e26687. doi.org/10.1371/journal.pone.0026687

Lehotzky RE, Partch CL, Mukherjee S, Cash HL, Goldman WE, Gardner KH, Hooper LV. 2010. Moecular basis for peptidoglycan recognition by a bacterial lectin. PNAS 107: 7722 - 7727

Lenz EA, Bramanti L, Lasker HR, Endmunds PJ. 2015. Long-term variation of octocoral populations in St. John, US Virgin Islands. Coral Reefs 34:1099–1109

Lévesque M, Feng Y, Jones RA, Martin P. 2013. Inflammation drives wound hyperpigmentation in zebrafish by recruiting pigment cells to sites of tissue damage. Dis Model Mech 6:508-515

Libro S, Kaluziak S, and Vollmer S. 2013. RNA-seq Profiles of Immune Related Genes in the Staghorn Coral Acropora cervicornis Infected with White Band Disease. PLoS ONE 8(11): e81821. doi:10.1371/journal.pone.0081821

Logan DDK, LaFlamme AC, Weis VM, Davy SK. Flow-cytometric characterization of the cell-surface glycans of symbiotic dinoflagellates (Symbiodinium spp.). J. Phycol. 46:525–533

Lõhelaid H and Samel N. 2018. Eicosanoid Diversity of Stony Corals Mar Drugs 16:doi:10.3390/md16010010

Maia TM, Gogendeau D, Pennetier C, Janke C, Basto R. 2013. Bug22 influences cilium morphology and the post- translational modification of ciliary microtubules. Biol Open 3:138–151

Mayfield AB, Chen YJ, Liu CY, Chen CS. 2018. The proteomic response of the reef coral Pocillopora acuta to experimentally elevated temperatures. PLoS ONE 13(1): e0192001

Menzel LP and Bigger CH. 2015. Identification of Unstimulated Constitutive Immunocytes, by Enzyme Histochemistry, in the Coenenchyme of the Octocoral Swiftia exserta. Bio Bull 229: 199-208

Mydlarz LD and Harvell CD. 2007. Peroxidase activity and inducibility in the sea fan coral exposed to a fungal pathogen. Comp Biochem Physiol Part A 146: 54–62

Mydlarz LD and Palmer CV. 2011. The presence of multiple phenoloxidases in Caribbean reef-building corals. Comp Biochem Physiol A Mol Integr Physiol 159:372–378

Mydlarz LD, Holthouse SF, Peters EC, Harvell CD. 2008. Cellular Responses in Sea Fan Corals: Granular Amoebocytes React to Pathogen and Climate Stressors. PLoS ONE 3(3): e1811. doi:10.1371/journal.pone.0001811

Mydlarz LD, Fuess LE, Mann MT, Pinzon JH, Gochfeld DJ. 2016. Cnidarian Immunity: From Genomes to Phenomes. In: Goffredo S, Dubinsky Z. The Cnidaria, Past, Present, and Future. 10.1007/978-3-319-31305-4_28.

Nappi AJ, Christensen BM. 2005. Melanogenesis and associated cytotoxic reactions: Applications to insect innate immunity. Insect Biochem Mol Biol 35:443-59

Nesvizhskii A. 2014. Proteogenomics: concepts, applications and computational strategies. Nat. Meth. 11:1114-1125

Oksanen J, Blanchet FG, Friendly M, Kindt R, Legendre P, McGlinn D, Minchin PR, O'Hara RB, Simpson GL, Solymos P, Stevens MHH, Szoecs E, Wagner H. 2018. vegan: Community Ecology Package. R package version 2.5-3. https://CRAN.R-project.org/package=vegan

Palmer CV, Bythell JC, Willis BL 2012. Enzyme activity demonstrates multiple pathways of innate immunity in Indo-Pacific anthozoans. Proc R Soc B 279:3879–3887

Piexoto RS, Rosado PM, de Assis Leite DC, Rosado AX, Bourne DG. 2017. Beneficial microorganisms for corals (BMC): proposed mechanisms for coral healthy and resilience. Front Microbiol 8: doi: 10.3389/fmicb.2017.00341

Prada C, Hellberg ME. 2013. Long prereproductive selection and divergence by depth in a Caribbean candelabrum coral. PNAS 110: 3961 - 3966

Proffitt MJ, Glenn J, Cesnik AJ, Jadhav A, Shortreed MR, Smith LM, Kavanaugh K, Cox LA, Olivier M. BMC Genomics 18:877 doi: 10.1186/s12864-017-4279-0

Ricaurte M, Schizas NV, Ciborowski P, Boukli NM. 2016. Proteomic analysis of bleached and unbleached Acropora palmata, a threatened coral species of the Caribbean. Mar Pollut Bull 107: 224–232

Rice ME, Harris GT. 2005. Comparing Effect Sizes in Follow-Up Studies: ROC Area, Cohen's d, and r. Law Hum Behav 5:615-20

Ruzicka RR, Colella MA, Porter JW, Morrison JM, Kidney JA, Brinkhuis V, Lunz KS, Macaulay KA, Martlett LA, Meyers MK, Colee J. 2013. Temporal changes in benthic assemblages on Florida Keys reefs 11 years after the 1997/1998 El Niño. Marine Ecology Progress Series 489: 125 – 141

Sethi T, Rintoul RC, Moore SM, MacKinnon AC, Salter D, Choo C, Chilvers ER, Dransfield I, Donnelly SC, Strieter R, Haslett C. 1999. Extracellular matrix proteins protect small cell lung cancer cells against apoptosis: a mechanism for small cell lung cancer growth and drug resistance in vivo. Nat Med 5: 662 - 668

Shikina S, Chen CJ, Chung YJ, Shao ZF, Liou JY, Tseng HP, Lee YH, Chang CF. Yolk Formation in a Stony Coral *Euphyllia ancora* (Cnidaria, Anthozoa): Insight Into the Evolution of Vitellogenesis in Nonbilaterian Animals. Endocrinology 154:3447–3459

Shiokawa M, Yamasaki S, Saijo S. 2017. C-type lectin receptors in anti-fungal immunity. Curr Opin Microbiol 40:123–130

Shnit-Orland M and Kushmaro A. 2008. Coral mucus - associated bacteria: a possible first line of defense. FEMS Microbiol Ecol 67:371–380

Stanley D. 2006. Prostaglandins and other eicosanoids in insects: Biological Significance. Annu Rev Entomol 51:25–44

Sugumaran M. 2002 Comparative Biochemistry of Eumelanogenesis and the Protective Roles of Phenoloxidase and Melanin in Insects. Pigment Cell Res 15: 2-9

Tailford LE, Crost EH, Kavanaugh D, Juge N. 2015. Mucin glycan foraging in the human gut microbiome. Front Genet 6:81. doi: 10.3389/fgene.2015.00081

Torchiano M. 2018. Efficient Effect Size Computation. R package version 0.7.4. http://github.com/mtorchiano/effsize/

Tybulewicz VJL, Falk G, Walker JE. 1984. Rhodopseudomonas blastica atp Operon Nucleotide Sequence and Transcription. J Mol Biol 174:185-214

Vu V. 2011. A ggplot2 based biplot. R package version 0.55. http://github.com/vqv/ggbiplot

Wall CB, Ricci CA, Mydlarz LD, Gates RD, Putnam HM. 2018. The effects of environmental history and thermal stress on coral physiology and immunity. Mar Biol 165:56

Warton DI, Wright ST, Wang Y. 2012. Distance-based multivariate analyses confound location and dispersion effects. Methods Ecol Evol 3:89–101

Wasserstein RL and Lazar NA. 2016. ASA Statement on Statistical Significance and P-Values. Am Stat 70:129-133

Weiskirchen R, Weiskirchen S, Tacke F. 2019. Organ and tissue fibrosis: molecular signals, cellular mechanisms and translational implications. Mol Aspects Med 65: 2 - 15

Wilhelm M, Schlegl J, Hahne JH, Gholami AM, Lieberenz M, Savitski MM, Ziegler E, Butzmann L, Gessulat S, Marx H, Mathieson T, Lemeer S, Schnatbaum K, Reimer U, Wenschuh H, Mollenhauer M, Slotta-Huspenina J, Boese JH, Bantscheff M, Gerstmair A, Faerber F, Kuster B. 2014. Mass-spectrometry-based draft of the human proteome. Nature 509: 582–587

Yuan D, Zou Q, Yu T, Song C, Huang S, Chen S, Ren Z, Xu A. 2014. Ancestral genetic complexity of arachidonic acid metabolism in Metazoa. Biochimica et Biophysica Acta 1841:1272–1284

Figure1 Field photos and histology of EBD. A) *E. calyculata* infectd with EBD; B) histological preparation showing melanin granules (arrows) present in granular amoebocytes; C) histological preparation showing accumulation of granular amoebocytes (arrows) in diseased *E. calyculata* epidermis; D) histological preparation showing fungal hyphae (arrow) in diseased *E. calyculata* tissue

Figure 2 Abundance of proteins in functional categories per coral sample

Figure 3 Comparison of total protein abundance between healthy and diseased states. A) total abundance of proteins for sequences found only in either healthy or diseased state ($p = 0.05$, Cohen's $d = 3.18$); and B) total abundance of proteins for sequences found in both healthy and diseased states ($p = 0,05$; Cohen's $d = -3.18$). (*****) represents significant effect for non-parametric t-tests ($p < 0.05$). (◆) represents large effect size values. Effect size was calculated using Cohen's *d* estimation. Y-axis denotes peptide spectral matches (i.e., PSMs).

Figure 4 PCA plot comparing disease states to functional categories. Salmon represents healthy corals; teal represents diseased corals

Figure 5 Proteins with large effect size values for A) reproduction, B) cell structure/remodeling, and C) energy and metabolism functional categories. ~82% most influential sequences for each functional category. (*****) represents significant effect for non-parametric t-tests ($p < 0.05$). (◆) represents large effect size values. Effect size was calculated using Cohen's *d* estimation. Y-axis denotes peptide spectral matches (i.e., PSMs).

Figure 6 Proteins with large effect size values for A) inflammation, B) lectin, C) antimicrobial, D) melanin synthesis, and E) "first line defense" immunity categories. (*****) represents significant effect for non-parametric t-tests ($p < 0.05$). (◆) represents large effect size values. Calculated using Cohen's *d* estimation. Y-axis denotes peptide spectral matches (i.e., PSMs).

Appendix 3A: Tables and Figures

TABLES

Table 1. Proteins identified that were also differentially expressed in transcriptome analysis. *Eunicea* sequence is transcript sequence identified in the protein spectra extracts. Proteins that agree with transcriptome were found in differential abundance between healthy and diseased corals with large effect sizes (i.e., large biological significance). Proteins that do not agree with transcriptome represent those with medium to negligible effect sizes.

Eunicea sequence	Protein name	P-value	Effect size	Agrees with transcript?
comp40293_c0_seq1.p1	C-type lectin domain family 4 member G	0.037 *	1.22 ◆	Yes
comp41554_c0_seq1.p1	Histone H2A type 1	0.2752	0.90 ◆	Yes
comp47621_c0_seq1.p1	Heat shock cognate 70 kDa protein	0.1266	0.94 ◆	Yes
comp54096_c0_seq2.p1	Carbonic anhydrase 7 (EC 4.2.1.1) (Carbonate dehydratase VII) (Carbonic anhydrase VII) (CA-VII)	0.1266	1.25 ◆	Yes
comp55982_c0_seq1.p1	Matrilin-2	0.5127	0.30	No
comp59151_c0_seq1.p1	Insoluble matrix shell protein 1 (IMSP1) (Fragment)	0.7963	-0.38	No
comp57545_c0_seq5.p1	Tubulin beta-4 chain	0.8273	-0.10	No
comp52644_c0_seq1.p1	Villin-1	0.5127	-0.66	No

(*) represents statistical significance ($p < 0.05$). (◆) represents large effect size values (Cohen's d *> 0.8).*

Table 2. Statistical comparison and SIMPER analysis showing the influence of each functional group driving differences between disease states and comparison of functional group protein abundance between healthy and diseased states.

	Average	Cumsum	P-value	Effect size
Reproduction	0.022	0.23	0.4	-1.26 ◆
Cell structure/remodeling	0.02	0.43	0.2	1.58 ◆
Unknown	0.02	0.60	0.7	-0.01
Immunity	0.01	0.74	0.4	1.13 ◆
Energy and metabolism	0.01	0.82	0.4	-1.62 ◆
Cell process	0.01	0.89	0.2	-1.11 ◆
Transcription/translation	0.00	0.93	0.1	2.30 ◆
Miscellaneous	0.00	0.96	0.7	-0.08
Chaperone	0.00	0.98	1	0.07
GTP/GTPase	0.00	0.99	0.2	-1.63 ◆
Vesicle associated	0.00	1	1	-0.13

"Average" represents average contribution to overall dissimilarity. "Cumsum" represents cumulative contribution to overall dissimilarity. (*) represents statistical significance ($p < 0.05$). (◆) represents large effect size values (Cohen's d *> 0.8).*

Table 3. SIMPER analysis showing the influence of proteins within each functional group that contribute to the most influential functional groups driving differences between disease states. ~82% most influential protein sequences per functional category are reported with the exception of the miscellaneous category and the transcription/translation category.

~82% most influential proteins in influential categories (table 3)

	Eunicea sequence	Protein name	average	cumsum
Reproduction				
	comp52470_c1_seq1.p1	Vitellogenin	0.53	0.97
Cell structure/remodeling				
	comp57938_c0_seq1.p1	Collagen alpha-2(I) chain	0.03	0.23
	comp34831_c0_seq1.p1	Tetratricopeptide repeat protein 28	0.03	0.44
	comp52695_c0_seq5.p1	Actin, cytoplasmic	0.01	0.53
	comp52695_c0_seq2.p1	Actin, cytoplasmic	0.01	0.62
	comp58210_c0_seq6.p1	Collagen alpha-1(XXVII) chain B	0.01	0.67
	comp41844_c0_seq1.p1	Actin, cytoplasmic	0.01	0.72
	comp57930_c0_seq2.p1	Filamin-A	0.00	0.75
	comp57545_c0_seq5.p1	Tubulin beta-4 chain	0.00	0.78
	comp41220_c0_seq1.p1	Tubulin alpha-1D chain	0.00	0.80
Unknown				
	comp19870_c0_seq1.p1		0.11	0.64
	comp48155_c0_seq1.p1		0.02	0.77
	comp54556_c0_seq3.p1		0.01	0.84
Immunity				
	comp54994_c0_seq1.p1	Arachidonate 5-lipoxygenase	0.08	0.31
	comp54994_c0_seq3.p1	Arachidonate 5-lipoxygenase	0.03	0.43
	comp54994_c0_seq5.p1	Arachidonate 5-lipoxygenase	0.02	0.51
	comp58711_c0_seq2.p1	Arachidonate 5-lipoxygenase	0.01	0.56
	comp56187_c0_seq1.p1	Synaptic vesicle membrane protein VAT-1 (quinone oxidoreductase)	0.01	0.60
	comp57865_c0_seq1.p1	Mucin-2 (Fragment)	0.01	0.64
	comp46142_c0_seq1.p1	Cytosolic non-specific dipeptidase	0.01	0.68
	comp58569_c0_seq1.p1	Dual oxidase 2	0.01	0.71
	comp56187_c0_seq4.p1	Synaptic vesicle membrane protein VAT-1 (quinone oxidoreductase)	0.01	0.74

comp47113_c0_seq1.p1	Galectin-4	0.01	0.77
comp56071_c0_seq1.p1	Arachidonate 5-lipoxygenase	0.01	0.80
comp40293_c0_seq1.p1	C-type lectin domain family 4 member G	0.01	0.82
Energy and metabolism			
comp53386_c0_seq1.p1	Acidic amino acid decarboxylase GADL1	0.06	0.24
comp50791_c0_seq1.p1	Phosphoenolpyruvate carboxykinase, cytosolic [GTP]	0.05	0.42
comp54586_c0_seq1.p1	Transketolase-like protein 2	0.03	0.55
comp44352_c0_seq1.p1	Fructose-bisphosphate aldolase, muscle	0.03	0.65
comp59137_c0_seq1.p1	ATP synthase subunits region ORF 7	0.018	0.72
comp54576_c0_seq1.p1	6-phosphogluconate dehydrogenase, decarboxylating	0.01	0.76
comp58035_c0_seq8.p1	Choline transporter-like protein 2	0.01	0.80
comp55166_c0_seq2.p1	Pyruvate carboxylase, mitochondrial	0.01	0.83
Most influential protein determined by SIMPER in select additional categories			
Miscellaneous			
comp54101_c0_seq1.p1	Cilia- and flagella-associated protein 91	0.06	0.27

"Average" represents average contribution to overall dissimilarity. "Cumsum" represents cumulative contribution to overall dissimilarity.

Table 4. Statistical comparison of influential proteins in functional categories between healthy and disease states. Proteins reported were ~82% most influential sequences found in each group by SIMPER analysis (table 3)

	P-value	Effect Size
Reproduction		
Vitellogenin	0.23	1.28 ◆
Cell structure/remodeling		
Actin	0.51	-0.03
Collagen	0.51	-1.24 ◆
Filamin-A	0.13	-1.17 ◆
Tetratricopeptide repeat protein	0.51	-0.04
Tubulin	0.28	-0.56
Energy and metabolism		
Fructose-bisphosphate aldolase	0.64	0.66
Phosphoenolpyruvate carboxykinase	0.64	0.36
Acidic amino acid decarboxylase GADL1	0.64	0.30
6-phosphogluconate dehydrogenase	0.35	0.56
Transketolase-like protein	0.64	-0.28
Pyruvate carboxylase	0.35	0.85 ◆
Choline transporter-like protein 2	0.16	-1.18 ◆
ATP synthase subunits region ORF 7	0.06	2.79 ◆

Bold effect sizes represent large effect size values. (*) represents statistical significance ($p < 0.05$). (◆) represents large effect size values (Cohen's d *> 0.8).*

Table 5. Statistical comparison of protein abundance in each immunity category between disease states. Proteins reported for each immunity categories with large effect sizes (table S3). Arachidonate 5-lipoxygnase is the only protein reported for inflammation because it comprised the majority of PSMs attributed to that category.

		P-value	Effect Size
Inflammation			
	Arachidonate 5-lipoxygenase	0.13	-1.37 ◆
Lectin			
	C-type lectin	0.04 *	-1.22 ◆
	Gaelctin	0.05 *	2.27 ◆
Antimicrobial			
	Chitinase	0.13	-1.31 ◆
Melanin synthesis			
	Laccase	0.83	-0.18
First-line defense			
	Collagen	0.51	-1.24 ◆
	Cilia- and flagella-associated protein	0.05 *	-3.84 ◆
	Mucin	0.05 *	-1.98 ◆

Bold effect sizes represent large effect size values. (*) represents statistical significance ($p < 0.05$). (◆) represents large effect size values (Cohen's d > *0.8).*

FIGURES

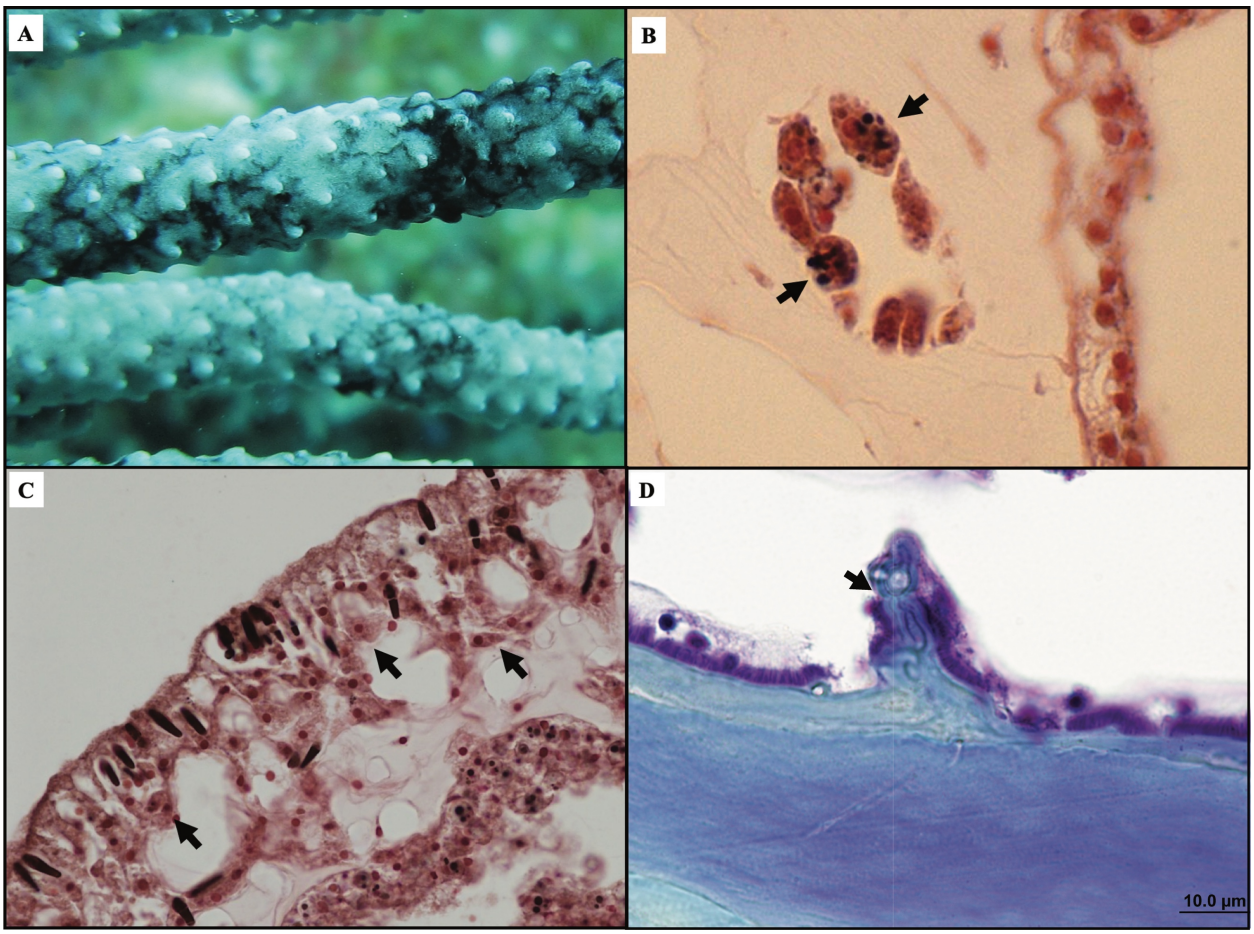

Figure 1

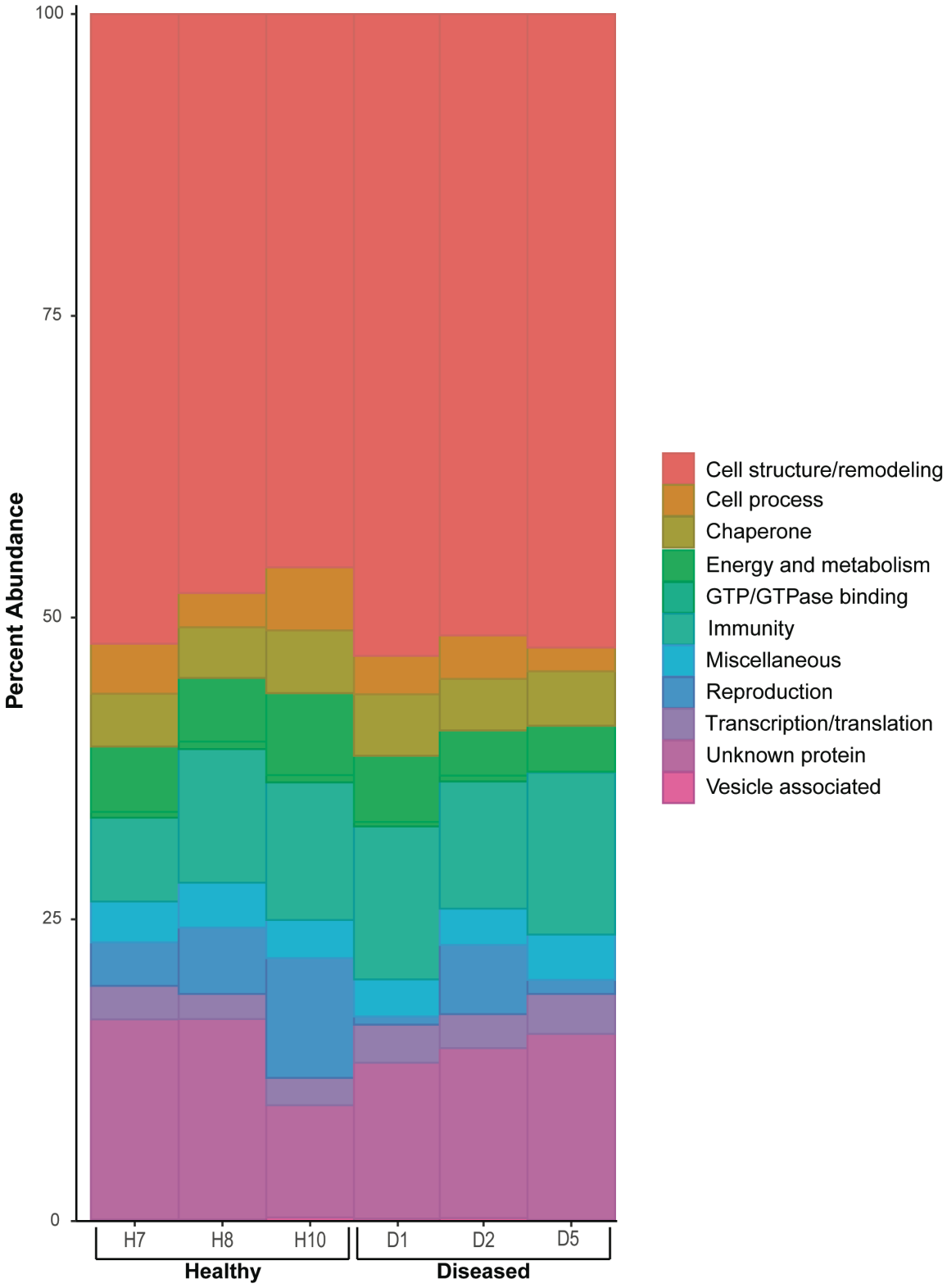
100
75
50
25
0
Percent Abundance
H7
H8
H10
D1
D2
D5
Healthy
Diseased
Cell structure/remodeling
Cell process
Chaperone
Energy and metabolism
GTP/GTPase binding
Immunity
Miscellaneous
Reproduction
Transcription/translation
Unknown protein
Vesicle associated

Figure 2

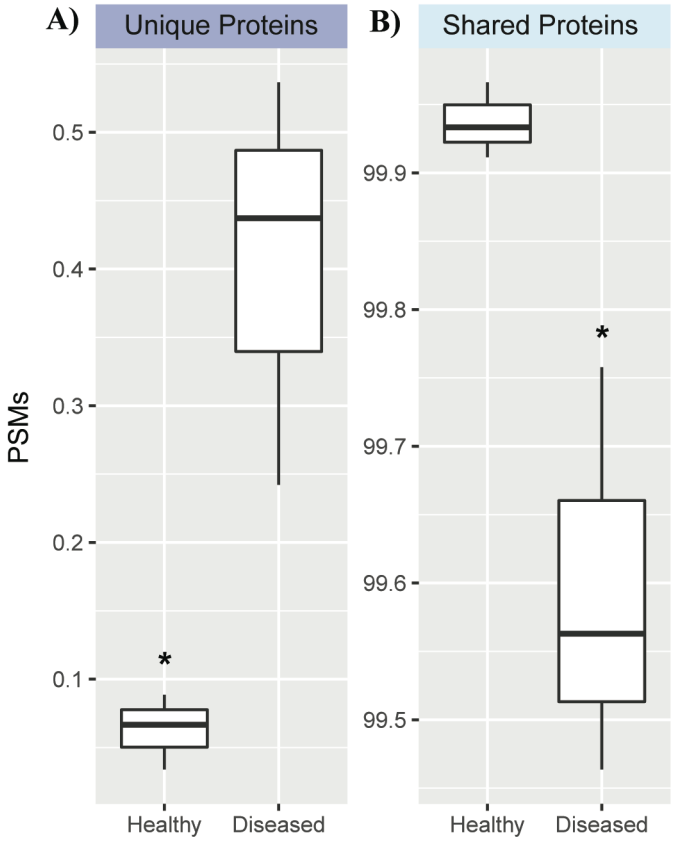
A)
Unique Proteins
B)
Shared Proteins
PSMs
0.5
0.4
0.3
0.2
0.1
99.9
99.8
99.7
99.6
99.5
*
*
Healthy
Diseased
Healthy
Diseased

Figure 3

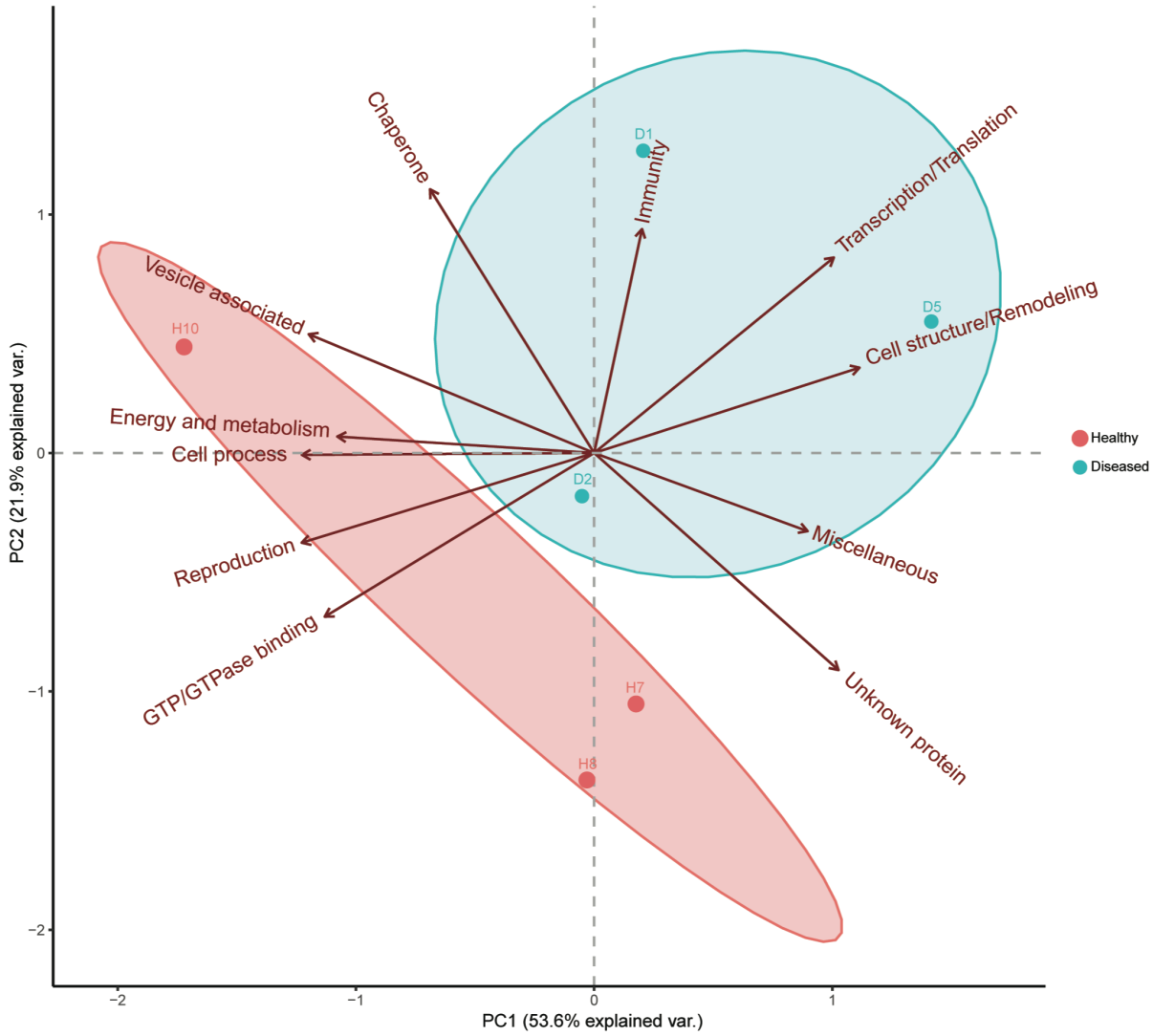
Chaperone
Immunity
Transcription/Translation
Cell structure/Remodeling
Miscellaneous
Unknown protein
GTP/GTPase binding
Reproduction
Cell process
Energy and metabolism
Vesicle associated
D1
D2
D5
H10
H7
H8
Healthy
Diseased
PC1 (53.6% explained var.)
PC2 (21.9% explained var.)
1
0
−1
−2
−2
−1
0
1

Figure 4

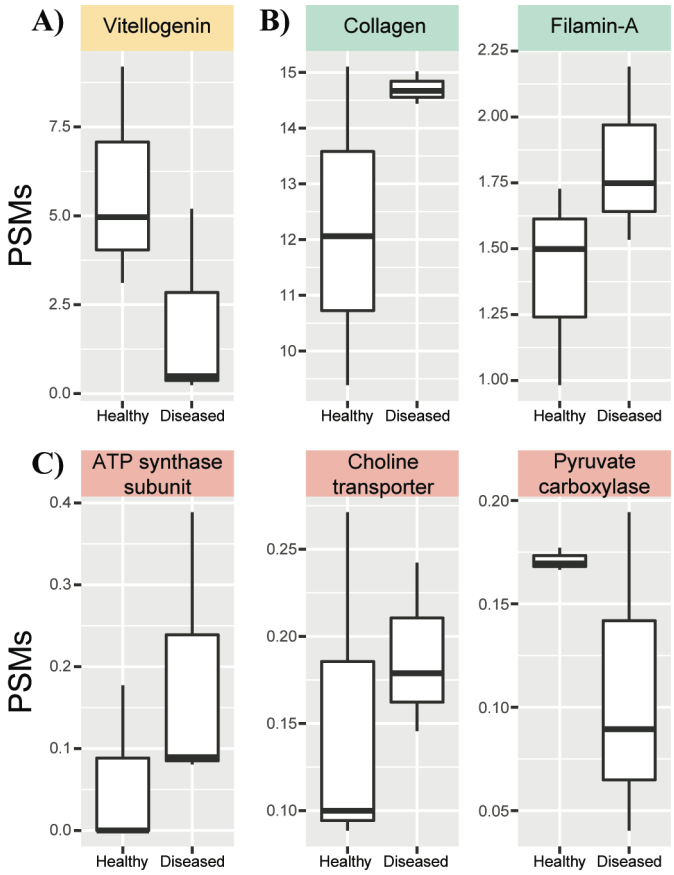
A)
Vitellogenin
B)
Collagen
Filamin-A
C)
ATP synthase subunit
Choline transporter
Pyruvate carboxylase
PSMs
PSMs
Healthy
Diseased

Figure 5

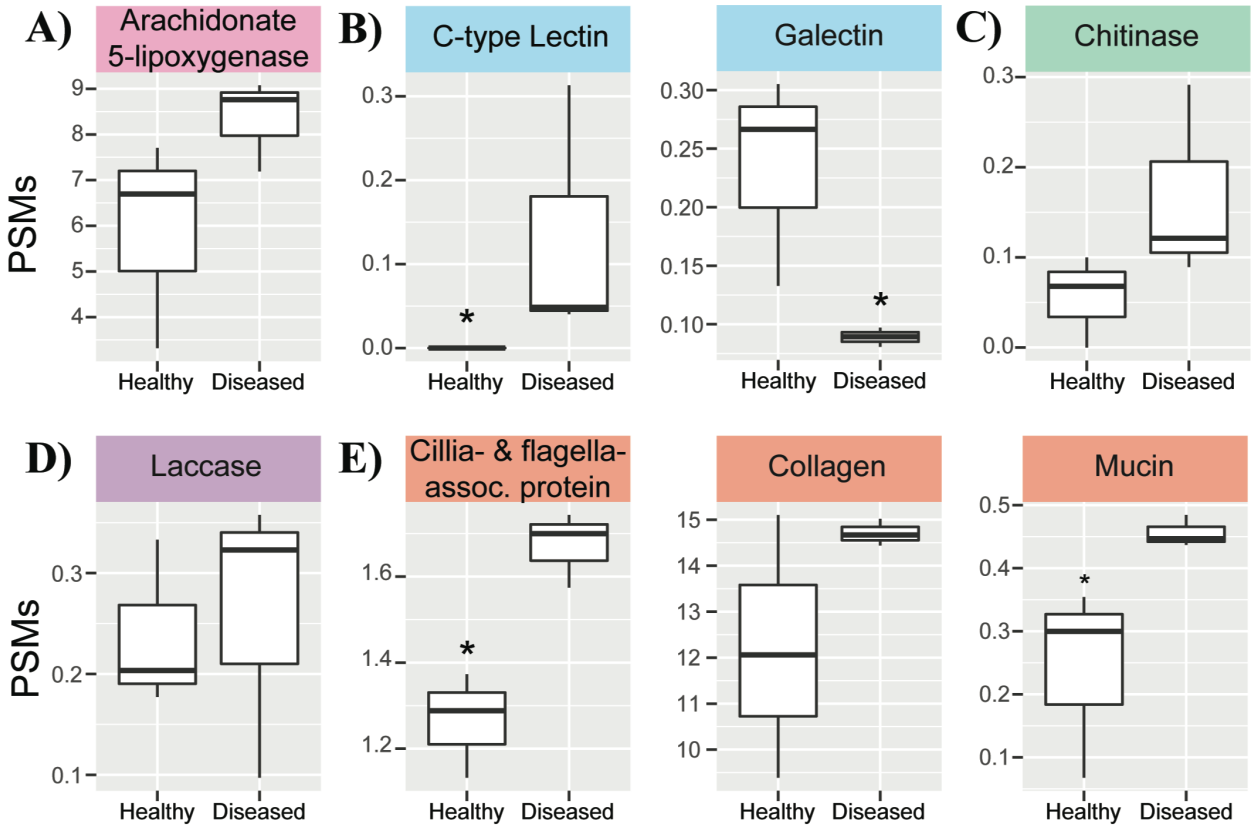
A)
Arachidonate 5-lipoxygenase
B)
C-type Lectin
Galectin
C)
Chitinase
D)
Laccase
E)
Cillia- & flagella-assoc. protein
Collagen
Mucin
PSMs
Healthy
Diseased

Figure

Appendix 3B: Supplementary Material

Table S1. Proteins identified within each functional group. *Eunicea* sequence is transcript sequence identified in the protein spectra extracts

Functional category	*Eunicea* sequence	Uniprot accession	Protein name	Protein classification (type or GO term)	Species	Score	Evalue
Cell structure/remodeling							
	comp41844_c0_seq1.p1	P12716	Actin, cytoplasmic	Actin/Tubulin	*Pisaster ochraceus*	490	1.00E-175
	comp52695_c0_seq5.p1	P12716	Actin, cytoplasmic	Actin/Tubulin	*Pisaster ochraceus*	715	0
	comp52695_c0_seq2.p1	P12716	Actin, cytoplasmic	Actin/Tubulin	*Pisaster ochraceus*	773	0
	comp41585_c1_seq1.p1	Q25379	Actin, cytoskeletal 3 (Fragment)	Actin/Tubulin	*Lytechinus pictus*	229	9.00E-78
	comp55541_c0_seq1.p1	P05094	Alpha-actinin-1	Actin/Tubulin binding	*Gallus gallus*	1225	0
	comp52009_c0_seq1.p1	P05099	Cartilage matrix protein	Extracellular matrix protein	*Gallus gallus*	56.6	3.00E-07
	comp47607_c0_seq1.p1	P34121	Coactosin	Actin/Tubulin binding	*Dictyostelium discoideum*	75.9	2.00E-15
	comp58210_c0_seq6.p1	A0MSJ1	Collagen alpha-1(XXVII) chain B	Extracellular matrix protein	*Danio rerio*	291	7.00E-81
	comp57938_c0_seq1.p1	P02466	Collagen alpha-2(I) chain	Extracellular matrix protein	*Rattus norvegicus*	551	3.00E-169
	comp57930_c0_seq2.p1	Q8BTM8	Filamin-A	Actin/Tubulin binding	*Mus musculus*	624	0
	comp43915_c0_seq1.p1	Q7JQD3	Gelsolin-like protein 1	Actin/Tubulin severing	*Lumbricus terrestris*	371	1.00E-126
	comp49179_c0_seq1.p1	Q7JQD3	Gelsolin-like protein 1	Actin/Tubulin severing	*Lumbricus terrestris*	382	4.00E-131
	comp59151_c0_seq1.p1	P86982	Insoluble matrix shell protein 1 (Fragment)	Extracellular matrix protein	*Stylophora pistillata*	90.5	3.00E-21
	comp50597_c0_seq1.p1	A0JMA9	Katanin p60 ATPase-containing subunit A-like	Actin/tubulin severing	*Xenopus laevis*	622	0
	comp56891_c0_seq5.p1	B5X3X5	Katanin p60 ATPase-containing subunit A1	Actin/tubulin severing	*Salmo salar*	229	4.00E-70
	comp55982_c0_seq1.p1	O00339	Matrilin-2	Extracellular matrix protein	*Homo sapiens*	203	2.00E-52
	comp45314_c0_seq1.p1	O00339	Matrilin-2	Extracellular matrix protein	*Homo sapiens*	77.4	9.00E-14

	comp56304_c0_seq1.p1	O42401	Matrilin-3	Extracellular matrix protein	*Gallus gallus*	114	3.00E-26
	comp57713_c0_seq4.p1	O88818	Plastin-3	Actin/Tubulin binding	*Cricetulus griseus*	654	0
	comp41665_c0_seq1.p1	P18320	Profilin	Actin/Tubulin binding	*Heliocidaris crassispina*	233	4.00E-79
	comp52212_c0_seq2.p1	P26043	Radixin	Actin/Tubulin binding	*Mus musculus*	704	0
	comp34831_c0_seq1.p1	Q96AY4	Tetratricopeptide repeat protein 28	Cell cycle	*Homo sapiens*	63.9	6.00E-12
	comp44743_c0_seq1.p1	Q5XFX0	Transgelin-2	Actin/Tubulin binding	*Rattus norvegicus*	150	6.00E-45
	comp35611_c0_seq1.p1	Q95VA8	Tropomyosin	Actin/Tubulin binding	*Trichinella spiralis*	159	2.00E-46
	comp51910_c0_seq1.p1	P18258	Tubulin alpha-1 chain	Actin/Tubulin	*Paracentrotus lividus*	647	0
	comp41220_c0_seq1.p1	Q2HJ86	Tubulin alpha-1D chain	Actin/Tubulin	*Bos taurus*	825	0
	comp57545_c0_seq10.p1	P11833	Tubulin beta chain	Actin/Tubulin	*Paracentrotus lividus*	600	0
	comp33082_c0_seq1.p1	O17449	Tubulin beta-1 chain	Actin/Tubulin	*Manduca sexta*	489	3.00E-173
	comp57545_c0_seq5.p1	P41937	Tubulin beta-4 chain	Actin/Tubulin	*Caenorhabditis elegans*	859	0
	comp52644_c0_seq1.p1	Q62468	Villin-1	Actin/tubulin severing	*Mus musculus*	592	0
	comp57942_c0_seq1.p1	O46037	Vinculin	Actin/Tubulin binding	*Drosophila melanogaster*	702	0
	comp59033_c0_seq1.p1	G8HTB6	ZP domain-containing protein	Extracellular matrix protein	*Acropora millepora*	141	1.00E-35
Cell process							
	comp49892_c0_seq1.p1	O93477	Adenosylhomocysteinase B	nucleic acid and protein metabolism	*Xenopus laevis*	697	0
	comp50625_c0_seq1.p1	Q66I24	Argininosuccinate synthase	Nitric oxide metabolism	*Danio rerio*	609	0
	comp52826_c0_seq1.p1	Q5XGM3	Betaine--homocysteine S-methyltransferase 1	Methylation associated	*Xenopus laevis*	566	0
	comp49643_c0_seq1.p1	A5PKH3	Fumarylacetoacetase	nucleic acid and protein metabolism	*Bos taurus*	631	0
	comp57380_c0_seq1.p1	Q95334	Glutamyl aminopeptidase	nucleic acid and protein metabolism	*Sus scrofa*	654	0

	comp52518_c0_seq1.p1	Q4JHE3	L-amino-acid oxidase	Amino acid transport and metabolism	*Oxyuranus scutellatus scutellatus*	142	6.00E-35
	comp49092_c0_seq5.p1	O94760	N(G),N(G)-dimethylarginine dimethylaminohydrolase 1	Nitric oxide metabolism	*Homo sapiens*	232	8.00E-75
	comp51054_c0_seq1.p1	Q5XI79	Protein arginine methyltransferase NDUFAF7, mitochondrial	Methylation associated	*Rattus norvegicus*	355	8.00E-119
	comp52631_c0_seq1.p1	Q11011	Puromycin-sensitive aminopeptidase	nucleic acid and protein metabolism	*Mus musculus*	1141	0
	comp54622_c0_seq1.p2	Q27245	Putative aminopeptidase W07G4.4	nucleic acid and protein metabolism	*Caenorhabditis elegans*	344	1.00E-111
	comp55076_c1_seq2.p1	Q59990	Putative cytochrome P450 120	retonoic acid metabolism	*Synechocystis sp.*	131	1.00E-32
	comp54551_c0_seq1.p1	O34363	Putative L-amino-acid oxidase YobN	nucleic acid and protein metabolism	*Bacillus subtilis*	124	6.00E-29
	comp49651_c0_seq1.p1	Q2KJC6	S-adenosylmethionine synthase isoform type-1	Methylation associated	*Bos taurus*	245	8.00E-80
	comp51052_c0_seq1.p1	P23787	Transitional endoplasmic reticulum ATPase	ATPase	*Xenopus laevis*	1380	0
	comp21067_c0_seq1.p1	P79781	Ubiquitin-40S ribosomal protein S27a	Ubiquitin/Ubiquitination associated	*Gallus gallus*	263	1.00E-90
	comp50028_c0_seq3.p1	Q29504	Ubiquitin-like modifier-activating enzyme 1	Ubiquitin/Ubiquitination associated	*Oryctolagus cuniculus*	1425	0
Chaperone							
	comp48034_c0_seq1.p1	P41932	14-3-3-like protein 1	Chaperone	*Caenorhabditis elegans*	323	1.00E-110
	comp48682_c0_seq1.p1	Q90593	Endoplasmic reticulum chaperone BiP	Chaperone	*Gallus gallus*	1095	0
	comp54417_c0_seq1.p1	P08108	Heat shock cognate 70 kDa protein	Chaperone	*Homo sapiens*	1070	0
	comp47621_c0_seq1.p1	P09189	Heat shock cognate 70 kDa protein	Chaperone	*Petunia hybrida*	877	0
	omp55924_c0_seq1.p1	P24724	Heat shock protein 90	Chaperone	*Theileria parva*	649	0
	comp81509_c0_seq1.p1	O44001	Heat shock protein 90	Chaperone	*Eimeria tenella*	306	6.00E-99
	comp77242_c0_seq1.p1	P30946	Heat shock protein HSP 90-alpha	Chaperone	*Oryctolagus cuniculus*	495	2.00E-171
	comp54031_c0_seq1.p1	Q90474	Heat shock protein HSP 90-alpha 1	Chaperone	*Danio rerio*	1091	0
	comp46956_c0_seq1.p1	P54985	Peptidyl-prolyl cis-trans isomerase	Chaperone	*Homo sapiens*	268	6.00E-92

	comp49209_c0_seq1.p1	Q17770	Protein disulfide-isomerase 2	Chaperone	*Caenorhabditis elegans*	572	0
	comp49073_c0_seq1.p1	Q8JG64	Protein disulfide-isomerase A3	Chaperone	*Gallus gallus*	366	8.00E-123
	comp56309_c0_seq1.p1	P13667	Protein disulfide-isomerase A4	Chaperone	*Homo sapiens*	672	0
	comp53174_c0_seq1.p1	Q63081	Protein disulfide-isomerase A6	Chaperone	*Rattus norvegicus*	529	0
Energy and metabolism							
	comp54576_c0_seq1.p1	P52209	6-phosphogluconate dehydrogenase, decarboxylating	Lipid biosynthesis	*Homo sapiens*	780	0
	comp53386_c0_seq1.p1	A6QM00	Acidic amino acid decarboxylase GADL1	Lipid metabolism	*Bos taurus*	65.9	1.00E-09
	comp51504_c0_seq1.p1	O15992	Arginine kinase	arginine kinase activity	*Anthopleura japonica*	388	8.00E-129
	comp53403_c0_seq1.p1	P19483	ATP synthase subunit alpha, mitochondrial	ATP biosynthetic process	*Bos taurus*	905	0
	comp48986_c0_seq1.p1	P00829	ATP synthase subunit beta, mitochondrial	ATP biosynthetic process	*Bos taurus*	861	0
	comp59137_c0_seq1.p1	P05450	ATP synthase subunits region ORF 7	ATP biosynthetic process		45.4	2.00E-05
	comp58035_c0_seq8.p1	Q6IP59	Choline transporter-like protein 2	Lipid biosynthesis	*Xenopus laevis*	573	0
	comp58035_c0_seq6.p1	Q6IP59	Choline transporter-like protein 2	Lipid biosynthesis	*Xenopus laevis*	573	0
	comp44352_c0_seq1.p1	P53445	Fructose-bisphosphate aldolase, muscle	Glycolysis		517	0
	comp52379_c0_seq1.p1	P51469	Glyceraldehyde-3-phosphate dehydrogenase	Glycolysis	*Xenopus laevis*	518	0
	comp56446_c0_seq1.p1	Q63060	Glycerol kinase	Lipid biosynthesis	*Rattus norvegicus*	629	0
	comp55780_c0_seq1.p1	P0DPA6	L-tryptophan decarboxylase	Lipid biosynthesis	*Psilocybe cubensis*	249	1.00E-76
	comp50791_c0_seq1.p1	P07379	Phosphoenolpyruvate carboxykinase, cytosolic [GTP]	Gluconeogenesis	*Rattus norvegicus*	808	0
	comp55166_c0_seq2.p1	P11498	Pyruvate carboxylase, mitochondrial	Gluconeogenesis	*Homo sapiens*	1588	0
	comp58500_c0_seq2.p2	Q9EQS0	Transaldolase	Pentose phosphate pathway	*Rattus norvegicus*	451	2.00E-159
	comp54586_c0_seq1.p1	Q9D4D4	Transketolase-like protein 2	Pentose phosphate pathway	*Mus musculus*	804	0
GTP/GTPase binding							
	comp57212_c1_seq4.p1	P61209	ADP-ribosylation factor 1	GTP/GTPase binding	*Drosophila melanogaster*	356	1.00E-126

	comp56273_c0_seq8.p1	Q6ZP65	BICD family-like cargo adapter 1	GTP/GTPase binding	*Homo sapiens*	67	2.00E-10
	comp41530_c0_seq1.p1	P21856	Rab GDP dissociation inhibitor alpha	GTP/GTPase binding	*Bos taurus*	601	0
	comp41497_c0_seq1.p1	P52565	Rho GDP-dissociation inhibitor	GTP/GTPase binding	*Homo sapiens*	206	1.00E-66
Immunity							
	comp52717_c0_seq1.p1	Q02356	AMP deaminase 2	Antioxidant	*Rattus norvegicus*	664	0
	comp54994_c0_seq3.p1	P12527	Arachidonate 5-lipoxygenase	acute inflammatory response	*Rattus norvegicus*	179	2.00E-46
	comp54994_c0_seq1.p1	P09917	Arachidonate 5-lipoxygenase	acute inflammatory response	*Homo sapiens*	183	6.00E-48
	comp58711_c0_seq2.p1	P09917	Arachidonate 5-lipoxygenase	acute inflammatory response	*Homo sapiens*	166	5.00E-41
	comp56071_c0_seq1.p1	P09917	Arachidonate 5-lipoxygenase	acute inflammatory response	*Homo sapiens*	521	1.00E-171
	comp54994_c0_seq5.p1	P51399	Arachidonate 5-lipoxygenase	acute inflammatory response	*Mesocricetus auratus*	168	1.00E-44
	comp40293_c0_seq1.p1	Q6UXB4	C-type lectin domain family 4 member G	lectin	*Homo sapiens*	73.6	4.00E-15
	comp54096_c0_seq2.p1	P43166	Carbonic anhydrase 7	Antioxidant	*Homo sapiens*	258	3.00E-85
	comp54434_c0_seq1.p1	Q9PWF7	Catalase	Antioxidant	*Rugosa rugosa*	682	0
	comp52150_c0_seq2.p1	Q13231	Chitotriosidase-1	Chitinase	*Homo sapiens*	362	9.00E-121
	comp52150_c0_seq1.p1	Q13231	Chitotriosidase-1	Chitinase	*Homo sapiens*	308	1.00E-100
	comp46142_c0_seq1.p1	Q9D1A2	Cytosolic non-specific dipeptidase	Apoptosis regulation	*Mus musculus*	516	3.00E-180
	comp40474_c0_seq1.p1	O43293	Death-associated protein kinase 3	Apoptosis regulation	*Homo sapiens*	169	4.00E-47
	comp58569_c0_seq1.p1	Q8HZK2	Dual oxidase 2	Antioxidant	*Sus scrofa*	1241	0
	comp51694_c0_seq9.p1	Q28193	Furin	TGF-Beta activation	*Bos taurus*	294	4.00E-88
	comp47113_c0_seq1.p1	P38552	Galectin-4	lectin	*Rattus norvegicus*	211	2.00E-65
	comp55281_c0_seq1.p1	P70627	Glutamate carboxypeptidase 2	Apoptosis regulation	*Rattus norvegicus*	370	9.00E-119
	comp56647_c0_seq1.p1	Q9NWZ3	Interleukin-1 receptor-associated kinase 4	innate immune response	*Homo sapiens*	104	4.00E-22
	comp51513_c0_seq1.p1	O59896	Laccase	Melanin synthesis	*Pycnoporus cinnabarinus*	119	3.00E-27
	comp54028_c0_seq1.p1	Q02079	Laccase-3	Melanin synthesis	*Thanatephorus cucumeris*	145	1.00E-35

	comp57865_c0_seq1.p1	Q62635	Mucin-2 (Fragment)	Mucus production	*Rattus norvegicus*	130	7.00E-30
	comp51366_c0_seq1.p1	P97346	Nucleoredoxin	Antioxidant	*Mus musculus*	278	1.00E-88
	comp53653_c0_seq2.p1	Q9EQZ5	Prostaglandin reductase 1	leukotirene inactivation	*Cavia porcellus*	288	3.00E-94
	comp53890_c1_seq1.p1	P81926	Superoxide dismutase [Cu-Zn]	Antioxidant	*Halocynthia roretzi*	209	3.00E-69
	comp56187_c0_seq1.p1	Q8JFV8	Synaptic vesicle membrane protein VAT-1 (quinone oxidoreductase)	Melanin synthesis	*Danio rerio*	363	9.00E-121
	comp56187_c0_seq4.p1	Q8JFV8	Synaptic vesicle membrane protein VAT-1 (quinone oxidoreductase)	Melanin synthesis	*Danio rerio*	200	3.00E-60
	comp40437_c0_seq1.p1	P48733	Uromodulin	Inflammation	*Bos taurus*	50.1	3.00E-07
Miscellaneous							
	comp49149_c0_seq1.p1	P86733	BPTI/Kunitz domain-containing protein (Fragment)	Protease inhibitor	*Homo sapiens*	134	3.00E-40
	comp54101_c0_seq1.p1	Q7Z4T9	Cilia- and flagella-associated protein 91	Cilia development	*Homo sapiens*	769	0
	comp52255_c0_seq2.p1	Q54PR9	Counting factor 60	Cell-counting factor	*Dictyostelium discoideum*	193	4.00E-56
	comp53454_c0_seq1.p1	F7E235	Failed axon connections homolog	Failed axon connections	*Xenopus tropicalis*	158	4.00E-42
	comp55869_c0_seq9.p1	P80426	Serotransferrin-1	Iron binding	*Salmo salar*	158	1.00E-41
	comp55869_c0_seq6.p1	P80429	Serotransferrin-2	Iron binding	*Salmo salar*	156	3.00E-41
	comp51801_c0_seq1.p1	Q96BD0	Solute carrier organic anion transporter family member 4A1	Transporter	*Homo sapiens*	224	2.00E-62
	comp56093_c0_seq3.p1	O75152	Zinc finger CCCH domain-containing protein 11A	Zinc finger	*Homo sapiens*	96.3	2.00E-20
Reproduction							
	comp57129_c0_seq1.p1	Q96J94	Piwi-like protein 1	Gamete-associated protein	*Homo sapiens*	904	0
	comp52470_c1_seq1.p1	Q91062	Vitellogenin	Gamete-associated protein	*Ichthyomyzon unicuspis*	100	8.00E-20
Transcription/translation							
	comp50614_c2_seq1.p1	P23396	40S ribosomal protein S3	Ribosomal protein	*Homo sapiens*	426	3.00E-152
	comp47077_c0_seq1.p1	Q58DT1	60S ribosomal protein L7	Ribosomal protein	*Bos taurus*	338	3.00E-117
	comp58714_c0_seq1.p1	Q5RC02	Alanine--tRNA ligase, cytoplasmic	tRNA ligase	*Pongo abelii*	1206	0

comp53529_c0_seq2.p1	Q2KJG3	Asparagine--tRNA ligase, cytoplasmic	tRNA ligase	*Bos taurus*	791	0
comp51864_c0_seq1.p1	Q3SYZ4	Aspartate--tRNA ligase, cytoplasmic	tRNA ligase	*Bos taurus*	723	0
comp43297_c0_seq1.p1	Q9YIC0	Elongation factor 1-alpha	translational elongation	*Oryzias latipes*	452	2.00E-159
comp24090_c0_seq1.p1	Q9YIC0	Elongation factor 1-alpha	translational elongation	*Oryzias latipes*	699	0
comp52959_c0_seq1.p1	Q92005	Elongation factor 1-alpha	translational elongation	*Danio rerio*	825	0
comp58423_c0_seq1.p2	Q90705	Elongation factor 2	translational elongation	*Gallus gallus*	1446	0
comp53943_c0_seq1.p1	P41250	Glycine--tRNA ligase	tRNA ligase	*Homo sapiens*	843	0
comp41554_c0_seq1.p1	Q4R3X5	Histone H2A.J	Histone	*Macaca fascicularis*	197	2.00E-65
comp48421_c0_seq1.p1	Q5ZMD6	Histone H2A.Z	Histone	*Gallus gallus*	231	4.00E-79
comp49296_c0_seq1.p1	Q6PC60	Histone H2B	Histone	*Danio rerio*	205	1.00E-68
comp55152_c0_seq2.p1	P02299	Histone H3	Histone	*Drosophila melanogaster*	273	6.00E-95
comp54266_c0_seq8.p1	Q6LAF1	Histone H4	Histone	*Dendronephthya klunzingeri*	202	9.00E-68
comp56543_c0_seq1.p1	F7AEX0	UV-stimulated scaffold protein A	RNA polymerase binding	*Xenopus tropicalis*	273	7.00E-83

Unknown

comp109396_c0_seq1.p1
comp19870_c0_seq1.p1
comp21074_c0_seq1.p1
comp41681_c0_seq1.p1
comp44698_c0_seq1.p1
comp48155_c0_seq1.p1
comp48518_c1_seq1.p1
comp50669_c0_seq1.p1
comp50827_c0_seq1.p1
comp51354_c1_seq1.p1
comp54556_c0_seq3.p1

	comp58897_c1_seq1.p1						
Vesicle associated							
	comp55337_c0_seq3.p1	Q05204	Lysosome-associated membrane glycoprotein 1	Lysosome-associated protein	*Bos taurus*	73.2	2.00E-13
	comp58716_c0_seq4.p1	P46461	Vesicle-fusing ATPase 1	Golgi vesicle docking	*Drosophila melanogaster*	833	0

Annotation achieved through NCBI-BLAST algorithm against the reviewed Uniprot database (or, in instances where a match was absent against the reviewed database, annotation was achieved against the TrEMBL Uniprot database). Unknown proteins are sequences that could not be identified by homology to either the reviewed or TrEMBL databases.

Table S2. Statistical comparison of total protein abundance for functional categories between healthy and diseased states.

	P-value	Effect Size
Cell structure/remodeling	0.2	1.58 ◆
Cell process	0.2	-1.11 ◆
Chaperone	1	0.07
Energy and metabolism	0.4	-1.59 ◆
GTP/GTPase binding	0.2	-1.64 ◆
Immunity	0.4	1.13 ◆
Miscellaneous	0.7	-0.08
Reproduction	0.4	-1.26 ◆
Transcription/translation	0.1	2.30 ◆
Unknown	0.7	-0.01
Vesicle associated	1	-0.13

Functional groups encompass total protein abundance for sequences found in each group. Bold effect sizes represent large effect size values. (*) represents statistical significance ($p < 0.05$). (◆) represents large effect size values (Cohen's d *> 0.8).*

Table S3. Comparison of total protein abundance for immunity categories between healthy and diseased states.

	P-value	Effect Size
Antioxidant	0.28	0.59
Inflammation	0.28	1.13 ◆
Lectin	0.83	-0.09
Antimicrobial	0.13	1.31 ◆
Apoptosis	0.83	0.17
Melanin synthesis	0.23	-1.39 ◆
First-line defense	0.05 *	1.74 ◆

Immunity categories encompass total protein abundance for sequences found to have roles in each group. Bold effect sizes represent large effect size values. (*) represents statistical significance ($p < 0.05$). (◆) represents large effect size values (Cohen's d *> 0.8).*

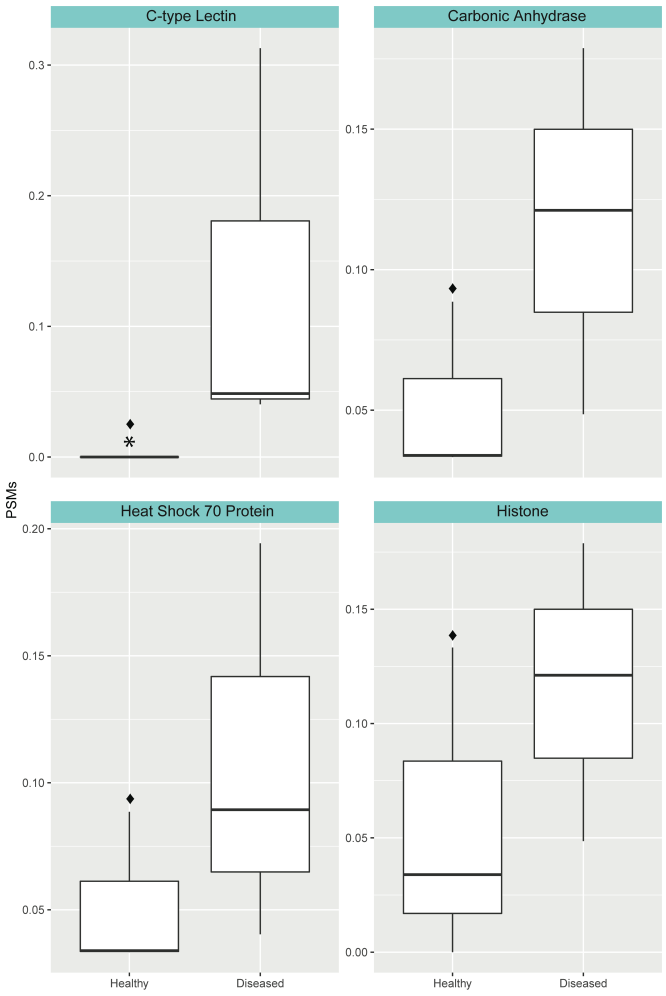

Figure S1 Abundance of proteins found in concordance with transcriptomic differentially expressed genes. (*) represents significant effect for non-parametric t-tests ($p < 0.05$). (◆) represents large effect size values. Effect size was calculated using Cohen's d estimation. Y-axis denotes peptide spectral matches (i.e., PSMs).

Chapter 4

Interactions between microclimate, symbiotic partner, and immunity reveal convergent survival strategies in populations of the Hawai`i coral, *Montipora capitata*, during consecutive bleaching seasons

Ricci CA, Wall CB, Wen AD, Mydlarz LD, Gates RD, Putnam HM

ABSTRACT

Bleaching events are increasing in frequency, and some areas are predicted to experience annual bleaching events within the next decade. Recently, elevated seawater temperatures coupled with strong El Niño Southern Oscillation conditions (2014 – 2017) produced the longest global bleaching event on record (Hughes et al. 2017; NOAA 2017), with many of the world's coral reefs experiencing repeated bleaching events over multiple years (Bahr et al. 2015a; Hughes et al. 2017; NOAA 2017). This presented a unique stress to explore the effects of environment, symbiotic partner, physiology, and immunity on bleaching outcomes. Natural laboratories within Kāne`ohe Bay were taken advantage of to elucidate the role of each component during this stress. Dominant symbiotic partner affected overall physiology while immunity primarily displayed either reef-specific responses or season-specific responses. Immune parameters ultimately converged on a similar pattern, demonstrating that specific interactions between the coral host, symbiotic partner, and environmental factors can influence the mechanisms by which this is achieved. This study thus provides important perspective on the impacts of consecutive bleaching events.

INTRODUCTION

Corals rely on a mutualism with dinoflagellates in the family Symbiodiniaceae to persist in oligotrophic tropical waters. Because heterotrophy alone cannot support corals, these symbionts will supply their host with the energy necessary for vital life processes like growth (Little, van Oppen & Willis 2004), calcification (Colombo-Pallotta, Rodriguez-Roman & Iglesias-Prieto 2010), and reproduction (Edmunds & Spencer Davies 1986). This symbiosis is, however, threatened by elevated temperatures that induce coral bleaching, or symbiosis breakdown. Recently, elevated seawater temperatures coupled with strong El Niño Southern Oscillation conditions (2014 – 2017) produced the longest global bleaching event on record (Hughes et al. 2017; NOAA 2017), with many of the world's coral reefs experiencing repeated bleaching events over multiple years (Bahr et al. 2015a; Hughes et al. 2017; NOAA 2017).

Differences in thermotolerances of resident Symbiodiniaceae species can be instrumental in influencing coral resilience to bleaching. In current models of bleaching, reactive oxygen species putatively derived from symbiont photosystem breakdown are believed to elicit an immune response that ultimately results in symbiont loss (Nielsen, Petrou & Gates 2018). As such, symbiont robustness against heat stress is key to shaping bleaching outcomes, and examining immunity in the context of symbiosis is helpful in understanding underlying bleaching physiology.

Comparisons between *Cladocopium* and *Durusdinium* are typically made when comparing symbiont robustness. Both *Cladocopium* and *Durusdinium* species form symbioses with numerous species (Stat and Gates 2011; Baker 2003), however, *Cladocopium* species transfer more nutrients to their coral host than do their *Durusdinium* counterparts (Stat and Gates 2011; Baker 2003). *Durusdinium* species are therefore considered more parasitic, with

associations resulting in lower growth rates (Little, van Oppen & Willis 2004) and reduced reproductive fitness (Jones and Berklemans 2011). Importantly, coral energy reserves are predictive of coral resilience to bleaching (Grottoli et al. 2014), and access to less photosynthetically fixed carbon can have long term costs. Consequently, bleaching outcomes are shaped by the different components of the holobiont and the interaction between partners.

Similarly, the environment within which a coral resides is influential. Several studies examining temperature regimes have identified roles for existence on thermally variable reefs (Oliver & Palumbi 2011) and/or reefs with higher constitutive temperatures (Kenkel, Meyer & Matz 2013) for increasing coral resilience to bleaching stress. Other environmental factors such as increased pCO_2 concentrations can threaten coral calcifications rates (Andersson and Gledhill 2013) and exacerbate thermal stress effects. These and other studies have been instrumental in advancing our understanding of their effects on coral physiology, however, most studies are carried out in the short term (e.g., periods of several weeks to several months). Particularly when addressing thermal stress, studies are typically conducted within the context of a single bleaching event and it is unclear which factors (e.g., symbiont population structure, host genotype, environmental history, etc.), or combination thereof, will determine coral resilience in the face of consecutive bleaching events. Because bleaching may ultimately result from an immune response against Symbiodiniaceae, the effect of coral immune parameters on the outcomes of consecutive coral bleaching should be examined. Further, the coral immune system is responsive to heat (Mydlarz et al. 2008; Palmer et al. 2011a) and bleaching stress (Mydlarz et al. 2009; Pinzon et al. 2015), and maintaining high baseline immunity can even be protective against bleaching (Palmer, Blythell & Willis 2012).

Bleaching events are increasing in frequency, and some areas are predicted to experience annual bleaching events within the next decade (van Hooidonk, Maynard and Planes 2013). Therefore, the effect of environmental history on coral immunity in response to bleaching stress was examined on two distinct reefs in Kāne`ohe Bay (windward O`ahu, Hawai`i, USA). Within Kāne`ohe Bay, physical factors such as wave-driven forcing and seawater residence times (Lowe et al. 2009) have created a natural system with differing environmental regimes. This was taken advantage of to examine the physiology and active immune response of corals at two reefs to bleaching stress over two consecutive bleaching seasons. Here, we test for the influence of space/history on coral bleaching and recovery and parse these responses among corals with *Cladocopium*- or *Durusdinium*-dominant symbiont communities. The symbiont-specific information will inform whether responses differ among communities, identify differences in immunity and physiology among corals hosting *Cladocopium* and *Durusdinium* symbionts, and whether these responses differ due to environmental history.

METHODS

Study site

Study reefs have been previously described (Wall et al. 2018). In summary, reefs were located in Kāneʻohe Bay, Oʻahu, Hawaiʻi (21°26′06.0″N, 157°47′27.9″W). Kāneʻohe Bay is highly heterogeneous due to different physical forcing (i.e., wave, wind, tidal) among bay regions (Lowe et al. 2009). In the southern lagoon (i.e., Lilipuna), geographic isolation and resistance to wave-driven forcing reduce seawater mixing and produce prolonged seawater residence times (ca. 30–60 days; Lowe et al. 2009). Conversely, in the central lagoon (i.e., Reef 14) seawater residence times are reduced (ca. 10 days) due to greater wave-driven forcing and

oceanic influences (Lowe et al. 2009). These forces culminate in Lilipuna corals experiencing low-variability in pCO_2 and Reef 14 corals experiencing high-variability pCO_2 (Wall et a. 2018), among other unmeasured variables.

Benthic surveys and coral collections

Four sampling events corresponding to periods defined as a 'bleaching period' corresponding to the point of maximum thermal stress (10 October 2014 and 12 October 2015), and a post-bleaching 'recovery period' approximately 4 months after peak seawater warming (11 February 2015 and 26 February 2016). At each time point, benthic surveys were conducted at each reef site using a 20 m transect and a line-point-intersect at 1 m intervals. Transects were positioned parallel to natural contours of the reef, being the north-south axis of the fringing reef (Lilipuna) and the east-west axis of patch reef (Reef 14). At each reef, transects (n = 2) were placed within three distinct reef habitats: the reef flat (< 1 m), the reef crest (1 - 2 m), and the reef slope (ca. 3 m). Benthic community cover was recorded at the species level for reef corals (*Montipora capitata, Pocillopora* spp. (*P. acuta*, *P. damicornis*)*, Porites compressa*), and either crustose coralline algae (CCA), macroalgae, or sand/bare/turf. For corals, bleaching state was quantified categorically, being either non-bleached (i.e., appearing fully pigmented) or bleached (i.e., exhibiting degrees of tissue paling/pigment variegation or being wholly white). Coral cover was calculated as % benthic cover, and bleaching extent was calculated as % coral cover bleached.

At each sampling period, forty coral branch tips (< 4 cm length) of *M. capitata* were collected from corals along the reef crest at a depth of ca. 1 m (State of Hawai'i Department of Land and Natural Resources, Special Activity Permit 2015-17 and 2016-69). Immediately post

collection, corals were snap frozen in liquid nitrogen and returned to HIMB and stored at -80 °C. Subsequently, coral samples were photographed on dry ice, and while remaining frozen each colony was split in half along its longitudinal axis. One-half of each coral fragment was stored at HIMB (-80 °C) for physiological assays and qPCR. The corresponding fragment-halves were used for immunological assays and were shipped to the University of Texas at Arlington using using a dry-shipper charged with liquid nitrogen

DNA extraction and symbiont community analysis

Symbiodinium DNA was extracted by adding an isolate of coral tissue (500 μl) to 500 ul DNA buffer (0.4 M NaCl, 0.05 M EDTA) with 2 % (w/v) sodium dodecyl sulfate, following a modified CTAB-chloroform protocol (Cunning et al. 2016; dx.doi.org/10.17504/protocols.io.dyq7vv). Following DNA extraction, the composition of the symbiont community in *M. capitata* was assayed using quantitative PCR (qPCR) (Cunning et al. 2016) by quantifying specific actin gene loci corresponding to internal transcribed spacer (ITS2) region of rDNA for *Cladocopium* and *Durusdinium*, namely, strain C31 and D1a; respectively (D1a has since been reclassified as *D. trenchii*). These primers were chosen because these Symbiodiniaceae strains are known to be the numerically dominant symbionts of *M. capitata* in Kāne`ohe Bay (Cunning et al. 2016). Specificity of genus-level primers have been previously validated using a combination of Symbiodiniaceae ITS2 and actin gene sequencing (Cunning & Baker 2013). Duplicate qPCR reactions (10 μl) were run for each coral sample using a StepOnePlus platform (Applied Biosystems) set to 40 cycles, a relative fluorescence (ΔR_n) threshold of 0.01, and internal cycle baseline of 3 - 15. Symbiont genera detected in only one technical replicate were considered absent. The relative abundance of clade *Cladocopium* and

Durusdinium symbionts (i.e., C:D ratio) in each sample was determined from the ratio of amplification threshold cycles (C_T) for each genera (i.e., C_T^C, C_T^D) using the formula C:D = 2^(C_T^C - C_T^D), where clade-specific C_T values are normalized according to gene locus copy number and fluorescence intensity (Cunning et al. 2016). Coral colonies were determined to be *Cladocopium*- or *Durusdinium*-dominated based on numerical abundance of each clade from qPCR analysis (Innis et al. 2018).

Physiological metrics

The extraction and processing of coral and symbiont tissues were performed following established methods (Wall et al. 2018). Coral tissue was removed from the skeleton using an airbrush filled with filtered seawater (0.2 μm), yielding 10 - 30 ml of tissue slurry. Extracted tissues were briefly homogenized and subsampled for the following physiological metrics: *Symbiodinium* cell densities, total chlorophyll ($a + c_2$) concentrations, protein biomass, and the total organic biomass determined from as the ash-free dry weight (AFDW) of coral + algae tissues. Both the archival tissue slurry and tissue aliquots were stored at -20 °C.

All physiological metrics were normalized to the surface area (cm^2) of coral skeleton using the paraffin wax-dipping technique (Stimson and Kinzie 1991). *Symbiodinium* counts obtained were measured by replicate cell counts (n = 6 - 10) on a haemocytometer, and expressed as *Symbiodinium* cells cm^{-2}. Chlorophyll *a* was quantified by concentrating algal cells through centrifugation (13,000 rpm × 3 min) and extracting pigments in the algal pellet in 100 % acetone for 36 h in darkness at -20 °C. Spectrometric absorbances were measured (λ = 630 and 663 nm) and chlorophyll *a* concentrations were quantified using the equations for dinoflagellates (Jeffrey and Humphrey 1975) and expressed as ug chlorophyll *a* cm^{-2}. Total protein

concentration (soluble + insoluble) were quantified using the Pierce BCA (bicinchoninic acid) Protein Assay Kit (Pierce Biotechnology, Waltham, MA). Protein solubilization was achieved by adding 1 M NaOH and heating (90 °C) for 60 min, followed by the neutralizing to ca. pH 7.5 with 1 N HCl. Protein was measured spectrophotometrically (λ = 562 nm) against a bovine serum albumin standard and expressed as mg protein cm^{-2}. Total fraction of organic biomass was measured by drying a subsample of coral tissue at 60 °C in pre-burned aluminum pans followed by burning in a muffle furnace (450 °C) for 4 h; the difference between the dried and burned masses is the AFDW and expressed as mg cm^{-2}.

Immunological assays

Coral immunology was assessed following previously established protocols for protein extractions and enzymatic assays (Mydlarz et al. 2009, 2010; Palmer et al. 2010, 2011a; Mydlarz & Palmer 2011). Briefly, 3–4 mL of coral tissue slurry was obtained by airbrushing with coral extraction buffer (100 mM TRIS buffer + 0.05 mM dithiothreitol). The resulting slurry was homogenized for 1 min on ice using a hand-held tissue homogenizer (Powergen 125, Fisher Scientific, Waltham, Massachusetts). For melanin concentration estimates, 1 mL of the tissue slurry was freeze-dried for 24 h using a VirTis BTK freeze-dryer (SP Scientific, Warminster, Pennsylvania). The remaining slurry was centrifuged at 4 °C at 2500×*g* (Eppendorf 5810 R centrifuge, Hamburg, Germany) for 5 min to remove cellular debris, and enzymatic assays were performed on aliquots of the supernatant, representing a cell-free extract or soluble protein extract of the host coral. All assays were run in duplicate on separate 96-well microtiter plates using a Synergy HT multidetection microplate reader using Gen5 software (Biotek Instruments,

Winooski, Vermont). Protein concen- trations were estimated using the RED660 protein assay (G Biosciences, Saint Louis, Missouri) against a bovine serum albumin standard curve.

Antioxidant profile

Antioxidant enzymes catalase (CAT) and superoxide dismutase (SOD) were measured. CAT is monitored as a change in absorbance after 25 mM hydrogen peroxide is added to crude protein extract and 50 μL of 10 mM PBS (pH 6.0). CAT activity was estimated as the mM H2O2 scavenged min−1 mg protein−1. SOD activity was analyzed using a commercially available kit (SOD determination kit #19160; Sigma-Aldrich, St. Louis, Missouri) following manufacturer's instructions and expressed as SOD activity mg protein−1. SOD activity was estimated by comparing the absorbance of samples at 450 nm to a positive and negative standard after incubating 10 μL of crude protein extract with manufacturer-provided reagents.

Melanin synthesis pathway

Prophenoloxidase (PPO) activity and melanin (MEL) concentration per sample were used to study the mela- nin synthesis pathways. PPO activity was determined by incubating 20 μL of protein extract and 50 μL of 10 mM phosphate buffered saline (PBS) (pH 7.0) at room tempera- ture with 20 μL of trypsin (0.2 mg mL−1 concentration) for 30 min. 20 μL of 25 mM l-DOPA (Sigma-Aldrich) was then added as a substrate. PPO activity was estimated as change in absorbance min−1 mg protein−1. MEL concentration was estimated using a weighed freeze- dried portion of initial tissue slurry. Melanin was allowed to extract for 48 h in 400 μL of 10 M NaOH after a brief period of bead- beating with 1-mm glass beads. 65 μL of extracted mela- nin was used to determine endpoint absorbance at 495 nm and resulting values were standardized to

a standard curve of commercial melanin (Sigma-Aldrich) and calibrated to µg melanin mg tissue−1.

Statistical analysis

Ecological data (*Montipora capitata* percent cover and percent bleached) were tested in a linear model in R package *lme4* (Douglas et al. 2015) with site (Lilipuna or Reef 14) and status (bleached or recovery) as the main effects and sampling period as a nested effect in status. Overall responses of symbiont physiology (symbiont density and chlorophyll *a* cm^{-2}), coral physiology (total coral protein concentration and coral biomass), antioxidant response (catalase and superoxide dismutase activity), and the melanin synthesis pathway (prophenoloxidase activity and total melanin content) were assess by multivariate generalized linear models using the R package 'MCMCglmm' (Hadfield 2010). Main effects were specified as site and status with sampling period as a nested effect in status. Univariate physiology and immunity response variables were analyzed using a linear model with site (Lilipuna, Reef 14), period (two bleaching and two recovery events), and symbiont community composition (*Cladocopium*- or *Durusdinium*-dominated) as fixed effects. Normal distribution and equal variance assumptions of ANOVA were examined by graphical representation of residuals and quantile:quantile plots. Where assumptions were not met, Box-Cox tests were performed (Box and Cox 1964) and data transformations applied in the package *MASS* (Venables and Ripley 2002). Analysis of variance tables (linear models) and analysis of deviance tables (linear mixed effect models) of type-II sum or squares were generated using the packages *car* (Fox and Weisberg 2011) and *lmerTest* (Kuznetsova et al. 2016). Immune parameters were examined in multivariate space because these data were not separated by coral and symbiont and therefore reflect holobiont responses.

Principal Component Analysis (PCA) was conducted on cumulative protein abundance for each functional group using the 'ggbiplot' function in the R package 'ggbiplot' (Vu 2011). All analyses were performed in *R*, version 3.4.3 (R Development Core Team 2018).

RESULTS

Benthic surveys

Montipora capitata cover declined at Reef 14 by 84 % after the first bleaching event, but not at Lilipuna. However, during the second bleaching event, populations remained stable (figure 1). Overall, the proportion of bleached *M. capitata* differed by site only ($p = 0.005$), with 62 % bleaching occurring at Reef 14 vs 25% at Lilipuna during the first bleaching event and 55 % bleaching occurring at Reef 14 vs 10% at Lilipuna during the second event. Bleached *M. capitata* was not observed during recovery surveys at Lilipuna (table 1).

Physiology metrics

Symbiont physiology differed by species ($p < 0.001$), site × symbiont interactions ($p < 0.001$), bleaching periods ($p = 0.003$) and site × status × symbiont interactions ($p = 0.048$)(table 2). *Symbiodinium* densities (cells cm^{-2}) showed overall declines during bleaching periods and increased post-bleaching ($p < 0.001$)(figure 2A), but symbiont densities did not differ between consecutive bleaching (October 2014 and October 2015) or recovery periods (February 2015 and February 2016)(table 3). Across all levels, corals with symbiont communities dominated by *Durusdinium* symbionts had 83 % higher symbiont densities relative to corals dominated by *Cladocopium* symbonts ($p < 0.001$). Period × symbiont interactions ($p = 0.033$) led to 58 % greater symbiont densities in *Durusdinium* relative to *Cladocopium* corals at both bleaching

periods, and 28 % and 40 % greater during the first and second recovery periods, respectively. Site influenced these effects [period × site × symbiont ($p = 0.012$)]. At Reef 14, symbiont density in *Durusdinium* corals were intermediate between low symbiont density *Cladocopium* (all sites) and high symbiont density Lilipuna *Durusdinium* corals. This pattern in *Durusdinium* corals reverse during the first recovery period and symbiont density were intermediate in Lilipuna *Durusdinium* corals and highest in Reef 14 *Durusdinium* corals. In subsequent periods, symbiont densities were consistently lower in *Cladocopium* relative to *Durusdinium* corals and did not differ among sites. Chlorophyll *a* concentrations (μg cm^{-2}) were lowest during bleaching relative to recovery periods (p <0.001), and lower at Lilipuna compared to Reef 14 ($p \leq 0.012$)(figure 2B). Period × symbiont (p = <0.001) effects showed no difference in chlorophyll *a* cm^{-2} during the first bleaching and recovery period (table 3). However, chlorophyll *a* was 38 % lower (second bleaching) and 21 % higher (second recovery) in *Cladocopium* corals relative to *Durusdinium* corals.

Overall coral physiology was primarily influenced by bleaching ($p < 0.001$) or recovery ($p < 0.001$) periods (table 2). Protein biomass was influenced by the period × site interaction (p = 0.002)(table 3), but this was limited to the first bleaching event where corals at Lilipuna had 32 % more protein than corals at Reef 14 (figure 2C). However, protein biomass did not differ among sites at all other periods. Coral protein (mg cm^{-2}) was influenced by symbiont type (p = 0.031), with *Durusdinium* corals having 9 % more protein than clade C corals (figure 2D).

Immunity metrics

Antioxidant response mainly showed differences resulting from different bleaching periods ($p = 0.001$), although there was a slight effect from site × status interactions (0.093)(table

4). Catalase (CAT) differed among periods (p <0.001), sites (p <0.001), the period × site interaction (p <0.001), and symbiont type (p = 0.002)(table 5). CAT was highest during bleaching events, being greatest at the second bleaching compared to the first bleaching period (figure 3A). CAT was lowest during both recovery periods and was not different at in the first or second recovery period. During the first year of bleaching and recovery, patterns in CAT activity at each time point were equivalent between sites. However, during the second year, CAT activity was higher at Lilipuna compared to Reef 14 within both both bleaching and recovery periods. CAT activity was also higher in clade D relative to clade C corals. Superoxide dismutase (SOD) increased through time (p <0.001)(figure 3B)(table 5) following the chronology of bleaching and recovery periods first bleaching period through the second recovery period. SOD was also higher in Lilipuna corals relative to those from Reef 14 (p = 0.028).

The melanin synthesis cascade differed by site (p = 0.021), status (p < 0.001), site × status interactions (p = 0.028) and different bleaching (p < 0.001) and recovery (p < 0.001) periods (table 4). Prophenoloxidase (PPO) was affected by periods (p <0.001), site (p = 0.041), and symbiont types (p = 0.043)(table 5). PPO was lowest during the second bleaching period and highest at second recovery period and intermediate at other time points (figure 3C). PPO was also higher at Reef 14 compared to Lilipuna and in *Durusdinium* corals relative to *Cladocopium* corals (p = 0.041). Melanin (MEL) differed among periods (p = 0.001) and the interaction of period × symbiont (p <0.001)(table 5). MEL was highest during the first bleaching event but had substantially decreased by the first recovery period (figure 3D). During the second year, MEL showed a similar pattern of increasing with bleaching and declined post-bleaching, however, the magnitude of MEL increase during second year bleaching was small relative to the first-year bleaching.

Overall bleaching and recovery patterns

Bleaching (figure 4A) and recovery (figure 4B) patterns separated by period (i.e., bleaching period one was distinct from bleaching period two; and recovery period one was distinct from recovery period two) regardless of reef site or dominant symbiont partner. Bleaching period one was primarily influenced by the melanin synthesis pathway while bleaching period two was influenced by antioxidant responses. Both recovery periods were influenced by components of the melanin synthesis pathway.

Variability for bleaching period one was greater than that of bleaching period two. Corals from Reef 14 dominated by *Durusdinium* symbionts showed the greatest variability for bleaching period one. For bleaching period two, *Durusdinium*-dominated corals displayed the most variability regardless of reef site. Recovery periods one and two displayed similar overall variances. However, in contrast to bleaching periods, *Durusdinium*-dominated corals from Reef 14 showed the least variation in response during recovery period two.

DISCUSSION

Consecutive bleaching seasons are a unique stress, as some effects may last even a year after bleaching (Pinzon et al. 2015). This implies that some aspects of coral immunity and physiology may not fully recover before a second assault occurs. Alternatively, each bleaching season may affect corals differently and highlights the need for multiple mechanisms when coping with bleaching stress. Natural laboratories within Kāne`ohe Bay were thus taken advantage of to elucidate the role of microhabitat and individual components of the holobiont in stress responses. This study provides rare insight into the role of inducible immunity during

annual bleaching events and demonstrates the importance of environmental history and symbiotic partner in determining coral responses to these stresses.

Dominant symbiotic partner affected overall physiology to a greater degree than immunity. Differences were apparent in all parameters of physiology measured. In particular, *Durusdinium*-dominant corals maintained higher symbiont cells cm^{-2}. They also maintained higher biomass, especially in those from Lilipuna. Conversely, this was only minimally influential on coral immunity. Differences were primarily observed in catalase during the first bleaching event and in superoxide dismutase during the first recovery period. In both instances, *Durusdinium*-dominant corals from Lilipuna displayed the highest activity. *Cladocopium*-dominant corals from Lilipuna, and *Cladocopium*- and *Durusdinium*-dominant corals from Reef 14, differed only marginally.

The melanin synthesis cascade was the most responsive parameter during the first bleaching event, while catalase was highly responsive to the second bleaching event. Additionally, superoxide dismutase levels rose steadily throughout the study period and was highest during the final recovery period. These patterns show the importance of considering each component of the holobiont, as immunity primarily displayed either reef-specific responses or season-specific responses despite the influence of symbiotic partner on physiology. It may be that immunity reveals the favorable state for survival in the face of consecutive bleaching, and that the coral host and the symbiotic partner can differentially contribute to the overall holobiont response to achieve the same end.

Coral cover and bleaching prevalence at each site may be particularly relevant when discerning survival strategies for each population. *Montipora capitata* cover declined at Reef 14 after the first bleaching event, but not at Lilipuna. Additionally, a larger proportion of *M.*

capitata bleached during this time at Reef 14 than did at Lilipuna. However, during the second bleaching event populations remained stable at both sites and only moderate bleaching occurred. Taking into account the dynamic and reef-specific regulation of immune parameters, it appears that Lilipuna corals display the favorable immune state. Corals at Reef 14, on the other hand, appear to have undergone selection during the first bleaching season, with the remaining population demonstrating a similar robustness to bleaching stress as those at Lilipuna.

Mechanisms conferring thermal tolerance in reef corals have been extensively investigated. For example, coral existence in thermally variable (Oliver and Palumbi 2011) or thermally elevated (Kenkel, Meyer & Matz 2013) environments have demonstrated resistance to bleaching. Additionally, some corals have demonstrated bleaching resistance associated with higher energy stores (Grottoli et al. 2014) or higher rates of heterotrophic feeding rates (Grottoli, Rodrigues and Palardy 2006). In Kāne`ohe Bay, *M. capitata* appear to display two tactics when faced with repeated bleaching: 1) frontloading (Barshis et al. 2013), or the higher constitutive expression of, superoxide dismutase (SOD); and 2) immune resilience, similar to transcriptome resilience (Seneca and Palumbi 2015), and here defined as the induction of an immune response and subsequent return to normal levels.

Frontloading of heat shock protein and immune-related genes (Barshis et al. 2013), metabolic genes (Kenkel, Meyer & Matz 2013), and stress response genes (Barfield et al. 2018) are associated with higher thermotolerance in some corals. It is hypothesized to be a baseline strategy for long-term heat acclimation (Barshis et al. 2013). The antioxidant SOD catalyzes the dismutation of the superoxide anion (O_2^-) to H_2O_2 and O_2, while H_2O_2 is further broken down to O_2 and water by catalase (Mydlarz et al. 2016). It is not clear why one parameter would be frontloaded and not others, however, one hypothesis is that it relieves some of the burden of

synthesizing sufficient levels at the time of bleaching (Barshis et al. 2013). Conversely, it may indicate that *M. capitata* were experiencing chronic stress, as the study period encompassed El Niño conditions in addition to record-breaking temperatures. Some corals increase their metabolic rates in response to increased temperatures (Edmunds, Cumbo and Fan 2011), which would in turn increase the need for antioxidants due to reactive oxygen species as a metabolic byproduct (Das and Roychoudhury 2014). Indeed, SOD is upregulated in direct response to increased metabolic activity (Hassan and Fridovich 1977).

In some corals, higher baseline immunity is also associated with thermotolerance (Barshis et al. 2013; Palmer, Blythell & Willis 2010). However, *M. capitata* constitutive immunity does not appear to be as influential as inducible immunity when surviving repeated bleaching given that, prior to the study period, Lilipuna corals displayed lower constitutive levels of both catalase and superoxide dismutase (Wall et al. 2018). Instead, we show evidence that the different initial levels ultimately converge on a similar pattern, and that specific interactions between the coral host, symbiotic partner, and environmental factors must influence the mechanisms by which this is achieved. In particular, melanin and catalase displayed strong responses, and then a drop back down to, or near to, recovery levels. This was especially true for catalase. Of note, although Lilipuna corals display a higher catalase response, bleaching differed only marginally. Therefore, the extent of the response may be less important that the actual ability to respond.

Both the antioxidant response and the melanin synthesis cascade are important for coping with stress events. The melanin synthesis cascade, for example, is vital for wound healing (Palmer et al. 2011; Rodríguez-Villalobos, Work, & Calderon-Aguilera 2016) and is implicated in symbiont UV protection (Palmer et al. 2010; Palmer et al. 2011a). Antioxidants are similarly

vital for mitigating cellular damage during immune responses (Pourova et al. 2010) and increased metabolic activity (Frisard and Ravussin 2006). Therefore, roles of the immune system span beyond disease and pathogen protection and has even been proposed as a general homeostasis mechanism (Palmer 2018). To this end, the coral animal must necessarily balance the contributions of its own responses and that of the symbiont to achieve total holobiont homeostasis.

Corals and Symbiodiniaceae respond to stress in distinct manners. Specifically, while corals can exhibit large transcriptional changes in response to heat (Leggat et al. 2011), transcriptomic profiles of resident symbionts remain minimally altered (Leggat et al. 2011; Barshis et al. 2011). This is in contrast to observable drops in photosynthetic capacity (Wall et al. 2018; Kemp et al. 2014), increased production of reactive oxygen species (McGinty, Pieczonka, & Mydlarz 2012), and increased production of nitric oxide (Hawkins and Davy 2012). These responses naturally invoke the need for antioxidative protection in the coral host, although the simultaneous regulation of other immune responses is necessary to prevent the removal of the symbiont. Indeed, failure to do so can result in symbiosis breakdown and ultimately lead to coral bleaching. On a broad scale, misregulation of immune responses may therefore contribute to global coral declines.

CONCLUDING REMARKS

Functional immunity and physiological parameters were measured to provide a phenotype, and thus context, to previous transcriptional studies examining holobiont responses to stress. Environmental history was found to shape coral host and symbiont physiology and subsequent responses to repeated bleaching. However, corals ultimately converged on the same

immune patterns despite reef of origin, demonstrating that differential contributions of each partner to the overall holobiont response achieves a favorable immune state for repeat bleaching survival. This study thus provides important perspective on the impacts of consecutive bleaching events.

Papahānaumokuākea Marine National Monument (Northwestern Hawaiian Islands) experienced up to 91% coral bleaching in some areas during the 2014 heat wave (Couch et al. 2017) that was encompassed in this study. Similarly, the Great Barrier Reef lost 30% of coral cover during the record breaking 2016 heatwave (Hughes et al. 2018) that occurred shortly after this study. The global decline of coral reefs due to elevated sea surface temperatures will likely be accelerated as bleaching events are predicted to become annual phenomena. Therefore, understanding their impacts and capacity to shape future reefs is of vital importance.

REFERENCES

Andersson AJ, Gledhill D (2013) Ocean Acidification and Coral Reefs: Effects on Breakdown, Dissolution, and Net Ecosystem Calcification. Ann Rev Mar Sci 5:321 – 348

Baker A (2003) Flexibility and Specificity in Coral-Algal Symbiosis: Diversity, Ecology, and Biogeography of Symbiodinium. Annu Rev Ecol Evol Syst 34:661 – 689

Barfield SJ, Aglyamova GV, Bay LK, Matz MV (2018) Contrasting effects of Symbiodinium identity on coral host transcriptional profiles across latitudes. Mol Ecol 27:3103 - 3115

Barshis DJ, Ladner JT, Oliver TA, Seneca FO, Traylor-Knowles N, Palumbi SR (2013) Genomic basis for coral resilience to climate change PNAS 110:1387 – 1392

Barshis DJ, Ladner JT, Oliver TA, Palumbi SR (2014) Lineage-specific transcriptional profiles of Symbiodinium spp. unaltered by heat stress in a coral host. Mol Biol Evol 31:1343-1352

Box GEP, Cox DR (1964) An analysis of transformations. J R Stat Soc Ser B Methodol 26:211 - 252

Colombo-Pallotta MF, Rodríguez-Román A, Iglesias-Prieto R (2010) Calcification in bleached and unbleached *Montastraea faveolata*: evaluating the role of oxygen and glycerol. Coral Reefs 29: 899 – 907

Couch CS, Burns JHR, Liu G, Steward K, Gutlay TN, Kenyon J, et al. (2017) Mass coral bleaching due to unprecedented marine heatwave in Papahānaumokuākea Marine National Monument (Northwestern Hawaiian Islands). PLoS ONE 12(9): e0185121. https://doi.org/10.1371/journal.pone.0185121

Cunning R, Baker AC (2013) Excess algal symbionts increase the susceptibility of reef corals to bleaching. Nat Clim Chang 3:259 – 262

Cunning R, Ritson-Williams R, Gates RD (2016) Patterns of bleaching and recovery of Montipora capitata in Kāne'ohe Bay. Mar Ecol Prog Ser 551:131-139

Das K, Roychoudhury A (2014) Reactive oxygen species (ROS) and response of antioxidants as ROS-scavengers during environmental stress in plants. Front environ sci 2:53

Douglas Bates, Martin Maechler, Ben Bolker, Steve Walker (2015). Fitting Linear Mixed-Effects Models Using lme4. Journal of Statistical Software, 67(1), 1-48. <doi:10.18637/jss.v067.i01>

Edmunds PJ, Davies PS (1989) An energy budget for *Porites porites* (Scleractinia), growing in a stressed environment. Coral Reefs 8: 37 – 43

Edmunds PJ, Cumbo V, Fan TY (2011) Effects of temperature on the respiration of brooded larvae from tropical reef corals. J Exper Biol 214:2783 – 2790

Frisard and Ravussin (2006) Energy Metabolism and Oxidative Stress: Impact on the Metabolic Syndrome and the Aging Process. Endocr 29:27–32

Grottoli AG, Rodrigues LJ, Palardy JE (2006) Heterotrophic plasticity and resilience in bleached corals. Nature 440:1186 - 1189

Grottoli AG, Warner ME, Levas SJ, Aschaffenburg MD, Schoepf V, McGinley M, Baumann J, Matsui Y (2014) The cumulative impact of annual coral bleaching can turn some coral species winners into losers. Glob Chang Biol 20:3823–3833

Jarrod D Hadfield (2010). MCMC Methods for Multi-Response Generalized Linear Mixed Models: The MCMCglmm R Package. Journal of Statistical Software, 33(2), 1-22. URL http://www.jstatsoft.org/v33/i02/

Hawkins TD, Davy SK (2012) Nitric Oxide Production and Tolerance Differ Among *Symbiodinium* Types Exposed to Heat Stress. Plant Cell Physiol 53:1889 – 1898

Hughes TP, Kerry JT, Álvarez-Noriega M, Álvarez-Romero JG, Anderson KD, Baird AH, Babcock RC, Beger M, Bellwood DR, Berkelmans R, Bridge TC, Butler IR, Byrne M, Cantin NE, Comeau S, Connolly SR, Cumming GS, Dalton SJ, Diaz-Pulido G, Eakin CM, Figueira WF, Gilmour JP, Harrison HB, Heron SF, Hoey AS, Hobbs JA, Hoogenboom MO, Kennedy EV, Kuo CY, Lough JM, Lowe RJ, Liu G, McCulloch MT, Malcolm HA, McWilliam MJ, Pandolfi JM, Pears RJ, Pratchett MS, Schoepf V, Simpson T, Skirving WJ, Sommer B, Torda G, Wachenfeld DR, Willis BL, Wilson SK (2017) Global warming and recurrent mass bleaching of corals. Nature 543:373-377

Hughes TP, Kerry JT, Baird AH, Connolly SR, Dietzel A, Eakin CM, Heron SF, Hoey AS, Hoogenboom MO, Liu G, McWilliam MJ, Pears RJ, Pratchett MS, Skirving WJ, Stella JS, Torda G (2018) Global warming transforms coral reef assemblages. Nature 556:492-496

Innis T., Cunning R., Ritson-Williams R., Wall CB, Gates RD. Coral Reefs (2018) 37: 423. https://doi.org/10.1007/s00338-018-1667-0

John Fox and Sanford Weisberg (2019). An {R} Companion to Applied Regression, Third Edition. Thousand Oaks CA: Sage.
URL: https://socialsciences.mcmaster.ca/jfox/Books/Companion/

Jones AM, Berkelmans R (2011) Tradeoffs to Thermal Acclimation: Energetics and Reproduction of a Reef Coral with Heat Tolerant Symbiodinium Type-D. J Mar Biol (2011) Article ID 185890

Kenkel CD, Meyer E, Matz MV (2013) Gene expression under chronic heat stress in populations of the mustard hill coral (*Porites astreoides*) from different thermal environments. Mol Ecol 22:4322 – 4334

Kuznetsova A, Brockhoff PB, Christensen RHB (2017). "lmerTest Package: Tests in Linear Mixed Effects Models." *Journal of Statistical Software*, 82(13), 1–26. doi: 10.18637/jss.v082.i13.

Leggat W, Seneca F, Wasmund K, Ukani L, Yellowlees D, Ainsworth TD (2011) Differential Responses of the Coral Host and Their Algal Symbiont to Thermal Stress. PLoS ONE 6(10): e26687. doi:10.1371/journal.pone.0026687

Little AF, van Oppen MJ, Willis BL (2004) Flexibility in algal endosymbioses shapes growth in reef corals. Science. 304:1492 – 1494

Lowe RJ, Falter JL, Monismith SG, Atkinson MJ (2009) A numerical study of circulation in a coastal reef-lagoon system. J Geophys Res 114:C06022

McGinty ES, Pieczonka J, Mydlarz LD (2012) Variations in reactive oxygen release and antioxidant activity in multiple Symbiodinium types in response to elevated temperature. Microb Ecol 64:1000-10007

Mydlarz LD, Holthouse SF, Peters EC, Harvell CD (2008) Cellular Responses in Sea Fan Corals: Granular Amoebocytes React to Pathogen and Climate Stressors. PLoS One 3: e1811

Mydlarz LD, Couch CS, Weil E, Smith G, Harvell CD (2009) Immune defenses of healthy, bleached and diseased Montastraea faveolata during a natural bleaching event. Dis Aquat Organ 87:67-78

Mydlarz LD, McGinty ES, Harvell CD (2010) What are the physiological and immunological responses of coral to climate warming and disease? J Exp Biol 213:934–945

Mydlarz LD, Palmer CV (2011) The presence of multiple phenoloxi- dases in Caribbean reef-building corals. Comp Biochem Physiol A Mol Integr Physiol 159:372–378

Mydlarz LD, Fuess LE, Mann MT, Pinzon JH, Gochfeld DJ (2016) Cnidarian Immunity: From Genomes to Phenomes. In: Goffredo S, Dubinsky Z. The Cnidaria, Past, Present, and Future. 10.1007/978-3-319-31305-4_28.

Nielsen DA, Petrou K, Gates RD (2018) Coral bleaching from a single cell perspective. ISME J 12:1558 - 1567

NOAA (2017) Tides and Currents. Mokuoloe, Hawaii, Station ID: 1612480. National Oceanic and Atmospheric Administra- tion, USA. https://tidesandcurrents.noaa.gov/stationhom e.html?id=1612480. [Accessed March 2017]

NOAA (2018) Tides and Currents. Mokuoloe, Hawaii, Station ID: 1612480. National Oceanic and Atmospheric Administration, USA. https://tidesandcurrents.noaa.gov/stationhome.html?id=1612480. [Accessed June 2018]

Oliver TA, Palumbi SR (2011) Do fluctuating temperature environments elevate coral thermal tolerance?. Coral Reefs 30:429–440

Palmer CV, Bythell JC, Willis BL (2010) Levels of immunity parameters underpin bleaching and disease susceptibility of reef corals. FASEB J 24:1935–1946

Palmer CV, McGinty ES, Cummings DJ, Smith SM, Bartels E, Mydlarz LD (2011a) Patterns of coral ecological immunology: variation in the responses of Caribbean corals to elevated temperature and a pathogen elicitor. J Exp Biol 214:4240 – 4249

Palmer CV, Traylor-Knowles NG, Willis BL, Bythell JC (2011) Corals Use Similar Immune Cells and Wound-Healing Processes as Those of Higher Organisms. PLoS ONE 6(8): e23992. doi:10.1371/journal.pone.0023992

Palmer CV, Bythell JC, Willis BL (2012a) Enzyme activity demonstrates multiple pathways of innate immunity in Indo-Pacific anthozoans. Proc Biol Sci 279: 3879–3887

Palmer CV, Bythell JC, Willis BL (2012) Enzyme activity demonstrates multiple pathways of

innate immunity in Indo-Pacific anthozoans. Proc Biol Sci 279:3879 – 3887

Palmer CV (2018) Immunity and the coral crisis. Commun Biol 1:91 doi: 10.1038/s42003-018-0097-4

Pinzón JH, Kamel B, Burge CA, Harvell CD, Medina M, Weil E, Mydlarz LD (2015) Whole transcriptome analysis reveals changes in expression of immune-related genes during and after bleaching in a reef-building coral. R Soc Open Sci 2:140214

Rodríguez-Villalobos JC, Work TM, Calderon-Aguilera LE (2016) Wound repair in Pocillopora. J Invertebr Pathol. Sep;139:1-5

Seneca FO, Palumbi SR (2015) The role of transcriptome resilience in resistance of corals to bleaching. Mol Ecol 24:1467 - 1484

Stat M, Gates RD (2011) Clade D Symbiodinium in Scleractinian Corals: A Nugget of Hope, a Selfish Opportunist, an Ominous Sign, or All of the Above?. J Mar Biol (2011) Article ID 730715

Stimson J, Kinzie RA III (1991) The temporal pattern and rate of release of zooxanthellae from the reef coral *Pocillopora damicornis* (Linnaeus) under nitrogen-enrichment and control conditions. J Exp Mar Biol Ecol 153:63 - 74

van Hooidonk R, Maynard JA, Planes S (2013) Temporary refugia for coral reefs in a warming world. Nat Clim Chang 3:508–511

Venables WN, Ripley BD (2002) Modern applied statistics with S-PLUS, 4th edn. Springer, New York

Vu V. 2011. A ggplot2 based biplot. R package version 0.55. http://github.com/vqv/ggbiplot

Wall CB, Ricci CA, Foulds GE, Mydlarz LD, Gates RD, Putnam HM (2018) The effects of environmental history and thermal stress on coral physiology and immunity. Mar Biol 165:56

Appendix 4A: Tables and Figures

TABLES

Table 1. Statistical analysis of *Montipora capitata* cover and bleaching status for Lilipuna and Reef 14 sites

Dependent var.	*Effect*	*Estimate*	*Std. Error*	*t value*	*Pr(>|t|)*
M. capitata cover	(Intercept)	0.4917	0.1205	4.08	**0.002**
	Site	0.2582	0.1391	1.856	0.093
	Status	-0.2134	0.1704	-1.252	0.239
	Site x Status	-0.3212	0.1968	-1.632	0.134
	Recovery x Period	-0.3136	0.1391	-2.254	**0.048**
	Bleached x Period	0.2173	0.1391	1.562	0.149
M. capitata bleached	(Intercept)	0.22917	0.09971	2.298	**0.044**
	Site	0.40833	0.11514	3.546	**0.005**
	Status	-0.2625	0.14102	-1.861	0.092
	Site x Status	-0.175	0.16283	-1.075	0.308
	Recovery x Period	-0.10833	0.11514	-0.941	0.369
	Bleached x Period	0.06667	0.11514	0.579	0.575

Site = two reef locations (Lilipuna and Reef 14); *Status* = bleaching and recovery; *Period* = Four events [first bleaching (October 2014), first recovery (February 2015), second bleaching (October 2015), second recovery (February 2016)]

Table 2. Multivariate general linear mixed model analysis of physiology parameters for symbionts and coral.

		post.mean	l-95% CI	u-95% CI	eff.samp	pMCMC
Symbiont physiology	(Intercept)	12.35427	12.21645	12.4973	2000	**<5e-04**
	Site	0.11447	-0.05427	0.28005	2000	0.159
	Status	0.20071	-0.00736	0.41903	2000	0.063
	Symbiont	0.76594	0.59463	0.92213	2000	**<5e-04**
	Site x Status	-0.12497	-0.37617	0.12441	2000	0.331
	Site x Symbiont	-0.45204	-0.68635	-0.21991	2000	**<5e-04**
	Status x Symbiont	-0.13353	-0.39016	0.10352	2000	0.28
	Recovery x Period	-0.0769	-0.19638	0.04533	2075	0.207
	Bleached x Period	0.18577	0.07243	0.3086	2000	**0.003**
	Site x Status x Symbiont	0.33863	0.01486	0.67702	2000	**0.048**
		post.mean	l-95% CI	u-95% CI	eff.samp	pMCMC
Coral physiology	(Intercept)	3.815076	3.696285	3.956838	2143	**<5e-04**
	Site	-0.090558	-0.246469	0.071407	2399	0.276
	Status	0.176048	-0.017448	0.386559	2197	0.086
	Symbiont	0.077729	-0.070558	0.242	2000	0.352
	Site x Status	0.036989	-0.218494	0.264853	2000	0.762
	Site x Symbiont	-0.066011	-0.284128	0.158368	2000	0.542
	Status x Symbiont	-0.037261	-0.266433	0.191589	2000	0.766
	Recovery x Period	-0.460213	-0.577238	-0.355607	2000	**<5e-04**
	Bleached x Period	0.543536	0.432594	0.65211	2000	**<5e-04**
	Site x Status x Symbiont	-0.002546	-0.356947	0.296846	2000	0.996

Site = two reef locations (Lilipuna and Reef 14); *Status* = bleaching and recovery; *Period* = Four events [first bleaching (October 2014), first recovery (February 2015), second bleaching (October 2015), second recovery (February 2016)]; *Symbiont* = symbiont community dominated by *Cladocopium* or *Durusdinium* species

Table 3. Statistical analysis of environmental history and bleaching event effects on *Symbiodinium* and *Montipora capitata* physiology.

Dependent variable	*Effect*	*SS*	*df*	*F*	*P*
Symbiodinium cm^{-2}	Period	1.108×10^{13}	3	9.470	**<0.001**
	Site	3.068×10^{10}	1	0.079	0.797
	Symbiont	5.640×10^{13}	1	144.647	**<0.001**
	Period × Site	4.604×10^{12}	3	3.936	**0.009**
	Period × Symbiont	3.461×10^{12}	3	2.959	**0.033**
	Site × Symbiont	8.347×10^{11}	1	2.141	0.144
	Period × Site × Symbiont	4.342×10^{12}	3	3.712	**0.012**
	Residual	1.174×10^{14}	301		
chlorophyll *a* cm^{-2}	Period	85.343	3	11.986	**<0.001**
	Site	23.851	1	10.049	**0.002**
	Symbiont	3.414	1	1.438	0.231
	Period × Site	7.037	3	0.988	0.399
	Period × Symbiont	66.062	3	9.378	**<0.001**
	Site × Symbiont	0.069	1	0.029	0.865
	Period × Site × Symbiont	12.746	3	1.790	0.149
	Residual	714.410	301		
chlorophyll *a* $cell^{-1}$	Period	19.268	3	6.870	**<0.001**
	Site	5.957	1	6.382	**0.012**
	Symbiont	181.229	1	193.843	**<0.001**
	Period × Site	4.064	3	1.449	0.229
	Period × Symbiont	14.105	3	5.029	**0.002**
	Site × Symbiont	3.234	1	3.459	0.064
	Period × Site × Symbiont	6.149	3	2.192	0.089
	Residual	278.608	298		
protein cm^{-2}	Period	0.058	3	0.722	0.540
	Site	0.053	1	1.980	0.160
	Symbiont	0.126	1	4.706	**0.031**
	Period × Site	0.412	3	5.135	**0.002**
	Period × Symbiont	0.035	3	0.440	0.725
	Site × Symbiont	0.011	1	0.394	0.530
	Period × Site × Symbiont	0.048	3	0.596	0.618
	Residual	8.020	300		

Period = Four events [first bleaching (October 2014), first recovery (February 2015), second bleaching (October 2015), second recovery (February 2016)]; *Site* = two reef locations (Lilipuna and Reef 14); *Symbiont* = symbiont community dominated by *Cladocopium* or *Durusdinium* species. *SS* = sum of squares and *df* = degrees of freedom

Table 4. Multivariate general linear mixed model analysis of immunity parameters

Dependent	*Effect*	post.mean	l-95% CI	u-95% CI	eff.samp	pMCMC
Antioxidants	(Intercept)	117810	42684	192137	2000	**0.003**
	Site	-64250	-158628	26177	2000	0.173
	Status	-59432	-165451	35452	2000	0.273
	Symbiont	52018	-37193	145724	2223	0.257
	Site x Status	99727	-6751	227769	2000	0.093
	Site x Symbiont	-52345	-171213	64704	2237	0.371
	Status x Symbiont	-29454	-140412	80048	2000	0.613
	Recovery x Period	5993	-79344	95013	2000	0.893
	Bleached x Period	155354	71257	239066	2000	**0.001**
	Site x Status x Symbiont	-19830	-154977	124398	2299	0.780
		post.mean	l-95% CI	u-95% CI	eff.samp	pMCMC
Melanin synthesis	(Intercept)	-2.66719	-2.93713	-2.38058	1813	**<5e-04**
	Site	-0.39651	-0.74326	-0.06436	1995	**0.021**
	Status	-2.33934	-2.75081	-1.90932	1759	**<5e-04**
	Symbiont	-0.10404	-0.40788	0.23292	2000	0.549
	Site x Status	0.62604	0.13674	1.21432	1858	**0.028**
	Site x Symbiont	0.07112	-0.41438	0.52135	2000	0.768
	Status x Symbiont	-0.14592	-0.67058	0.3296	1697	0.583
	Recovery x Period	-3.27933	-3.54864	-3.01634	1656	**<5e-04**
	Bleached x Period	-1.27829	-1.50975	-1.03632	2000	**<5e-04**
	Site x Status x Symbiont	-0.04161	-0.79221	0.64455	1779	0.912

Site = two reef locations (Lilipuna and Reef 14); *Status* = bleaching and recovery; *Period* = Four events [first bleaching (October 2014), first recovery (February 2015), second bleaching (October 2015), second recovery (February 2016)]; *Symbiont* = symbiont community dominated by *Cladocopium* or *Durusdinium* species

Table 5. Statistical analysis of environmental history and bleaching event effects on antioxidant enzymes and immune activity of *Montipora capitata.*

Dependent variable	*Effect*	*SS*	*df*	*F*	*P*
Catalase (CAT)	Period	3048.497	3	117.049	**<0.001**
	Site	185.209	1	21.334	**<0.001**
	Symbiont	80.983	1	9.328	**0.002**
	Period x Site	228.314	3	8.766	**<0.001**
	Period x Symbiont	57.881	3	2.222	0.086
	Site x Symbiont	1.590	1	0.183	0.669
	Period x Site x Symbiont	22.454	3	0.862	0.461
	Residual	2526.337	291		
Peroxidase (POX)	Period	1.657	3	16.504	**<0.001**
	Site	0.121	1	3.619	0.058
	Symbiont	0.001	1	0.042	0.838
	Period x Site	0.089	3	0.884	0.450
	Period x Symbiont	0.363	3	3.612	**0.014**
	Site x Symbiont	0.018	1	0.547	0.460
	Period x Site x Symbiont	0.014	3	0.138	0.937
	Residual	9.502	284		
Superoxide dismutase (SOD)	Period	1.349×10^{10}	3	83.207	**<0.001**
	Site	2.631×10^{8}	1	4.867	**0.028**
	Symbiont	8.110×10^{7}	1	1.500	0.222
	Period x Site	9.381×10^{7}	3	0.578	0.630
	Period x Symbiont	2.319×10^{8}	3	1.430	0.234
	Site x Symbiont	3.041×10^{7}	1	0.378	0.539
	Period x Site x Symbiont	1.021×10^{8}	3	0.630	0.596
	Residual	1.616×10^{10}	299		
Prophenoloxidase (PPO)	Period	8.112	3	207.503	**<0.001**
	Site	0.055	1	4.227	**0.041**
	Symbiont	0.054	1	4.135	**0.043**
	Period x Site	0.002	3	0.051	0.985
	Period x Symbiont	0.020	3	0.510	0.676
	Site x Symbiont	0.069×10^{-3}	1	0.005	0.942

	Period x Site x Symbiont	0.001	3	0.031	0.993
	Residual	3.857	296		
Melanin (MEL)	Period	1.713	3	1133.636	**<0.001**
	Site	0.001	1	1.112	0.292
	Symbiont	0.013×10^{-5}	1	0.000	0.987
	Period x Site	0.016	3	10.241	**<0.001**
	Period x Symbiont	0.002	3	1.276	0.283
	Site x Symbiont	9.972×10^{-5}	1	0.198	0.657
	Period x Site x Symbiont	0.257×10^{-3}	3	0.170	0.917
	Residual	0.150	297		

Period = Four events [first bleaching (October 2014), first recovery (February 2015), second bleaching (October 2015), second recovery (February 2016)]; *Site* = two reef locations (Lilipuna and Reef 14);S*ymbiont* = symbiont community dominated by clade C or D *Symbiodinium* spp. *SS* = sum of squares and *df* = degrees of freedom

FIGURES

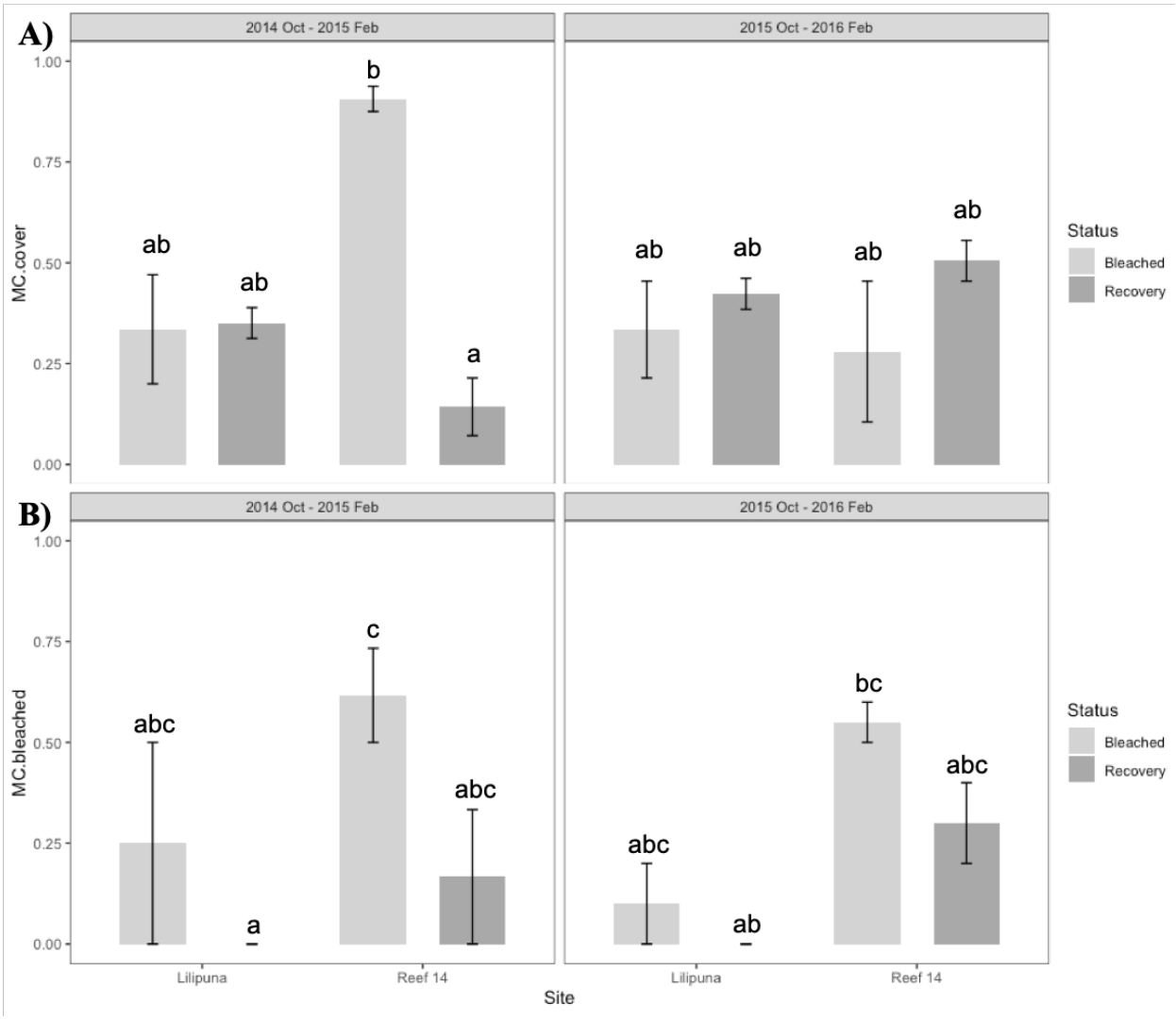

Figure 1 Field surveys documenting M. captitata *cover (A) and* M. captiata *that bleached (B) during the first (2014 Oct - 2015 Feb) and second (2015 Oct - 2015 Feb) bleaching seasons. Y axis represents percent abundance*

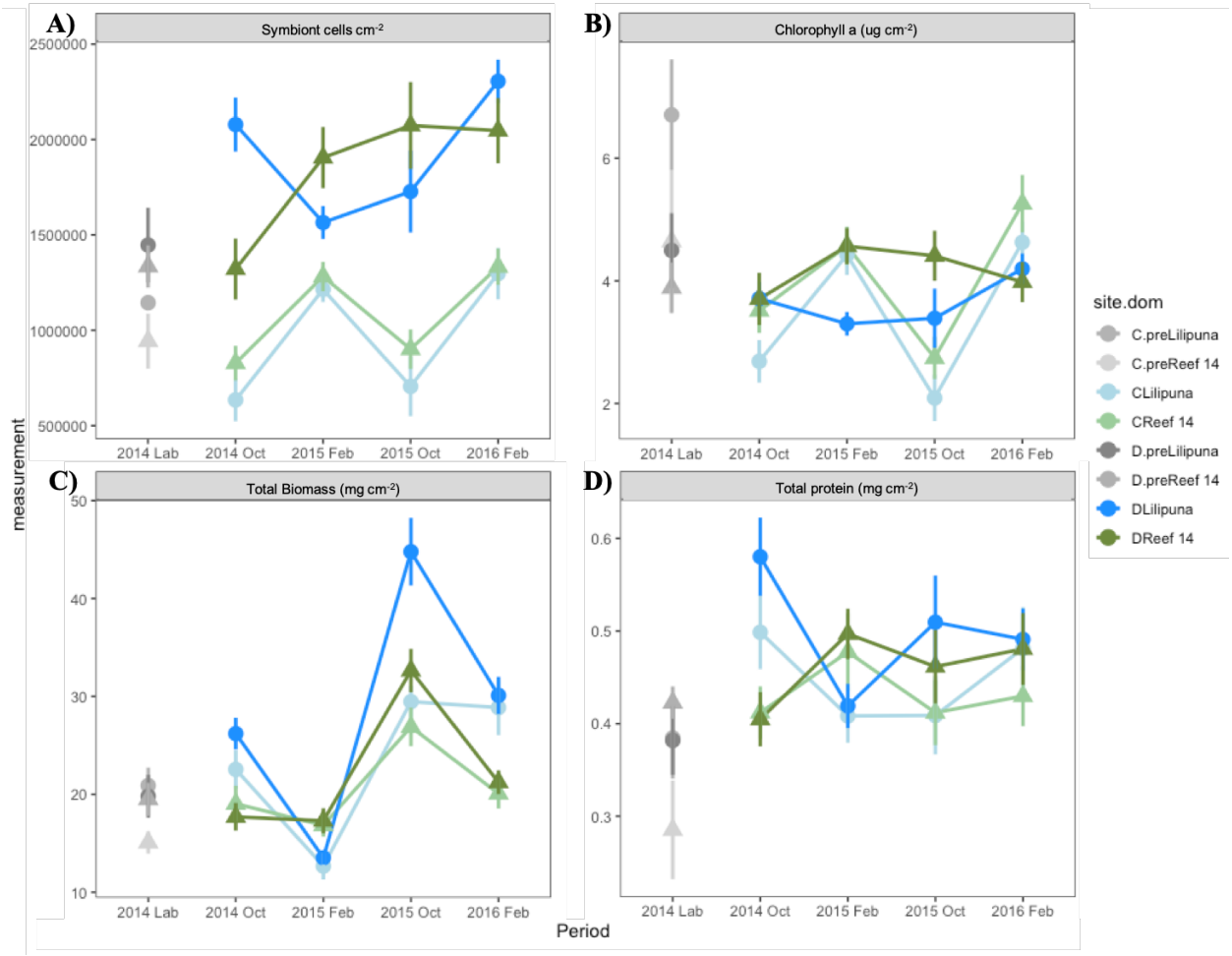

Figure 2 Symbiont (A-B) and coral (C-D) physiology parameters. Dark hues represent Durusdinium *dominated corals, light hues represent* Cladocopium *dominated corals. Circles and blue hues represent Lilipuna corals, green hues and triangle represent Reef 14 corals*

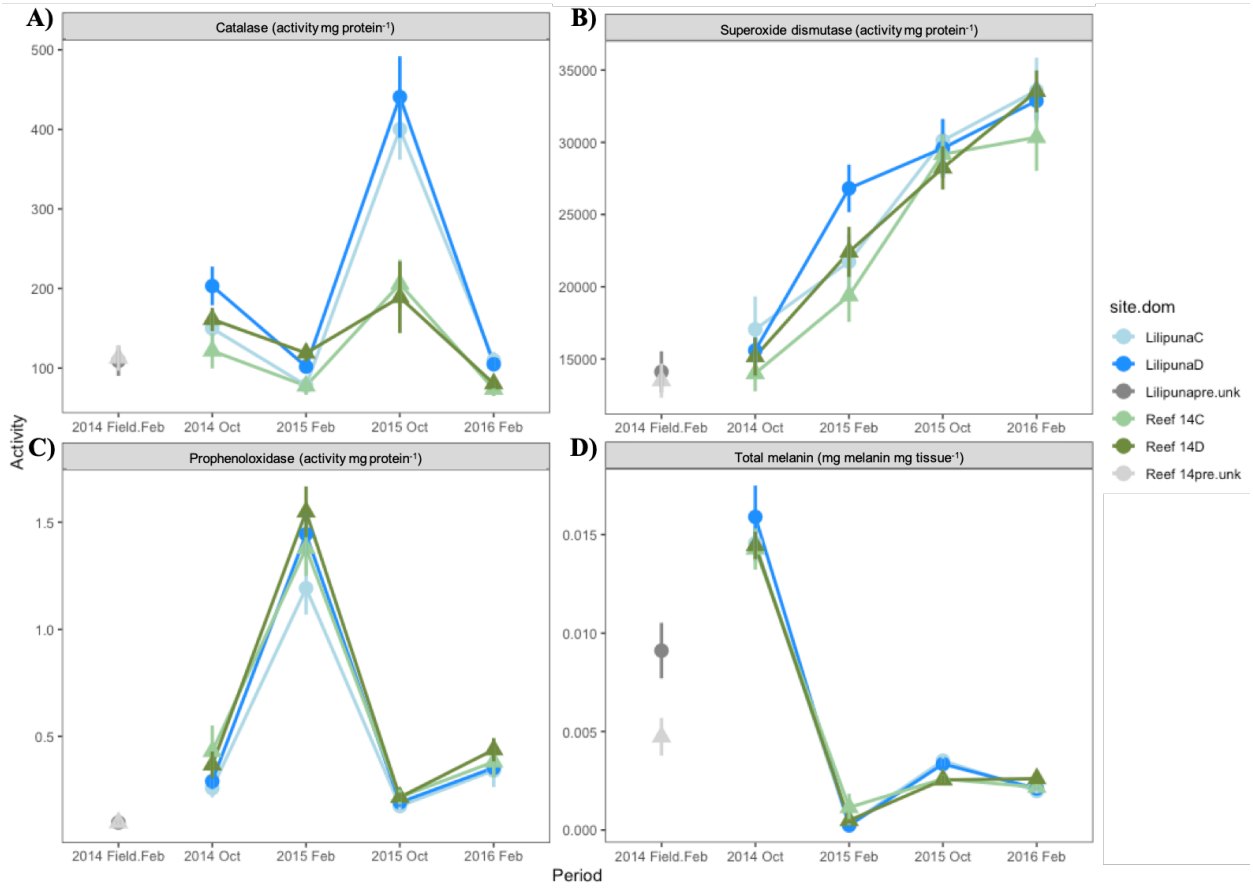

Figure 3 Immunity parameters for Lilipuna (circles with blue hues) and Reef 14 (triangles with green hues) corals. Darker hues represent Durusdinium *dominated corals, lighter hues represent* Cladocopium *dominated corals*

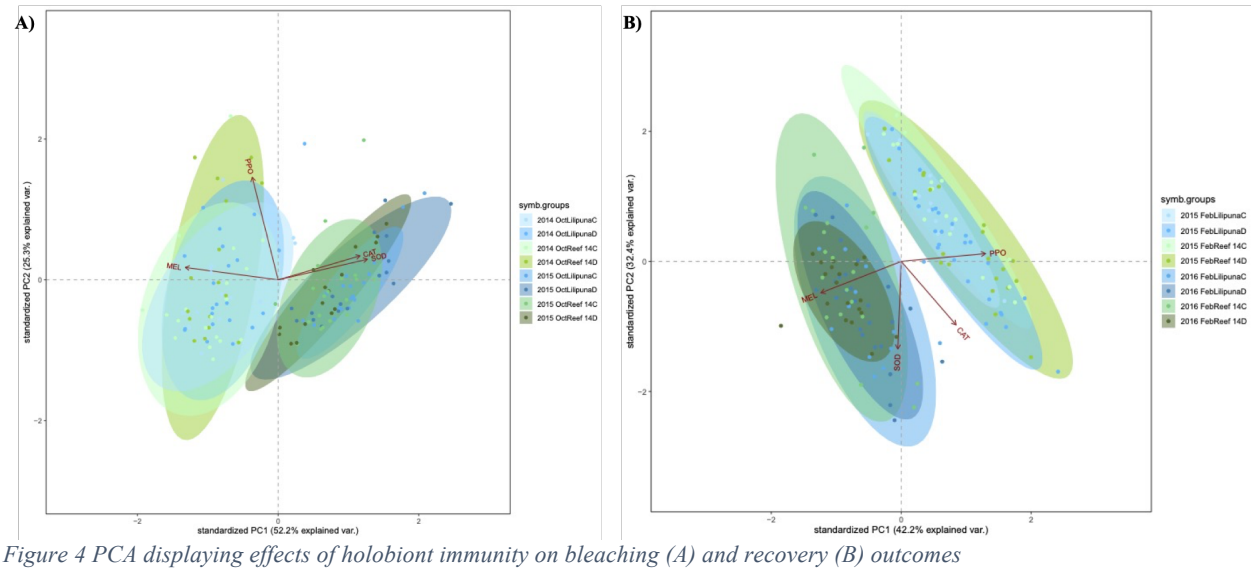

Figure 4 PCA displaying effects of holobiont immunity on bleaching (A) and recovery (B) outcomes

Chapter 5

Conclusions and Discussion

The coral immune system plays multiple roles in addition to pathogen defense and clearance. For example, it is plays roles during wound healing (Palmer et al. 2011; Rodríguez-Villalobos, Work, & Calderon-Aguilera 2016) and ocean acidification (Kaniewska et al. 2012). Additionally, it is pivotal for symbiosis, both during establishment and breakdown. Specifically, during symbiont infection, incompatible partners elicit widespread transcriptional changes that include the induction of immune genes (Voolstra et al. 2009). Further, in current bleaching models, reactive oxygen species putatively derived from the symbiont are believed to elicit an immune response that results in its loss (Nielsen, Petrou & Gates 2018). Therefore, the importance of the immune system cannot be overstated and should be examined under multiple contexts.

Coral immune responses are specific to the type of stress

Corals, like all invertebrates, do not possess an adaptive immune system. Despite this, a high degree of specificity can be achieved by the invertebrate innate immune system. For example, in the water flea, *Daphnia magna*, increased host fitness against the bacterial pathogen *Pasteuria ramosa* was observed when mothers were previously exposed to the bacteria (Little et al. 2003). Corals in particular can discriminate between preferred and non-preferred Symbiodiniaceae species during partner selection (e.g., Voolstra et al. 2009; Wood-Charlson et al. 2006). In addition to organism-specific responses, immunity is also specific to the type of stress experienced. Namely, it appears that mechanisms important for coral responses to disease overlap with, but are not the same as, those that are important for temperature stress.

Four processes comprise the initiation and implementation of an immune response: 1) immune recognition; 2) intracellular signaling; 3) effector responses; and 4) tissue repair (Mydlarz et al. 2016). As such, the signal input received by the coral must necessarily determine the outcome. Effector responses such as inflammation and the production of antimicrobial compounded were induced in *Eunicea calyculata* infected with *Eunicea* Black Disease (EBD). In addition, physiological responses such as increased mucus production and the reinforcement of the extracellular matrix were observed, and are likely a strategy to prevent further infiltration by etiological or other agents. In contrast, during temperature stress, arms of immunity falling under tissue repair (Mydlarz et al. 2016) appear to be induced. Specifically, during bleaching stress, both melanin synthesis and antioxidant production were induced. Antioxidants may be particularly vital to this stress, as some corals increase their metabolic activity in response to increased temperature (Edmunds, Cumbo and Fan 2011), and reactive oxygen species are a natural byproduct of this process.

Melanin synthesis is essential for both temperature and disease stress responses

Melanin synthesis is vital for both temperature and disease stress. In *Eunicea calyculata* infected with EBD, melanin was systemically synthesized in response to the etiological pathogen. Similarly, in *Montipora captiata* undergoing bleaching stress, melanin synthesis was also increased. Although it was not visually obvious such as that in diseased *E. calyculata*, melanin was likely synthesized throughout the entire polyp in *M. capitata* as well.

The melanin synthesis pathway begins with the proteolytic cleavage of inactive prophenoloxidase to the active phenoloxidase and, through a series of intermediate reactions, ultimately leads to the production and deposition of melanin into coral tissues (Mydlarz and

Palmer 2011; Nappi and Christensen 2005). During infection, its main function is the encapsulation and/or walling off of the pathogen. The systemic deposition of melanin in *E. calyculata* tissues is thus of note. If the etiological agent is indeed a fungal pathogen, it may explain the EBD phenotype. However, a second possibility is the systemic induction of inflammatory responses, which can induce subsequent melanin synthesis (Lavesque et al. 2013).

The role of melanin production in response to temperature stress is less clear. However, it may serve as an early acclimatization mechanism (Wall et al. 2018), as melanin synthesis can occur relatively quickly after cleavage of the proenzyme. Indeed, the sea fan, *Gorgonia ventalina*, displayed melanization in response to elevated temperatures (Mydlarz et al. 2008), and higher constitutive levels of melanin and melanin-containing granular cells have also been documented in coral species considered resistant to thermal bleaching (Palmer et al. 2010). Conversely, it may primarily serve a UV-protective role, perhaps for resident Symbiodiniaceae species (Palmer et al. 2010; Vijayan et al. 2017), as high temperature would typically occur with high irradiance in the field.

Potential responses to a malfunctioning symbiont resemble responses to a pathogen

The symbiosis between corals and Symbiodiniaceae is initiated through phagocytosis of the symbiont cell and, by mechanisms as of yet unknown, the phagosome is prevented from fusing with the lysosome (Mohamed et al. 2016), allowing it to mature into a symbiosome. Elements that allow the persistence and maintenance of the coral-Symbiodiniaceae symbiosis are also currently unknown, however, active immune suppression by the symbiont is believed to be a factor. This is evidenced by phenomena such as some corals displaying decreased diseased susceptibility when bleached (Merselis, Liman & Rodriguez-Lanetty 2018) and the upregulation

of immune-suppressing TGF-β in coral hosts during symbiosis establishment (Berthelier et al. 2017). Therefore, aspects activating an immune response may have adverse consequences for symbiosis.

Inflammation is a key immune response for corals against invading pathogens. This was particularly evident in *Eunicea calyculata* infected with EBD and has also been observed in sea fans (Mydlarz et al. 2008) and hard corals (Palmer, Mydlarz & Willis 2008). The initiation of this response begins with the detection of the pathogen via Pathogen Associated Molecular Patterns (PAMPs) by Pattern Recognition Receptors (PRRs; e.g., toll-like receptors, lectins, etc.). Downstream signaling upon detection results in the production of inflammatory cytokines (Nicolo et al. 2016). Importantly, many PRRs detect PAMPs at the cell surface of potential pathogens. Therefore, the increase of immune activating proteins at the cell surface of *Breviolum psygmophilum* in response to temperature stress is of note, particularly because of the increase in proteins known to induce inflammation. Dysfunction induced by temperature stress may therefore cause the coral to treat the symbiont as an invading pathogen, providing an alternative mechanism by which an immune response results in the clearance of Symbiodiniaceae.

Concluding remarks

This thesis contributes novel information to the field of coral biology. First, I show that elevated temperatures affect the cell surface of a Symbiodiniaceae species. This has implications for partner signaling during stress events. Second, I demonstrate that pathogen-specific immune responses can be detected in a soft coral host, and provide evidence for immune components driving a disease phenotype. As the molecular study of coral disease is still a new and emerging field, this work contributes further understanding of disease dynamics at the protein level.

Finally, I have investigated the role of the coral immune system during consecutive bleaching seasons and found that bleaching-resistant coral populations display specific patterns of inducible immunity. This gives important insight into mechanisms that promote coral population persistence in the face of annual bleaching events.

Coral reefs continue to be threatened by rising temperatures and disease outbreaks. Therefore, continued investigation into the mechanisms underlying bleaching and disease outcomes is crucial for informing policy and conservation initiatives. These works provide the first cell-surface proteome for a Symbiodiniaceae species and the first analysis of a coral immune response to consecutive bleaching seasons. Finally, they further the use of proteomics in this field, as the use of these techniques are still in its infancy. As such, they provide a framework for proteomic analysis within a non-model system.

REFERENCES

Berthelier J, Schnitzler CE, Wood-Charlson EM, Poole AZ, Weis VM, Detournay O (2017) Implication of the host TGFβ pathway in the onset of symbiosis between larvae of the coral *Fungia scutaria* and the dinoflagellate *Symbiodinium* sp. (clade C1f). Coral Reefs 36: 1263 - 1268

Edmunds PJ, Cumbo V, Fan TY (2011) Effects of temperature on the respiration of brooded larvae from tropical reef corals. J Exper Biol 214:2783 – 2790

Kaniewska P, Campbell PR, Kline DI, Rodriguez-Lanetty M, Miller DJ, et al. (2012) Major Cellular and Physiological Impacts of Ocean Acidification on a Reef Building Coral. PLoS ONE 7(4): e34659. doi:10.1371/journal.pone.0034659

Lévesque M, Feng Y, Jones RA, Martin P (2013) Inflammation drives wound hyperpigmentation in zebrafish by recruiting pigment cells to sites of tissue damage. Dis Model Mech 6:508-515

Little TJ, O'Connor B, Colegrave N, Watt K, Read AF (2003) Maternal transfer of strain-specific immunity in an invertebrate. Curr Biol 13:489-492

Mydlarz LD, Holthouse SF, Peters EC, Harvell CD (2008) Cellular Responses in Sea Fan Corals: Granular Amoebocytes React to Pathogen and Climate Stressors. PLoS One 3: e1811

Mydlarz LD, Fuess LE, Mann MT, Pinzon JH, Gochfeld DJ (2016) Cnidarian Immunity: From Genomes to Phenomes. In: Goffredo S, Dubinsky Z. The Cnidaria, Past, Present, and Future. 10.1007/978-3-319-31305-4_28.

Nicolo P, Matteo C, Daniela P, Aiti V (2016) Inflammatory response of the ascidian *Ciona intestinalis*. In: Ballarin L, Cammarata M. Lessons in immunity: From single-cell organisms to mammals. 10.1016/C2014-0-02427-6

Palmer CV, Mydlarz LD, Willis BL (2008) Evidence of an inflammatory-like response in non-normally pigmented tissues of two scleractinian corals. Proc R Soc B 275:2696-2693

Palmer CV, Bythell JC, Willis BL (2010) Levels of immunity parameters underpin bleaching and disease susceptibility of reef corals. FASEB J 24:1935–1946

Palmer CV, Traylor-Knowles NG, Willis BL, Bythell JC (2011) Corals Use Similar Immune Cells and Wound-Healing Processes as Those of Higher Organisms. PLoS ONE 6(8): e23992. doi:10.1371/journal.pone.0023992

Merselis DG, Lirman D, Rodriguez-Lanetty M (2018) Symbiotic immuno-suppression: is disease susceptibility the price of bleaching resistance? PeerJ 6: e4494. doi: 10.7717/peerj.4494

Mohamed AR, Cumbo V, Harii S, Shinzato C, Chan CX, Ragan MA, Bourne DG, Willis BL, Ball EE, Satoh N, Miller DJ (2016) The transcriptomic response of the coral Acropora digitifera to a competent Symbiodinium strain: the symbiosome as an arrested early phagosome. Mol Ecol 25:3127 – 3141

Nielsen DA, Petrou K, Gates RD (2018) Coral bleaching from a single cell perspective. ISME J 12:1558 – 1567

Rodríguez-Villalobos JC, Work TM, Calderon-Aguilera LE (2016) Wound repair in Pocillopora. J Invertebr Pathol. Sep;139:1-5

Vijayan V, Jasmin C, Anas A, Kuttan PS, Vinothkumar S, Subrayan PP, Nair S (2017) Sponge-associated bacteria produce non-cytotoxic melanin which protects animal cells from photo-toxicity. Appl Biochem Biotechnol 183:396–411

Wood-Charlson EM, Hollingsworth LL, Krupp DA, Weis VM (2006) Lectin/glycan interactions play a role in recognition in a coral/dinoflagellate symbiosis. Cell Microbiol 8:1985-1993